THE ROLE OF KENAF AND MONTMORILLONITE CLAY ON THE ENHANCEMENT OF THE PROPERTIES OF POLYHYDROXYBUTYRATE COMPOSITES

MUHAMMAD RAFIQ BIN MOHD ISA

FACULTY OF SCIENCE
UNIVERSITI MALAYA
KUALA LUMPUR
2022

THE ROLE OF KENAF AND MONTMORILLONITE CLAY ON THE ENHANCEMENT OF THE PROPERTIES OF POLYHYDROXYBUTYRATE COMPOSITES

MUHAMMAD RAFIQ BIN MOHD ISA

THESIS SUBMITTED IN FULFILMENT OF THE REQUIREMENTS FOR THE DEGREE OF DOCTOR OF PHILOSOPHY

DEPARTMENT OF CHEMISTRY

FACULTY OF SCIENCE

UNIVERSITI MALAYA

KUALA LUMPUR

2022

UNIVERSITI MALAYA

ORIGINAL LITERARY WORK DECLARATION

Name of Candidate: **MUHAMMAD RAFIQ BIN MOHD ISA**

Registration/Matric No: **SHC140085**

Name of Degree: DOCTOR OF PHILOSOPHY (PH.D)

Title of Project Paper/Research Report/Dissertation/Thesis ("this Work"):

THE ROLE OF KENAF AND MONTMORILLONITE CLAY ON THE ENHANCEMENT OF THE PROPERTIES OF POLYHYDROXYBUTYRATE COMPOSITES

Field of Study: **MATERIAL CHEMISTRY**

I do solemnly and sincerely declare that:

(1) I am the sole author/writer of this Work;
(2) This Work is original;
(3) Any use of any work in which copyright exists was done by way of fair dealing and for permitted purposes and any excerpt or extract from, or reference to or reproduction of any copyright work has been disclosed expressly and sufficiently and the title of the Work and its authorship have been acknowledged in this Work;
(4) I do not have any actual knowledge nor do I ought reasonably to know that the making of this work constitutes an infringement of any copyright work;
(5) I hereby assign all and every rights in the copyright to this Work to the University of Malaya ("UM"), who henceforth shall be owner of the copyright in this Work and that any reproduction or use in any form or by any means whatsoever is prohibited without the written consent of UM having been first had and obtained;
(6) I am fully aware that if in the course of making this Work I have infringed any copyright whether intentionally or otherwise, I may be subject to legal action or any other action as may be determined by UM.

Candidate's Signature Date 11/01/2022

Subscribed and solemnly declared before,

Witness's Signature Date 11/01/2022

Name:
Designation:

THE ROLE OF KENAF AND MONTMORILLONITE CLAY ON THE ENHANCEMENT OF THE PROPERTIES OF POLYHYDROXYBUTYRATE COMPOSITES

ABSTRACT

Kenaf reinforced and montmorillonite (MMT) modified polyhydroxybutyrate (PHB) composites were prepared using a twin-screw extruder and injection moulding machine. The influence of reinforcement content and surface treatment on the composites' mechanical, rheological and thermal properties was investigated. The samples were moulded into a bar and dumb-bell shaped specimens and subjected to dry-as-moulded, indoor, outdoor and soil burial conditions for four months. The composites were characterised for thermal, rheological and mechanical properties. The results were supported by images obtained from microscopy techniques such as field emission scanning electron microscopes (FESEM) and transmission electron microscopes (TEM). Weibull analysis of single fibre tensile test results indicates fibre damage due to a high concentration of sodium hydroxide or longer soak time. Kenaf reinforced PHB exhibited up to 21% improvement in Young's modulus. The presence of fibres in the polymer melt modified its flow behaviour from Newtonian (in pure PHB melt) to shear thinning behaviour. Fracture energy and critical strain energy release rate of the kenaf reinforced composite was increased with the addition of 20% kenaf fibres. FESEM image showed gaps between the PHB matrix and treated kenaf fibres, indicating that interfacial adhesion is still poor. However, the melt behaviour, such as the complex viscosity and storage modulus obtained through the rheological study of the treated kenaf PHB composites, shows improvement in interaction. Long term mechanical properties of treated kenaf composites also showed better performance. Energy dispersive X-ray mapping revealed that nanocomposites with clay content of 3 phr exhibited better dispersion than

nanocomposites with higher clay content. The mechanical properties of the MMT-modified PHB, such as the tensile and flexural modulus, were enhanced compared to neat PHB. From the rheological study, PHB and PHB nanocomposites modified with untreated MMT exhibited Newtonian fluid behaviour in the tested frequency range. However, for nanocomposites modified with acid-treated MMT, shear-thinning behaviour was observed at higher clay content. The nanocomposites also exhibited higher complex viscosity compared to PHB. From transmission electron microscopy analysis, exfoliation of the MMT was observed for the treated MMT nanocomposites at all clay loading. MMT-modified PHB has lower melting temperature when compared to neat PHB. Furthermore, it was found that the addition of MMT influenced the crystallisation behaviour of PHB. The presence of acid-treated MMT also reduced the degree of crystallinity with increasing clay content. MMT modification of PHB was shown to reduce the rate of PHB biodegradation when buried in the soil.

Keywords: polyhydroxybutyrate, green composites, biodegradable composites

PERANAN KENAF DAN MONTMORILLONITE TERHADAP PENINGKATAN SIFAT KOMPOSIT POLYHYDROXYBUTYRATE

ABSTRAK

Komposit PHB yang diperkuatkan serat kenaf dan dimodifikasi dengan montmorillonite (MMT) telah disediakan dengan menggunakan extruder skru kembar dan pengacuan suntikan. Pengaruh kandungan kenaf dan MMT serta kesan rawatan permukaan terhadap dua komponen tersebut telah dikaji. Komposit tersebut telah dibentuk menjadi bentuk bar dan dumbel dan seterusnya didedahkan kepada beberapa kondisi berbeza seperti di dalam bangunan, di luar bangunan dan ditanam di dalam tanah selama 4 bulan. Sifat termal, reologi dan mekanikal komposit telah dikaji dan pemerhatian telah disokong dengan teknik mikroskopi seperti mikroskop elektron imbasan (FESEM) dan mikroskop elektron transmisi (TEM). Analisis Weibull terhadap hasil ujian tegangan serat tunggal menunjukkan kerosakan serat kerana kepekatan natrium hidroksida yang tinggi atau masa rendaman yang berlebihan. PHB yang diperkuat kenaf mempamerkan peningkatan modulus Young hingga 21%. Kehadiran serat dalam leburan polimer mengubah tingkah laku alirannya dari Newtonian (dalam cairan PHB tulen) kepada tingkah laku penipisan ricih. Sifat hentaman PHB, seperti fracture energy dan critical strain energy release rate, telah meningkat dengan penambahan serat kenaf sebanyak 20%. Imej SEM menunjukkan jurang antara matriks PHB dan serat kenaf yang dirawat, menunjukkan bahawa lekatan antara muka masih lemah. Namun, tingkah laku cairan komposit kenaf PHB, seperti kelikatan kompleks dan modulus simpanan, menunjukkan peningkatan dalam interaksi. Sifat mekanikal jangka panjang komposit kenaf yang dirawat juga menunjukkan prestasi yang lebih baik. Pemetaan penyebaran tenaga sinar-X mendedahkan bahawa nanokomposit dengan kandungan MMT 3 phr menunjukkan penyebaran yang lebih baik

berbanding nanokomposit dengan kandungan MMT yang lebih tinggi. Sifat mekanikal PHB yang diubahsuai MMT, seperti modulus tegangan dan lenturan, ditingkatkan jika dibandingkan dengan PHB yang tulen. Dari analisis reologi, nanokomposit PHB yang diubahsuai dengan MMT yang tidak dirawat menunjukkan kelakuan cecair Newtonian dalam julat frekuensi yang dikaji. Walau bagaimanapun, untuk nanokomposit yang diubahsuai dengan MMT yang dirawat dengan asid, tingkah laku penipisan ricih diperhatikan pada kandungan MMT yang lebih tinggi. Nanokomposit juga menunjukkan kelikatan kompleks yang lebih tinggi berbanding PHB tulen. Dari analisis mikroskopi elektron transmisi, pengelupasan MMT diperhatikan untuk nanokomposit MMT yang dirawat pada semua kandungan MMT. PHB yang diubahsuai MMT mempunyai takat lebur yang lebih rendah jika dibandingkan dengan PHB yang tulen. Selanjutnya, didapati bahawa penambahan MMT mempengaruhi sifat penghabluran PHB. Kehadiran MMT yang dirawat asid juga mengurangkan tahap penghabluran selaras dengan peningkatan kandungan MMT. Pengubahsuaian PHB menggunakan MMT terbukti dapat mengurangkan kadar biodegradasi PHB ketika berada di dalam tanah.

Kata kunci: Polyhydroxybutyrate, komposit hijau, komposit boleh terbiodegradasi

ACKNOWLEDGEMENT

Firstly, I would like to thank the Government of Malaysia for funding my studies under the MyBrain15 program. I also wish to thank University Malaya for funding my research via the Postgraduate research fund (PPP) grant PG172-2015A.

I would like to express my most profound appreciation to my supervisors, Prof. Dr Aziz bin Hassan and Dr Nor Mas Mira binti Abdul Rahman, for their patience and guidance throughout my PhD journey. I would also like to extend my sincere thanks to Prof. Dr Zainal Arifin bin Mohd Ishak and his team at USM Nibong Tebal campus for their assistance with TEM.

I am incredibly grateful to my family for their support throughout my study period. I cannot begin to express my thanks to my wife and children, who have sacrificed a lot while continuing my studies. Without their tremendous understanding and encouragement in the past few years, it would be impossible to complete my study. I would also like to extend my deepest gratitude to my parents and siblings for their financial and moral support during this challenging period.

Thanks to my fellow Composite Materials and Polymer Research group members who have assisted me directly or indirectly throughout the research. I am also grateful to all the Department of Chemistry support staff who has helped me throughout my studies. Special mention to Mr Zul, who has been instrumental in running the research lab.

TABLE OF CONTENTS

LIST OF TABLES

LIST OF FIGURES

LIST OF SYMBOLS AND ABBREVIATIONS

ω	:	Angular frequency
η^*	:	Complex viscosity
G_c	:	Critical strain energy release rate
K_c	:	Critical stress intensity factor
R	:	Cross-head speed
X_c	:	Degree of crystallinity
d	:	Depth
ΔH_m	:	Enthalpy of melting
L_f	:	Fibre length
W	:	Fracture energy
G''	:	Loss modulus
T_m	:	Melting temperature
P	:	Peak load
P_F	:	Probability of failure
G'	:	Storage modulus
σ	:	Stress
L	:	Support span
N	:	Total number of fibres tested
m	:	Weibull modulus
W_f		Weight fraction
E	:	Young's modulus

ASTM	:	American Society for Testing and Materials
CP	:	Coffee waste particles
DAM	:	Dry-as-moulded
DCP	:	Dicumyl peroxide
D_n	:	Number average
DSC	:	Differential Scanning Calorimetry
DTp	:	Peak derivative temperature
D_w	:	Weight average
EDX	:	Energy Dispersive X-ray Analysis
FDA	:	Food and Drug Administration
FESEM	:	Field Emission Electron Microscope
FTIR	:	Fourier Transform Infrared Spectrometer
GPa	:	Gigapascal
HMDI	:	Hexamethylene diisocyanate
LG		levoglucosan
mm	:	milimeter
MMT	:	Montmorillonite
MPa	:	Megapascal
NaOH	:	Sodium hydroxide
OPEFB	:	Oil palm empty fruit bunch
PCL	:	Polycaprolactone
PHA	:	Polyhydroxyalkanoate
PHB	:	Polyhydroxybutyrate

PHV	:	Polyhydroxyvalerate
PLA	:	Poly(lactic acid)
PP	:	Polypropylene
RDGE	:	Resorcinol diglycidyl ether
$T_{50\%}$	:	50% degradation temperature
TDP	:	4,4'-thiodiphenol
TGA	:	Thermogravimetric Analyser
TGIC	:	Triglycidyl isocyanurate
T_{onset}	:	Onset temperature
UTM	:	Universal Testing Machine
WAXS	:	Wide Angle X-Ray Scattering
XRD	:	X-ray Diffraction Analysis

CHAPTER 1: INTRODUCTION

1.1 Overview

In 2016, it was reported that China imported over 60% of the world plastic waste. Its decision to stop importing waste plastic in 2018 caused a ripple that affected the whole world, drawing attention to a known but often-times ignored issue, the plastic crisis (Laura & Kennedy, 2018). As of 2017, a cumulative total of 8.3 billion metric tonnes of plastics have been manufactured globally (Geyer et al., 2017). Demand for more energy-efficient materials has increased the use of polymer composites in various industries. Polymer composites are used to produce various articles such as outdoor decking, car bumpers and aeroplane fuselages. Composites have high strength, high stiffness, and low density, which allows the fabrication of relatively lighter parts but with similar or superior strength compared to more traditional materials (Saba et al., 2016). Composites also offer unique opportunities compared to traditional materials, such as integrating multiple functions into a single system. However, because most polymer composites are complex systems comprised of two or more components, separating the components for recycling is cost-intensive (Pickering et al., 2016). The rapid historical growth of the use and disposal of the material has proved to be a challenge for solid waste management systems.

Currently, the most popular method for disposing of polymer composites is *via* landfill and incineration, and both methods impact the environment significantly. Globally, only 9% of the plastic wastes have been recycled, and the majority of the rest end up in landfills and into the ocean (Brooks et al., 2018). The statistic highlights the importance of shifting from traditional polymers to more environmentally friendly biodegradable plastics, especially for single-use applications such as product packaging and consumer products (Gross & Kalra, 2002). Plenty of biodegradable polymers can

potentially be used instead of conventional polymers. In particular, a bio-derived polyester, polyhydroxybutyrate (PHB), has a very high potential as a substitute.

Key characteristics such as biodegradability, recyclability and environmental safety, the hallmark of eco-friendly materials, have become increasingly important during the material selection process (Zhang et al., 2017). Several researchers have been working on green composites utilising resins from renewable resources such as poly(lactic acid) (PLA), polycaprolactone (PCL) and polyhydroxyalkanoates (PHA). PHAs are a range of naturally occurring polyesters that are growing in popularity. PHA can be extracted from the bacteria to yield a non-toxic, biocompatible and biodegradable polymer (Muhammadi et al., 2015).

Since their discovery, over 100 different polyesters of the same structure have been found. The two most widely studied of these are poly(3-hydroxybutyrate) (PHB) and polyhydroxyvalerate (PHV) (Muneer et al., 2020). These different types of PHA are categorised by their side groups. PHB has a simple -CH_3 side chain while PHV has a slightly more complex -CH_2-CH_3 side chain. PHB is an attractive substitute for petrochemical plastic due to its similar properties to polypropylene, biocompatibility, and biodegradability (Zhong et al., 2020). ASTM Committee on Plastic Technology defined biodegradable polymers as degradable plastic in which the degradation results from the action of naturally occurring microorganisms such as bacteria, fungi and algae. The Second International Scientific Workshop on Biodegradable Polymers and Plastics held in 1991 at Montpellier defines biodegradable polymer as a polymer in which the degradation is mediated at least partially by a biological system. PHB fits into both definitions. PHB undergoes surface erosion in the presence of many bacteria and moulds.

The erosion is mediated by extracellular enzymes, and the cell metabolises the degradation products. PHB is truly a biodegradable polymer.

Also, PHB is water-insoluble and resistant to hydrolytic degradation. However, pure PHB is very brittle, thus limiting its application (Li et al., 2016). This work will combine kenaf and montmorillonite with PHB to improve its mechanical and thermal properties. Kenaf fibres and montmorillonite are selected due to their low environmental impact.

1.2 Problem statement

Pure PHB is very brittle, thus limiting its practical application due to a brittle material's tendency for catastrophic failures. Catastrophic failures are hazardous because there are almost no signs of failure until too late. PHB has low nucleation density and slow crystallisation rates, leading to the formation of large spherulites (Wang et al., 2016). These large spherulites would produce cracks and are the reason for their brittleness. The addition of reinforcing fillers could improve the crystallisation behaviour of PHB. It is known that in polymer composite materials, some fillers may act as nucleation agents, encouraging the formation of smaller spherulites. Smaller crystal sizes would reduce the cracks in the polymer matrix, improving its mechanical properties.

Mohamed El-Hadi (2014) reported that the addition of trimethyl stearyl ammonium treated montmorillonite (MMT), a type of treated nanoclay, to PHB accelerated its crystallisation process and improved its thermal stability due to the MMT acting as a nucleating agent. In addition, the introduction of layered silicates such as montmorillonite would dramatically accelerate the biodegradation process of PHB due to smaller spherulites sizes (Maiti et al., 2003, 2007). PHB with nanoclay tends to crystallise faster, producing smaller spherulites, resulting in a higher inter-spherulitic area. These

inter-spherulitic regions are amorphous and are more susceptible to hydrolysis followed by consumption by the microorganisms. The introduction of more malleable fibres could also help to toughen the composite.

Natural fibres have several advantages: low density, biodegradability, good mechanical properties, low cost, and relatively abundant. Despite the advantages, natural fibres can absorb a significant amount of moisture and have poor interfacial adhesion with the polymeric matrix. To reduce the hydrophilicity and improve the fibre-matrix adhesion, removing oil and wax substances on the fibre surface is essential, achieved via surface treatment (Chandrasekar et al., 2017). Alkalisation involves soaking the natural fibres in sodium hydroxide solution and is one of the chemical methods of fibre surface treatment. Alkali treated kenaf fibres have been reported to absorb less moisture from the environment and produce composites with better mechanical properties than their untreated counterparts.

1.3 Aims and objectives

This research aims to improve the mechanical properties of PHB through the addition of kenaf fibres and modify the crystallisation behaviour of PHB via modification using MMT. To achieve this aim, the objectives of the experiment are:

1. To prepare kenaf fibre/PHB and MMT/PHB composites via compounding and injection moulding machine.

2. To study the effect of surface-treated kenaf fibre and MMT on the thermal and mechanical properties of the composite and its processability.

3. To study the long-term environmental exposure impact on the mechanical properties of the composites.

1.4 Research scope

Kenaf and mmt were combined with PHB to improve the thermal and mechanical properties. This study covers the influence of filler content, filler surface treatment and environmental exposure on the thermal and mechanical properties of the injection moulded composites. Thermal analysis was done using thermogravimetric analysis (TGA) and differential scanning calorimetry (DSC) to study the stability and crystallisation behaviour of the composite. Mechanical properties were characterised using a universal testing machine (UTM) for tensile and flexural properties and a drop tower impact tester for impact properties. The composite specimens were subjected to indoor, outdoor and soil burial for a maximum duration of four months. The mechanical properties were characterised after conditioning to investigate the effect of secondary crystallisation and biodegradation on its mechanical properties.

1.5 Thesis outline

Chapter one presents the research background, aim, objectives and scope of the study. The importance of advancing biodegradable composites technology was also explained.

Chapter two provides a review of literature on PHB and efforts done by other researchers to improve its properties. Gaps in the current knowledge are highlighted in this chapter.

Chapter three summarises the materials and methods implemented in the study. The details of the experimental setup are described in this chapter.

Chapter 4 presents the results obtained during the study and offers in-depth analysis and relevant discussions.

Chapter 5 presents the general conclusions from the study done in this exercise. Recommendations for future work are also included.

CHAPTER 2: LITERATURE REVIEW

2.1 Polyhydroxybutyrate

Polyhydroxybutyrate, or PHB, is a biodegradable polymer belonging to the polyhydroxyalkanoate (PHA) family of polyesters. It was first discovered inside *Bacillus megaterium* in the 1920s by Maurice Lemoigne, a French microbiologist (Sudesh et al., 2000). It is thought that bacteria store PHB for the same reasons as mammals store fat: as an energy source (Madison & Huisman, 1999). The polymer forms within the bacterial cells in discrete granules, with diameters between 100 and 800 nm. However, the number and size of the granules and the molecular weight of the polymer will vary depending on the type of bacteria, the growth conditions, and the extraction method (Anderson & Dawes, 1990; Poirier et al., 1995). The slight yellow colour of the polymer is due to residual cell debris left in the polymer post-extraction.

PHB is a thermoplastic material that is biodegradable in a microbial rich environment. In addition to its excellent barrier properties and insolubility in water, naturally, it draws interest as a food packaging material (Hankermeyer & Tjeerdema, 1999). Its thermoplastic behaviour allows it to be processed using conventional polymer processing methods such as extruders and injection moulding machines (Holmes, 1988). Its material properties have been reported to be similar to polypropylene (PP), a widely used petroleum-based polymer (Li et al., 2016; Marchessault & Yu, 2005; Muneer et al., 2020; Sudesh et al., 2000; Yu et al., 2006). It has remarkable mechanical properties such as high elastic modulus and tensile strength. Due to its biocompatibility, PHB has found critical applications in tissue engineering and biomedical applications such as sutures, thermogels, controlled drug release agents, tissue scaffolds and many more (Holmes,

1985; Manavitehrani et al., 2016; Meischel et al., 2016; Volova et al., 2003; Wu et al., 2016).

Microorganisms in soil and water can degrade PHAs by using PHA hydrolases and PHA depolymerases (Choi et al., 2004; Jendrossek & Handrick, 2002). The rate of degradation activities of these enzymes depends on the composition of the polymer and the environmental conditions. The degradation for PHB is typically a few months (in anaerobic sewage) to years (in seawater) (Madison & Huisman, 1999). The higher the population of microorganisms, the faster PHB articles will degrade in that environment. Exposure to UV light has been shown to accelerate the biodegradation process of PHAs (Shangguan et al., 2006). It is recommended that PHB articles be composted to minimise their ecological impact.

Table 2.1: Degradation rate for Biopol®.

Environment	Time for 100% weight loss (weeks)
Anaerobic sewage	6
Estuarine sediment	40
Aerobic sewage	60
Soil	75
Seawater	350

PHB has been applied in niche applications worldwide, given its mix of mechanical properties and tailorable biodegradability. Due to cultural and social factors,

disposable shaving razors are usually flushed down the toilet in Japan. PHB fabricated razor blades would degrade in sewage, minimising blockage and environmental issues (Lenz, 1995). The US Navy has also been using PHB-based utensils to reduce the amount of plastic waste generated by their ships (Council, 1996). PHB-based utensils would sink once disposed of at sea due to PHB's higher density compared to water. Microorganisms on the sea floor would disintegrate these wastes, something not possible with conventional plastics.

Figure 2.1: Articles fabricated from PHB (photo sourced from https://marymatuvi17.wordpress.com/).

Several issues are limiting the widespread adoption of PHB. Firstly, it has been widely reported that PHB is brittle. Brittleness observed in PHB has been attributed to the inability of the amorphous region of its polymeric chain to freely move as it is subjected to force (Righetti et al., 2019). PHB is produced, it has a highly regular structure - it is almost entirely isotactic, which means that all the side groups on the polymer chain

point in the same direction (Sudesh et al., 2000). This arrangement causes the chains to form helical structures, with the side groups all pointing away from the centre of the helix to minimise steric hindrance (Padermshoke et al., 2005). Carbonyl-methyl group interactions stabilise the helix conformation. The chains, therefore, pack together easily to form crystals, and the crystalline nature of the polymer makes it brittle and stiff (Barham & Keller, 1986). Furthermore, it is relatively more expensive to produce when compared to more conventional polymers (L. Yu et al., 2006). In 1997, the retail price for PHB was reported at around USD16 per kg, while PE and PP only cost less than USD1 per kg (Choi & Lee, 1997).

Another drawback is that it is difficult to process in a molten state because it starts to degrade at temperatures not much higher than its melting temperature (Gogolewski et al., 1993). At above 170°C, PHB starts to decrease molecular weight, and the degradation gets more severe over a longer duration of time (Avella et al., 2000). The thermal degradation mechanism for PHB is due to random scission at the ester group according to a β-hydrogen elimination (Doi et al., 1990). Lastly, PHB has poor resistance to acids and bases and can be dissolved in chlorinated solvents (Holmes, 1985). The mechanical properties of PHB have been reported to be dependent on its molecular weight (Grassie et al., 1984). The impact strength was reported to decrease from about 145 Jm^{-1} to about 30 Jm^{-1} as the molecular weight changes from 500,000 $gmol^{-1}$ to 200,000 $gmol^{-1}$.

Due to its immense potential, more effort has been taken to improve our PHB understanding, reduce processing costs, and modify its properties. The bacterial PHB production process can be modified to produce PHB copolymerised with PHV. This copolymerisation makes the structure more irregular and less crystalline. Therefore, the

copolymer is less brittle yet still biodegradable (Holmes, 1988). PHB-PHV copolymers exhibit isodimorphism. At less than 40 mol% HV, the HV units can crystalise in the PHB lattice. Isodimorphism allows the copolymer to exhibit similar high crystallinity as neat PHB, retaining good chemical and hydrolysis resistance.

Early development of PHB-HV copolymers contains up to 30% PHV content (Bauer & Owen, 1988). Copolymerising PHB with PHV has been shown to improve the ductility of the polymer. Wide Angle X-ray Scattering (WAXS) results suggest that the HV acts as distortion in the polymer lattice. The Young's modulus was reduced as HV% increases without significant change to its crystallinity. PHB was shown to have similar dynamic mechanical properties in the -30°C to 50°C range. However, the modulus for PHB-HV copolymers is severely affected by the difference in temperature, as indicated by the steep reduction in modulus value as the temperature increases (Owen, 1985). PHB with higher HV% also shows significantly lower flexural modulus and tensile strength, albeit with significantly higher elongation at break.

The melt strength of neat PHB is dependent on its molecular weight. Reduction of its molecular weight due to heat decomposition would reduce the resulting mechanical strength of the finished article and affect the ease of extrusion. Lower melt strength would result in repeated melt breakage, resulting in more wastage during processing. Due to its slow crystallisation, PHB melt is very sticky and quite challenging to handle compared to conventional polymers such as PE or PP.

2.2 Development of PHB composites

Improving the mechanical properties of PHB is vital to increase its adoption and improve its range of applications. While biodegradability and biocompatibility of PHB remain advantageous, strategies to tailor material architecture for toughening PHB are vital to tackle its shortcoming of embrittlement and thermal instability. Researchers have been attempting to improve the composites by using various reinforcements. However, most groups have focused on using natural or biobased reinforcement agents to preserve the products' ability to biodegrade fully.

Bodros et al. (2007) studied the mechanical properties of various biocomposites and compared them against glass fibre reinforced epoxy composite, a commonly used composite for structural application. The researchers found that some biocomposites can match the mechanical performance shown by the epoxy-glass fibre composites. However, the researchers noted that many factors must be optimised to achieve maximum performance.

Bucci et al. (2014) prepared and studied the mechanical and physical properties of PHB biocomposites reinforced with rice husk ash. The researchers reported up to 25% improvement in impact properties and 15% improvement in flexural strength. However, the modulus of elasticity is decreased with increasing ash content. This observation contradicts the reported hardness, where the shore hardness of the composites increases with increasing ash content. Furthermore, the authors also reported the increasing density of the composites with higher ash content and commented that it is a non-limiting factor. It has been a well-known fact that one of the allures of polymer composites have been its

weight-to-performance ratio. Therefore, it is more advantageous to reduce its overall density by employing a less dense reinforcement into a PHB composite.

Reis et al. (2015) reported that compounding PHB with milled coffee waste particles (CP) resulted in composites with improved thermal resistance. The researchers attribute a reduction in the X_c due to an imperfect PHB crystal arrangement resulting from introducing CP. The authors claimed that increasing CP content to up to 20% improved the impact strength. Upon closer study, it was observed that the actual improvement is only by 3 J/m, which is relatively negligible and within the potential error range. The fractured image presented did not show any significant change in the fracture behaviour of the materials. The researchers have suggested a pull-out fracture mode; however, no plastic deformation was observed on the actual fractured surface.

Smith et al. (2020) studied the synergistic effect of peroxide and agave fibre in fibre reinforced PHB composites prepared reactive extrusion. Analysis using optical microscopy showed a decrease in spherulite formation, indicating a controlled reduction of the crystalline region. The researchers suggested that the fibre-matrix adhesion was improved due to the introduction of organic peroxides. The addition of peroxides increases the tensile strength of the composites compared to systems without peroxides. However, the tensile strength value is still lower compared to the reported value for neat PHB. It is important to note that due to the intent of the researchers to employ the composites in food packaging, they were limited to a maximum of 1.5 wt. % organic peroxide in their composites to meet the Food and Drug Administration (FDA) requirements. Melo et al. (2012) also reported that peroxide treatment improved the mechanical properties of carnauba fibre reinforced PHB composites compared to

composites reinforced with untreated carnauba fibres. However, both composites still yield lower tensile strength compared to neat PHB.

Hosokawa et al. (2017) studied the mechanical properties of compression moulded PHB reinforced with random mats of sisal and coconut fibres. The researchers used a DSC to study the thermal degradation of the composites, which is quite unconventional. The composites exhibited higher crystallinity compared to neat PHB. The researchers also reported that composites reinforced with sisal exhibited similar performance to neat PHB, while coconut fibre reinforced PHB has lower mechanical properties than neat PHB. It was also reported that moisture absorption in the fibre reinforced samples post-conditioning has caused the mechanical strength of the composites to decrease.

Barkoula et al. (2010) studied the influence of manufacturing methods on the mechanical properties of short flax fibre reinforced PHB and PHB-HV composites. In general, injection moulded PHB composites exhibited lower impact strength than compression moulded. However, the shorter cycle time of injection moulding, higher reproducibility and capability of moulding more complex shapes makes injection moulding more advantageous in the long run.

Gunning et al. (2013) studied the mechanical and biodegradation performance of short natural fibres reinforced PHB composites prepared via extrusion and injection moulding. The fibres employed were hemp, jute and lyocell. The researchers reported a high level of fibre breakage during processing, which resulted in lower tensile and impact properties. The fibre breakage could be due to their selection of 200 rotations per minute (RPM) as the screw speed during the extrusion process. Higher RPM is usually used to

get higher shear rates during mixing to get excellent dispersion. However, fibre-fibre and fibre-machine interaction during the process can cause the fibres to break, resulting in fibres with a length less than the critical length. Therefore, it is crucial to optimise the processing speed used, especially where preservation of the aspect ratio is paramount.

Khoshnava et al. (2017) studied the mechanical properties of woven kenaf bast fibre/oil palm empty fruit bunches (OPEFB) hybrid reinforced PHB biocomposite as non-structural building materials. Optimal mechanical properties such as tensile and flexural strength were observed at 11 layers of kenaf/OPEFB mats. It was suggested that the addition of OPEFB improved the impact properties of the polymer matrix. On the other hand, kenaf bast fibres reduced the impact properties due to their brittle nature. The compression moulding process stated in the study involves a relatively long processing time at 180°C to thoroughly melt the polymer at the centre of the specimens. There is a very high probability that the PHB has started to degrade after extended exposure to the processing temperature.

Wong et al. (2004) successfully improved the mechanical properties of PHB by the introduction of 4,4'-thiodiphenol (TDP) treated flax fibres. TDP is known to form hydrogen bonding with many functional groups and was suggested to be responsible for the shift of the dynamic mechanical properties of the PHB matrix from brittle to ductile. However, there were no long-term properties reported for the composite. For PHB composites, it is essential to study the long-term mechanical properties due to their tendency for embrittlement. In some cases, the embrittlement might become even more severe due to the initially beneficial modification, reducing its practical service life.

2.3 Ageing in PHB and its composites

Ventura et al. (2017) studied the hydrothermal ageing effect on water uptake and tensile properties of compression moulded PHB/flax biocomposites. The effectiveness of fibre surface treatment such as wet/dry cycling, argon plasma and ethylene plasma was also studied. The hydrothermal ageing found that all the surface treatment studied was ineffective at preventing water uptake. The pseudo-Fickian behaviour of water diffusion in the composites was accelerated with increasing ageing temperature. Before ageing, all the composites presented higher stiffness and strength compared to neat PHB. A combination of wet/dry cycling and argon plasma yielded the best properties, indicating improved fibre-matrix adhesion. However, post-ageing, the mechanical properties were reduced due to fibre debonding and matrix damage due to the water uptake.

Sanchez-Safont et al. (2020) studied the compatibilisation effect of different reactive agents in PHB/natural fibre-based biocomposites. Four different compatibilisers were evaluated; dicumyl peroxide (DCP), hexamethylene diisocyanate (HMDI), resorcinol diglycidyl ether (RDGE), and triglycidyl isocyanurate (TGIC). Both fibres and reactive agents partly hindered secondary crystallisation, leading to lower crystallinity in aged composites for neat PHB. However, no apparent improvement in terms of fibre-matrix adhesion was observed.

Wang & Petru (2019) reported that surface treatment of flax fibres improved the damping properties of the composite under hygrothermal conditions. The four chemical treatments evaluated, alkalisation, silanisation, acetylation and alkali-silanisation, successfully reduced the flax fibres' water uptake. The storage modulus and glass transition temperature of the treated flax composites are higher than neat PHB, and the

peak value of the loss factor is lower than neat PHB specimens. The acetylation treated flax composites exhibit excellent damping performance in all dynamic mechanical properties.

The fibre surface needs to be modified to make natural fibres more suitable for reinforcing in PHB-based materials. Several chemicals could do the surface modification of fibre, and these have a specific effect on the fibre. Important properties may include mechanical strengths, moduli, interlaminar shear strength, bonding ability, water and chemical retention, flammability and thermal stability. Vinayagamoorthy (2020) has analysed different surface treatments and concluded that NaOH treatment is the best in elevating the majority of the fibre characteristics (Vinayagamoorthy, 2020). It has been proved that NaOH effectively improves the interfacial adhesion between the fibre and matrix and thus elevating the mechanical properties. In addition, NaOH elevates the interlocking and wetting of fibres with the matrix, thermal stability and storage modulus of the composites.

2.4 PHB nanocomposites

Bruno et al. (2008) evaluated PHB/nanoclay composite prepared using the solution intercalation method. The researchers reported that changes in PHB crystallinity were observed after incorporating organophilic nanoclay into the polymer matrix. These microstructural changes were detected by the variation of hydrogen nuclear relaxation time values and X-ray, which showed an increase in the clay interlamellar space due to the intercalation of the polymer in the clay between lamellae. It was also reported that the solvents used in the technique affect the organisation of the crystalline region directly, promoting better intercalation and behaving like a plasticiser. The method used in this

study is relatively simple. However, production on a larger scale is significantly more complicated due to the solvents used in the study, such as dimethyl chloride and tetrahydrofuran.

Manikandan et al. (2020) attempted to improve PHB barrier properties and chemical resistances by incorporating graphene nanoplatelets (Gr-NP) via the solution casting method. In comparison with pristine PHB, the PHB/Gr-NPs nanocomposite showed a higher melting temperature, thermal stability, and tensile strength along with a reduction in oxygen and water vapour permeability, respectively. The penetration of UV and visible light was significantly reduced with the addition of Gr-NPs. Furthermore, the cytotoxic effect of the prepared nanocomposite was found to be statistically insignificant compared to the pristine PHB.

Ollier et al. (2018) studied the influence of the content of untreated and modified bentonite on the thermal degradation of a biodegradable bacterial PHB matrix. The modified clay was first acid-activated, then silylated and further modified by cationic exchange treatment. The researchers reveal that the organic modifiers of the muti-treated clay promote the thermal degradation process leading to a significant reduction in the molecular weight of PHB. It was demonstrated that the incorporation of the bentonite did not modify the degradation mechanism of PHB and that the process can be well described by the Avrami–Erofeev random nucleation model, in which the reaction is controlled by initial random nucleation followed by overlapping.

PHB-based films, reinforced with bacterial cellulose or cellulose nanocrystals and plasticized using tributyrin or poly(adipate diethylene), were prepared by Seoane et al. (2017) via solvent casting. Contact angle measurements and calorimetric analysis proved

that cellulose nanocrystals aggregation, due to the hydrophilic nature of the filler, slows down the degradation rate of the composite. Increasing the filler content increases the biodegradation rate. In contrast, nanocomposites with bacterial cellulose behave similarly to neat PHB, possibly due to the lower hydrophilic character of this material. The addition of the two plasticisers contributed to a better dispersion of the nanoparticles by increasing the interaction between the cellulosic reinforcements and the matrix. Secondary recrystallisation occurring during incubation was found to reduce the biodegradation rate of the composites in compost.

The introduction of nanoclays into PHB has been shown to alter biodegradation, allowing for specialised applications such as nutrient release control in fertilisers (de Carvalho Arjona et al., 2021). The researchers prepared PHB nanocomposite encapsulated urea via the emulsion method. The nanoclay was introduced into the system to improve its processability, specifically the thermal stability. All the PHB/MMT microcapsules showed a higher temperature of degradation, indicating better thermal stability while maintaining biodegradability.

Ublekov et al. (2018) prepared a novel electrospun PHB/organomodified MMT nanocomposite fibrous scaffold via the electrospinning method. The addition of the modified MMT particles leads to significant amorphisation of the deposited fibrous scaffolds and dramatically improves the mechanical properties. The addition of 5 wt% organo-modified MMT in the 12 wt% PHB solution leads to a self-supporting 3D network fibrous scaffold formation. In the case of electrospun PHB mats, the addition of the nanoclay particles leads to a significant reduction of average fibre diameter and surface clay-filled pore structure formation, which is beneficial in its intended application as a tissue scaffold.

The effect of the surface properties of several silica nanoparticles on the dispersion and isothermal crystallisation kinetics of PHB nanocomposites were investigated by Lan & Sun (2017). Bare and PEG treated sol-gel silica nanoparticles were synthesized from commercially available hydrophobic and hydrophilic fumed silica. PEG treated silica nanoparticles were best dispersed in PHB matrix, as evidenced by TEM images. Values of the Avrami exponent, $n = 2.2 \pm 0.2$ for all the PHB/silica nanocomposites, indicated that the introduction of various silica nanoparticles did not alter the crystallisation mechanism of PHB. However, the crystallisation rate of PHB in the nanocomposites was significantly decreased due to the introduction of PEG treated silica. This decrease is because the rearrangement of the PHB polymer chains during crystallisation was limited by the interaction and chain entanglement between PHB and the grafted PEG on silica. It was also reported that the solvents used in the solvent casting process directly affect the organisation of the crystalline region, promoting better intercalation of the nanoparticles.

PHB/Cloisite 10A nanocomposite was prepared by solution casting method to study its water vapour permeability (Akin & Tihminlioglu, 2018). The researchers reported that the nanocomposite has reduced water vapour permeability compared to native PHB films. 3 wt% clay loaded composites exhibited optimal performance. In addition, the exfoliated structure was reported to be achieved at low clay loaded sample (1% w/w). However, at higher concentrations (3% w/w), the structure was found as intercalated. The barrier properties improvement was highly dependent on the dispersibility of Cloisite 10A in the PHB matrix. Reduction in water permeability is attributed to increasing tortuosity of the permeable channel formed due to the clay delamination.

Kaci et al. (2009) investigated the re-processability of PHB/organoclay nanocomposite by subjecting the material to multiple extrusion cycles in a single screw extruder running at 60 RPM. Evaluations were done after the first, third, fifth and seventh extrusion cycles, and tensile properties and morphology of the samples were determined. X-ray diffraction analysis showed that crystallinity tended to increase with the number of reprocessing cycles up to the fifth cycle and then decreased. In general, the mechanical properties of all systems decreased with reprocessing. As it is, PHB/nanocomposite is not suitable for recycling as the mechanical properties were reduced.

Nanoparticles were added into PHB for improving mechanical and thermal properties and for additional properties, such as antibacterial properties. For example, Jayakumar et al. synthesised PHB-silver nanocomposite using cheese whey permeate, a by-product of the dairy industry, as a substrate for growing *Bacillus megaterium* (Jayakumar et al., 2020). The nanocomposite showed comparatively higher mechanical strength and excellent thermal properties without compromising its flexibility. The barrier properties of the film were seen to improve significantly. However, the effect of silver on the biodegradation of the films was not carried out. If the biodegradation rate is severely impacted, then it could reduce the desirability of PHB as a food packaging material.

Kiran et al. (2017) prepared a nanocomposite by combining PHB with nano-melanin via solvent casting. The researchers reported that the nanocomposite film was homogeneous, smooth, without any cracks, and flexible. The film was crystalline and thermo-stable up to 281.9°C. The introduction of nano-melanin into PHB imbued the composite with anti-bacterial properties, especially for food packaging applications. However, no mechanical properties were reported in this study.

Biodegradable polyhydroxybutyrate/poly-3-caprolactone mats were fabricated by Avossa et al. (2021) via electrospinning for use as a medical dressing. The mats were modified with hybrid Melanin-TiO_2 nanostructures to improve their anti-bacterial properties. All the samples were reported to absorb a large amount of water, which is advantageous for a wound dressing. Coating the mats' surface with the melanin-TiO_2 coating was more effective than incorporation into the matrix. It was reported that melanin also provides a UV-shielding effect when incorporated into a composite (Roy & Rhim, 2021).

Several researchers have studied the viability of starch nano-particles as a reinforcement in polymer composites (Kim et al., 2015). Generally, the incorporation of starch nano-particles increases both the tensile strength and elastic modulus of the composites but decreases the elongation at break. However, Yu et al. (2008) reported that both the tensile strength and elongation was increased when PLA was reinforced with PCL-grafted starch nanoparticles. The rubbery PCL component was sufficient to provide enough flexibility for the nanocomposites, which contributed to the improvement of elongation. However, Young's modulus was reduced. Kim et al. (2015) also highlighted that nano-starch is less competitive than nano-cellulose as a reinforcement.

Nanocellulose can be categorised into cellulose nanocrystals, cellulose nanofibrils, and bacterial cellulose. Nanocellulose exhibits a high surface to volume ratio, excellent mechanical properties and good physical properties such as thermal, electrical and optical properties (Bhat et al., 2017). Although cellulose nanofibrils and nanocrystals are extracted from the same sources, both have a very distinct structure. Cellulose nanofibrils have a complex web-like structure, while cellulose nanocrystals have short rod-like structures (Zinge & Kandasubramanian, 2020).

Nanocellulose develop a network-like structure when incorporated in PHB, resulting in improved barrier and migration properties (Dhar et al., 2015). They have been shown to enhance the crystallization, mechanical behaviour and water resistance of PHB (Briassoulis et al., 2021). Frone et al. (2020) reported that crystalline nanocellulose has better adhesion with the polymer matrix than cellulose nanofibrils, making them more effective as reinforcing agents. However, to ensure minimal environmental and financial cost, the process of extracting nanocellulose must be environmentally friendly, ideally by upcycling agricultural wastes (Abral et al., 2019; Dufresne, 2013).

CHAPTER 3: MATERIALS AND METHODOLOGY

3.1 Materials

The PHB pellets were supplied by Tianan Biologic Materials (Ningbo, China). The selected grade was Enmat Y1000P, suitable for the extrusion and injection moulding process. The HV copolymer content is reported at 3%. The properties of the material, reported in the technical data sheet, are tabulated in Table 3.1. However, the manufacturer did not provide any standard testing method to characterise the properties.

Table 3.1: Properties of Enmat Y1000P.

Properties	Value
Specific gravity	1.25
Tensile strength (MPa)	39
Elongation at break (%)	2
Young's modulus (MPa)	2800 - 3500
Flexural modulus (MPa)	3520 - 4170
Notched Izod impact (J/m)	22
Melting point (°C)	170 - 176

Kenaf fibre bales were supplied by the National Kenaf and Tobacco Board (Kota Bharu, Malaysia) and processed into 3 mm short fibres by the Malaysian Agricultural Research and Development Institute (Serdang, Malaysia). Sodium hydroxide pellets were supplied by Merck (NJ, USA). Nanocor (IL, USA) supplied acid-treated and untreated MMT powder. The two grades of MMT used in this study are Nanomer PGV (untreated MMT, beige grey powder) and Nanomer 1.34TCN (MMT treated with 25–30 wt% methyl dihydroxy ethyl hydrogenated tallow ammonium, off-white powder) with a density of 776 kg/m^3 and 275 kg/m^3, respectively. Both MMTs were reported to have an average particle size of 16 μm.

Before alkali treatment, the kenaf fibres were rinsed with water and dried for 6 hours at 80°C in a conventional oven. Then, the fibres were soaked in a NaOH solution. NaOH concentration was varied at 2%, 4%, and 6% w/v with soak time of three, four, and five hours. The maximum amount of fibre treated is set at 5% weight of fibre over the volume of water. This limit is to ensure the alkali solution thoroughly wets each fibre strand. After soaking, the fibres were drained and rinsed with distilled water until the pH of the washing liquid was neutral. Finally, the treated fibres were dried using a vacuum oven at 80°C for 24 hours. A summary of the treatment condition is provided in Figure 3.1.

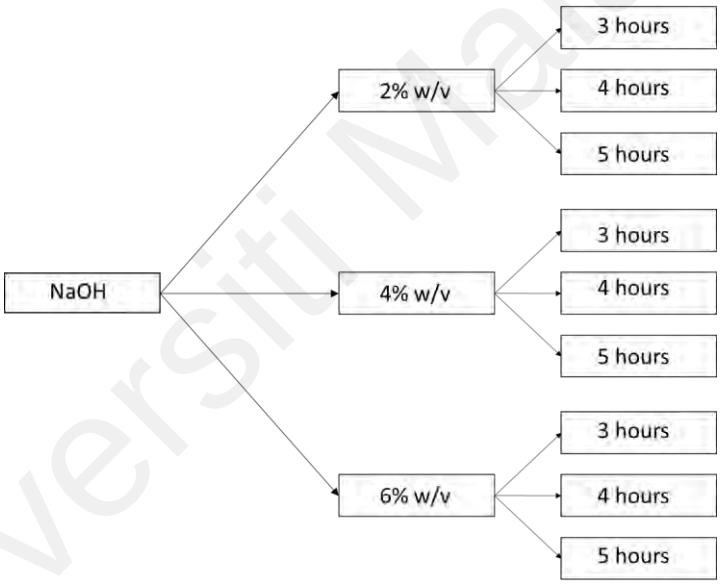

Figure 3.1: Summary of alkali treatment conditions.

3.2 Compounding and Injection Moulding

3.2.1 Preparation of kenaf/PHB composites

Two types of fibres were used to prepare two different composites: untreated and alkali-treated kenaf. The composites were first mixed using a BRABENDER KETSE 20/40 (Duisburg, Germany) twin-screw extruder with a processing temperature range

from 180°C to 190°C and screw speed at 80 RPM. The extruded composites were cut into pellets using a pelletiser (Brabender, Duisburg, Germany)

Then, the composite pellets were dried in a vacuum oven at 80°C for eight hours and fed into a BOY 55M injection moulding machine (DrBOY, Neustadt-Fernthal, Germany) and moulded both bar and dumbbell-shaped specimens according to ASTM D638 (2010). The barrel temperature zones were set at 180°C, 180°C, and 185°C from back to front. The nozzle temperature was set at 185°C. The screw speed was maintained at 50 RPM. The injection pressure was set at 45 to 55 bar and 50 s holding time.

The untreated fibre-reinforced composite was designated as UT, and the alkali-treated kenaf-reinforced composite was designated as CT. These acronyms are followed by a number referring to its fibre weight fraction (5%, 10%, or 20%).

3.2.2 Preparation of MMT/PHB nanocomposite

For each grade of montmorillonite, three different clay contents were used in the compounding process. The modification was done by dispersing the montmorillonite into the matrix using a BRABENDER KETSE 20/40 twin-screw extruder with a processing temperature range from 180°C to 190°C and screw speed at 200 RPM. Then, the extrudate was cut into pellets using a pelletiser.

The pellets were dried and fed into a BOY 55M injection moulding machine and moulded into both bar and dumbbell-shaped specimens according to ASTM D638. The barrel temperature zones were set at 180°C, 180°C and 185°C from back to the front. The nozzle temperature was set at 185°C. The screw speed was maintained at 50 RPM. The injection pressure was set at 45 to 55 bar and 50 seconds holding time. The composite pellets were compression moulded into 1 mm thickness sheets using a compression moulding machine for rheology tests. Samples mixed with untreated montmorillonite are

labelled as PGV, and samples mixed with treated montmorillonite as TCN. The acronym is followed by a number referring to its clay content, either 3, 6 or 9 parts per hundred parts of resin (phr).

The composition of specimens prepared is listed in Table 3.2.

Table 3.2: Formulation list.

Kenaf/PHB Composites	Untreated kenaf (%)	Treated kenaf (%)
PHB	-	-
UT5	5	-
UT10	10	-
UT20	20	-
CT5	-	5
CT10	-	10
CT20	-	20
MMT/PHB Composites	**Untreated MMT (phr)**	**Treated MMT (phr)**
PHB	-	-
PGV3	3	-
PGV6	6	-
PGV9	9	-
TCN3	-	3
TCN6	-	6
TCN9	-	9

3.3 Conditioning

The moulded specimens were subjected to four different conditions before mechanical testing was commenced. The conditions are dry-as-moulded, indoor, outdoor, and soil burial. For indoor, outdoor and soil burial, the specimens were left for two and four months before mechanical properties were evaluated.

3.3.1 Dry-as-moulded (DAM)

Specimens subjected to DAM condition are characterized immediately after moulding. This condition will serve as a reference for the other conditions.

3.3.2 Indoor

Specimens subjected to indoor conditions were left on the rack in the laboratory, away from direct sunlight. Any dirt or soiling was cleaned before testing.

3.3.3 Outdoor

Specimens subjected to outdoor conditions were mounted on custom racks, exposed directly to the weather, facing eastward. Any dirt or soiling was cleaned before testing.

3.3.4 Soil burial

Specimens subjected to soil burial were buried about one foot deep in garden soil, with at least 1 cm distance between each other. After the set duration, the samples were excavated and rinsed to remove lodged soil. The specimens were air-dried for 24 hours before testing.

3.4 Characterisation

3.4.1 Fibre characterisation

The composition of lignocellulosic fibres was determined according to the Acid Detergent Fibre - Neutral Detergent Fibre (ADF–NDF) method described by van Soest and Wine (1968). This analysis was done by the Malaysian Agricultural Research and Development Institute (MARDI).

Surface functional group changes were studied using a Fourier Transform-Infrared (FTIR). FTIR spectra were acquired using a Spectrum 400, Perkin Elmer FTIR (USA) spectrometer equipped with ATR. The fibres were mounted on an ATR accessory

before scanning. The spectra were obtained with an accumulation of 16 scans and with a resolution of 4 cm^{-1} and a spectral range from 4000–650 cm^{-1}.

The thermal stability of the fibre was studied using Perkin Elmer TGA 6 (USA) Thermogravimetric Analyser. For each sample, 5 to 7 mg of the fibre were placed in ceramic pans and heated from 50°C to 900°C under nitrogen atmosphere (flow rate: 20 mL/min) at a heating rate of 10°C/min.

The fibre surface morphology was examined using a Hitachi Field Emission Scanning Electron Microscopy (FESEM) model SU8220 (JP). The fibres were coated with platinum (layer thickness ~30 nm) to prevent charging on the surface.

The fibres were analysed using PANalytical Empyrean powder XRD (NL) to determine changes in crystallinity. The fibres were mounted on a circular sample holder. The XRD was performed using radiation of CuKα = 1.5458 Å at a diffraction angle (2θ) range of 10 to 50°. The crystallinity index (CrI) was calculated using the Highscore Plus software based on the method described by Segal et al. using the following equation (Segal et al., 1959):

$$(CrI) = \left(\frac{I_{002} - I_{am}}{I_{002}}\right) \times 100 \quad (3.1)$$

where I_{002} is the maximum intensity of the (002) lattice diffraction peak and I_{am} is the intensity scattered by the amorphous part of the sample. The diffraction peak for plane (002) is located at a diffraction angle of $2\theta = 27°$. The intensity scattered by the amorphous part was measured at a diffraction angle of around $2\theta = 11.0°$.

Single fibre tensile tests for the fibres were conducted according to ASTM C1557. For the analysis, 80 to 120 individual filaments of kenaf were randomly selected, measured and mounted onto a mounting tab made of manila paper. The setup is illustrated in Figure 3.2. Before starting the test, the mid-section of the mounting tab is cut.

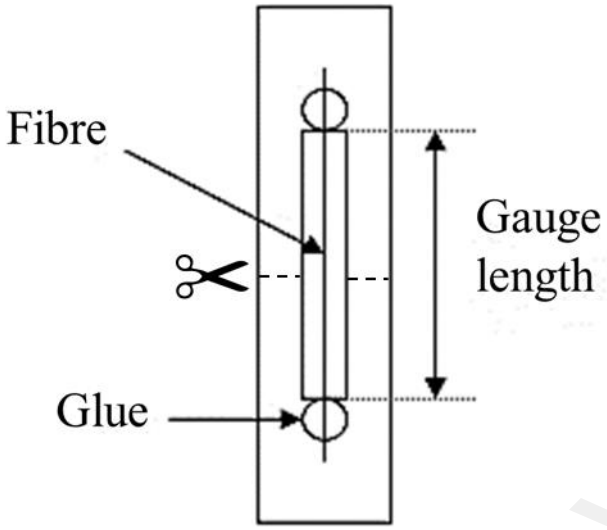

Figure 3.2: Mounting tab for single fibre tensile test.

Instron Universal Testing Machine model 3345 (USA) was used during testing. The test was carried out at a 1 mm/min cross-head speed with a 0.1 kN load cell. The fibre diameter was measured using a Leco IA-32 image analyser. Ten readings were taken per specimen, and the average values were used in the calculation done by the software. Data from the single fibre tests were analysed using a modified two-parameter Weibull distribution function. The probability of failure $P_F(\sigma)$ for a single fibre at stress, σ and length, L can be written as

$$P_F(\sigma, L) = 1 - exp\left(-\frac{L}{L_0}\left(\frac{\sigma}{\sigma_0}\right)^m\right) \tag{3.2}$$

where m is the Weibull modulus, σ_o is the characteristic strength, and L_o is the gauge length. The Weibull modulus is the measurement of the scatters in the data. The equation above was rearranged for testing at a fixed gauge length ($L=L_o$).

$$ln\left[ln\left(\frac{1}{1-P_F\,(\sigma)}\right)\right] = m.ln\sigma - m.ln\sigma_0 \quad (3.3)$$

The tensile strength values of the fibres were arranged in ascending order, and the probability of failure was assigned using an estimator given by

$$P_F(\sigma_i) = \frac{i - 0.5}{N} \quad (3.4)$$

where $P_F(\sigma_i)$ is the probability of failure corresponding to the *i*th strength value, and N is the total number of fibres tested.

3.4.2 Composite characterisation

3.4.2.1 Thermal analysis

The thermal stability of the composites was studied using a Perkin Elmer TGA 6 (Waltham, USA) thermogravimetric analyser. For each sample, 5 to 7 mg of the fibre was placed in ceramic pans and heated from 50°C to 900°C under a nitrogen atmosphere (flow rate: 20 mL/min) at a heating rate of 10°C/min.

A Perkin Elmer DSC6 (Waltham, USA) was used to study the phase transitions in the composites. Approximately 5 mg of the specimen was used for the analysis. A typical DSC run would consist of three steps. The first step involved heating from 50°C to 200°C. Then, the sample was cooled to 50°C and held for at least 1 min. The final step involved heating from 50°C to 200°C. These steps were performed under controlled conditions, with a heating and cooling rate of 10°C/min and under nitrogen atmosphere (flow rate: 20 mL/min). The first step was taken as a precaution to remove the thermal history of the materials. The melting temperature (T_m) and melting enthalpy (ΔH_m) were determined from the second heating run.

3.4.2.2 Rheology

The rheological behaviour of the composites under oscillatory shear flow was investigated using an Anton Paar MCR 301 rheometer (Anton Paar, Graz, Austria) with a CTD450 attachment. A parallel plate with a 25-mm diameter and 1-mm gap was used. A dynamic frequency sweep was conducted with 1% strain amplitude and an angular frequency ranging from 0.5 to 500 rad/s at 180°C.

3.4.2.3 Mechanical properties

Tensile tests were performed using an Instron 5569 Universal Testing Machine (Canton, NJ, USA) equipped with a 50 kN load cell and a mechanical extensometer (Instron, Canton, NJ, USA) with a cross-head speed of 10 mm/min^{-1}. The specimen dimension and shape were made following ASTM D638. The tests were performed at room temperature, and the extensometer jaw grip was set at 50 mm. A minimum of seven specimens per batch was tested to obtain the best reproducible results. For each batch of the specimen, the average values of Young's modulus (E), tensile strength (σ_{max}), and tensile strain (ε) were calculated by the Bluehill software (Instron, version 2.24, Canton, NJ, USA) from the stress over strain curve obtained. The E was calculated at 0.5% strain. A simplified diagram for the tensile testing setup is provided in Figure 3.3.

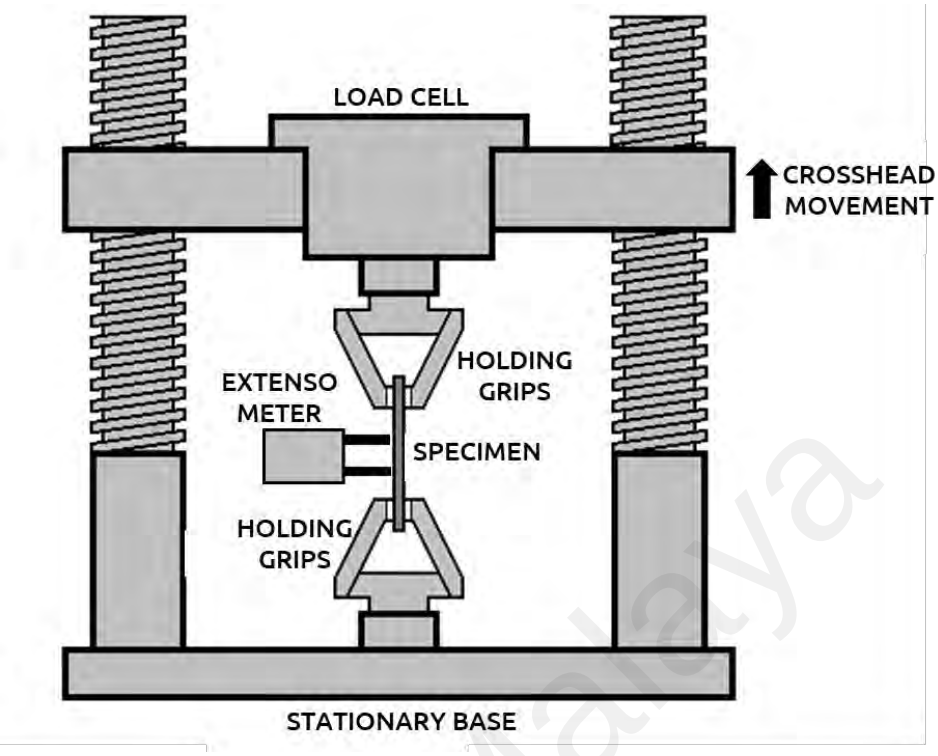

Figure 3.3: Tensile test setup.

Flexural tests were performed using an Instron 5569 universal testing machine (Canton, NJ, USA). The distance between the supports spans (L) was 50 mm, and the cross-head speed was 1.31 mm/min. The speed of the cross-head motion (R) was calculated by using

$$R = \frac{ZL^2}{6d} \tag{3.5}$$

where L and d are the specimen's support span (mm) and depth (mm), respectively, and Z, is the straining rate equal to 0.01. The test was conducted at room temperature. The specimen shape and dimension were prepared as per ASTM D790. Five specimens per batch were tested, and the averages were recorded. The flexural modulus and strength were calculated using the Bluehill® software (Instron, version 2.24, Canton, NJ, USA)

from the obtained flexural curve. A simplified diagram for the flexural testing setup is provided in Figure 3.4

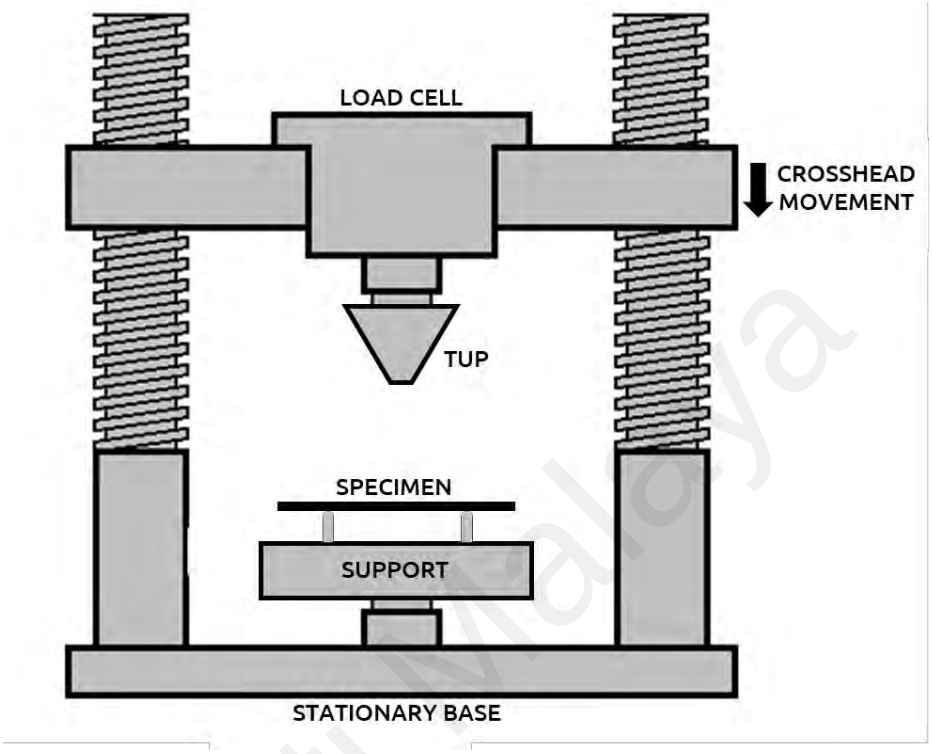

Figure 3.4: Flexural test setup.

The bar-shaped test specimens were notched using a Ray Ran notch cutter and tested using an Instron Dynatup 9210 Drop Tower Impact Tester with a V-shaped tup. The impactor weight was 6.45 kg, and the impactor velocity was set at 0.85 ms^{-1}. The notch depth to specimen depth ratio is set at 0.2. Only one notch depth is selected to reduce the amount of sample required (Hassan et al., 2011). The specimen dimension used is as stated in ASTM E23. At least ten specimens were tested for each sample. A simplified diagram for the impact test setup is provided in Figure 3.5.

For this study, a drop weight impact test was used. The test uses the free fall of known weight to supply the energy to break a beam shaped specimen. The kinetic energy

of the falling weight is adjusted by simply varying its drop height. Energy absorbed by the specimen is calculated as

$$U_t = \frac{W}{2g}(u_1^2 - u_2^2) \tag{3.6}$$

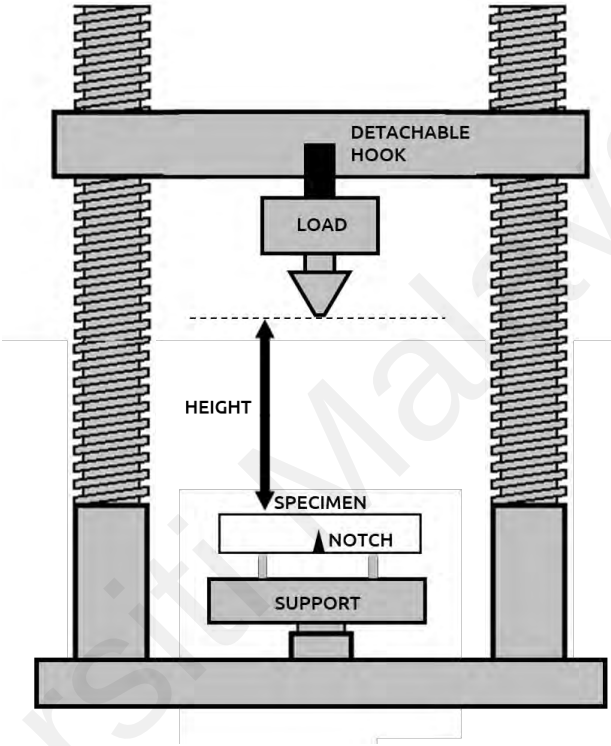

Figure 3.5: Impact test setup.

where W is the weight of the striking head, g is the acceleration due to gravity (9.8 ms^{-1}), u_1 is the velocity of the striking head just before impact ($= \sqrt{2gH}$), u_2 is the measured velocity of the striking head just after impact, and H is the drop height.

3.4.2.4 Field Emission Scanning Electron Microscope (FESEM)

The fractured surface of the composite specimens was examined using a Hitachi Field Emission Scanning Electron Microscopy model SU8220 (JP) to study the effect of

MMT on the fracture mechanics of the materials. EDX was used to map the dispersion of Al and Si in the composite to study MMT dispersion.

3.4.2.5 Transmission Electron Microscope (TEM)

The microstructure of the composite was also studied using a FEI Tecnai G2 transmission electron microscope. A thin layer of the samples was prepared using a microtome, and images were obtained at 200 kV. The interlaminar distance of the nanoclay was measured using the TEM images.

CHAPTER 4: RESULTS AND DISCUSSION

4.1 Fibre pretreatment

4.1.1 Fibre chemical composition

Major components in kenaf fibres are cellulose, hemicellulose and lignin. The effect of alkali treatment on the chemical composition of kenaf fibres was studied and the data obtained are listed in Table 4.1.

Table 4.1 Chemical composition of alkali-treated and untreated kenaf fibres.

	Cellulose (%)	Hemicellulose (%)	Lignin (%)
Untreated	58.1	16.1	14.1
2% 3 hr	67.6	9.0	10.1
2% 4 hr	65.4	9.5	10.7
2% 5 hr	67.6	13.1	7.8
4% 3 hr	67.6	11.8	8.8
4% 4 hr	72.8	12.7	7.9
4% 5 hr	69.0	9.1	8.7
6% 3 hr	69.0	9.7	9.4
6% 4 hr	68.7	10.4	9.1
6% 5 hr	74.1	12.2	6.3

In general, all treated fibres have lower lignin composition when compared to the untreated fibres. For example, fibres treated with 4% NaOH for 4 hours contain 7.9% lignin, while untreated fibres contain 14.1% lignin. Hemicellulose content was also reduced, from 16.1% in untreated fibres to 12.7% in fibres treated with 4% NaOH for 4 hours. Various studies have reported that alkaline treatment of natural fibres results in fibres with lower lignin content, cleaner surface due to removal of wax and oils, and increased crystallinity (Cai et al., 2015; Fiore et al., 2015; Kabir et al., 2012). Alkali sensitive hydroxyl groups in the molecules were broken down, reacted with water molecules, and removed from the fibre. A generalised reaction mechanism scheme for

this interaction has been suggested by Ferreira et al. (2019), and the schematic diagram of treated and untreated fibre (Mwaikambo & Ansell, 2002) are illustrated in Figure 4.1. The hydrophilicity of the fibres was reduced and produced a cleaner and rougher surface for adhesion with the polymer.

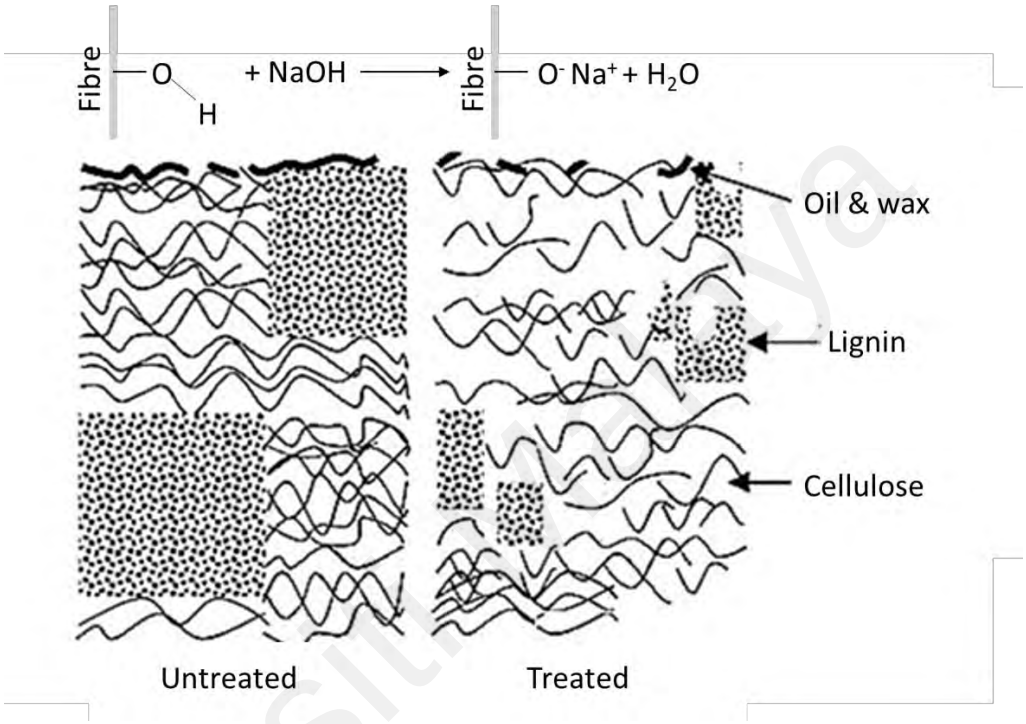

Figure 4.1: Generalised mechanism and schematic diagram for alkali treatment of cellulosic fibres.

It was also expected that increasing the soak time and solution concentration would lower lignin content and a higher cellulose percentage. The lower lignin content is due to a more potent reagent used or longer duration for the reagent to act. However, from the observation, this was not always the case. For example, fibres treated with 4% NaOH for 5 hours have higher lignin content than those treated with the same reagent for 4 hours. It is because natural fibres are not uniform in composition. Hemicellulose content was also expected to be reduced by the treatment. Meanwhile, it can also be observed that a

2% NaOH solution requires a longer soak time to be effective. The surface images of the treated and untreated fibres were captured using FESEM.

The surface of the untreated fibres is shown in Figure 4.2 (a). The surface is covered with impurities such as wax and debris. On the other hand, Figure 4.2 (d) shows the surface of kenaf fibre after being treated with 4% NaOH solution for 4 hours. The image provides visual evidence that the treatment was effective in removing impurities. The result from the chemical composition analysis also confirms that the percentage of hemicellulose and lignin was reduced after treatment. The lignin layer on the fibre's surface has been removed, and the surface is rougher, as supported by the results from the chemical composition analysis. A cleaner and rougher surface, in theory, should improve adhesion between the fibres and the matrix (Herrera-Franco & Valadez-González, 2005).

Figure 4.2 (b) and (c) are the surface images of fibres treated with 2% NaOH for 3 hours and 4% NaOH for 3 hours, respectively. From the image, it was observed that the surface of the fibres was partially cleaned for both treatment parameters. It is predicted that such fibres would produce weaker composites than the optimally treated fibres. However, chemical composition and surface analysis alone is insufficient to decide optimal treatment parameters. For example, fibres treated with higher concentrations of NaOH or longer times can all display similar surface profiles, yet, they exhibit subpar mechanical properties. It has been reported that prolonged exposure to NaOH can damage the fibres, reducing their mechanical properties (Krishnaiah et al., 2017). Sub-optimal NaOH concentration or soak time could lead to excessive delignification, introducing stress concentrator into the fibre structure.

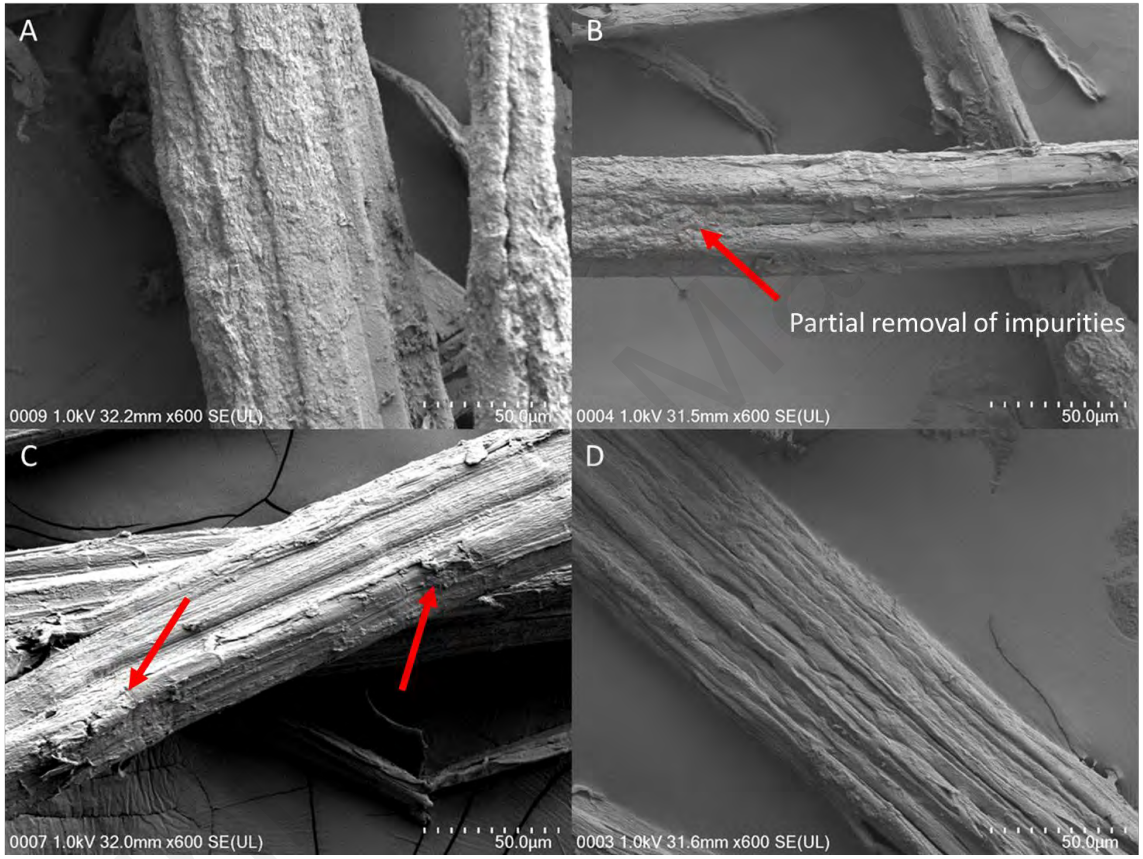

Figure 4.2: FESEM image of a) untreated fibre surface b) 2% NaOH for 3 hours, c) fibres treated with 4% NaOH for 3 hours, and d) fibre treated with 4% NaOH for 4 hours

4.1.2 FTIR

The fibres were analysed using FTIR, and the IR spectra were compared to study the effect of surface treatment on the fibres. The IR spectra for the fibres treated with 4% NaOH are shown in Figure 4.3.

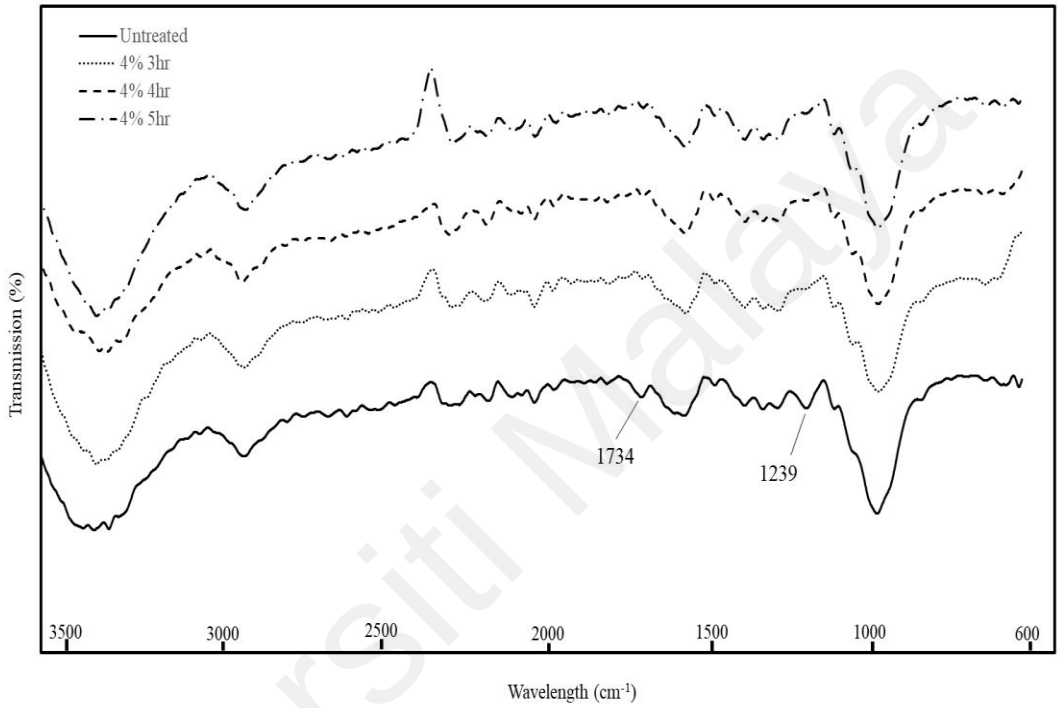

Figure 4.3: FTIR spectra of treated and untreated fibres.

All spectra had broad bands at 3400 cm^{-1} corresponding to free OH groups on cellulose molecules. Also, all spectra exhibited peaks related to the C-H stretching absorption between 2800 - 2900 cm^{-1}. The peaks at 1734 cm^{-1} are associated with C=O stretching of the acetyl group in hemicelluloses (El-Shekeil et al., 2012). It can also be attributed to the p-coumaric acids of lignin or hemicelluloses. The peak at 1239 cm^{-1} is attributed to the C-O stretch of the acetyl group of lignin (Sgriccia et al., 2008). These peaks are absent in the spectra of the treated fibres. The disappearance of these peaks indicates that most of the surface lignin and hemicelluloses were removed during the

treatment (Asim et al., 2016). Increasing the soak time also reduced the intensity of these peaks. The reduction indicate that more hemicellulose and lignin were removed from the fibre as the alkali soak time was increased.

4.1.3 TGA

TGA curves of untreated and treated kenaf fibres are provided in Figure 4.4.

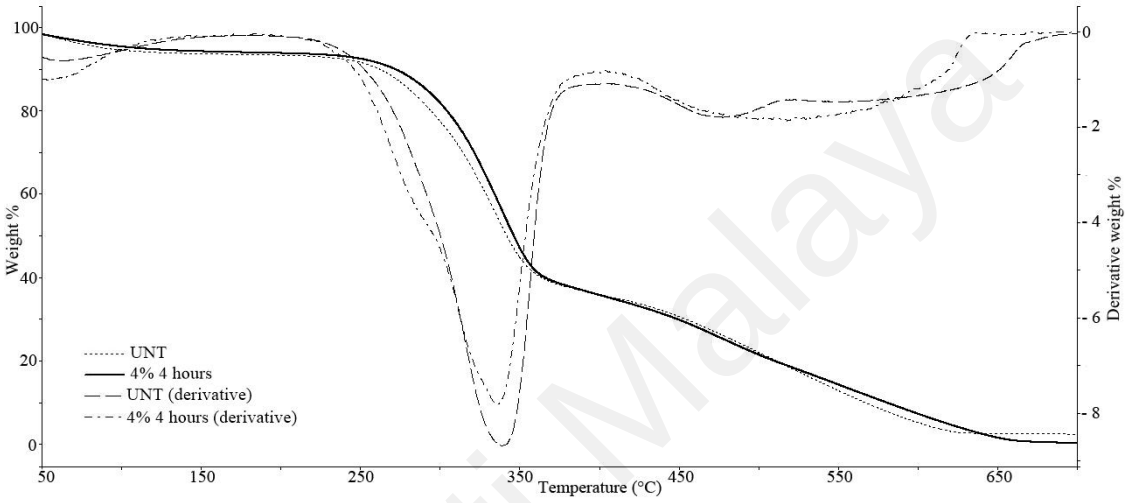

Figure 4.4: TGA curve for treated and untreated fibres.

The curves show that the degradation of natural fibres consists of multiple steps. The first mass loss occurs between 50 - 130°C and can be attributed to the removal of moisture from the sample. The second transition occurred between 250 - 350°C and resulted in a 50% weight loss. It can be attributed to the degradation of hemicellulose and cellulose (Ouajai & Shanks, 2005; Pang et al., 2015; H. Yang et al., 2007). Cellulose degradation begins with dehydration reactions, followed by chain scission with the elimination of condensation products and the production of carbon residue. The abrupt weight loss observed indicates that cellulose decomposed quickly, and products were released intensively within a short period. Arseneau (1971) has proposed that cellulose polymer tend to be carbonised at this relatively lower temperature through the

dehydration and cross-linking reaction. The dehydration of cellulose begins at temperatures as low as 210°C, resulting in the formation of anhydrocellulose. This compound is quite reactive and undergoes further reactions that produce CO, $C0_2$, H_20, and most residual char.

The next transition occurs in a broad region between 350 - 630°C, which can be attributed to the continued decomposition of lignin and tar or char from the decomposition of the main components (Yao et al., 2008). Lignin contains many aromatic rings with various branches, and the activity of the functional groups cover a wide range, which is why the degradation of lignin covers a wide range of temperatures (Yang et al., 2007). Depolymerisation of residual cellulose yielding the levoglucosan (LG) tar becomes significant at about 270°C and builds up rapidly. The amount of char produced at the end of the reaction will vary depending on factors such as heating rate (Shen & Gu, 2009). Overall, the thermal decomposition pathway for cellulose is very complex and speculative chemical pathways were proposed by Shen & Gu in Figure 4.5.

The 50% degradation temperature ($T_{50\%}$), onset temperature (T_{onset}) and peak derivative temperature (DT_P) for the fibres are listed in Table 4.2. From the table, alkali-treated fibres are more heat resistant than the untreated fibres as all treated fibres have higher values compared to the untreated fibres. The most obvious improvement is in the T_{onset}. T_{onset} is determined by extrapolating the starting temperature by determining the intersection of the starting-mass baseline and the tangent to the TGA curve at the maximum gradient as stated in ISO 11358-1. In this work, T_{onset} was determined for the second transition occurring between 250°C to 350°C. Therefore, T_{onset} can indicate the thermal stability of the fibres where a higher T_{onset} means better thermal stability, as the fibres can withstand higher temperature before degradation occurs.

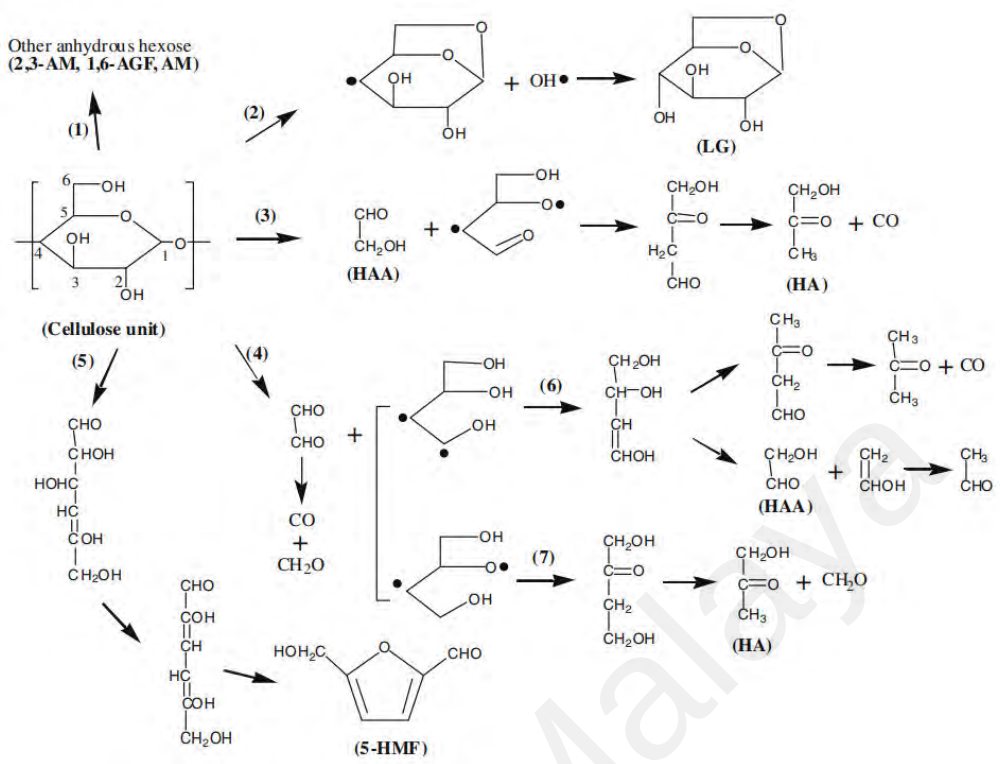

Figure 4.5: Speculative chemical pathways for direct conversion of cellulose molecules.

Table 4.2: Onset temperature, $T_{50\%}$ and DT_p of treated and untreated fibres.

Sample	T_{onset} (°C)	$T_{50\%}$ (°C)	DT_p (°C)
Untreated	259	341	337
2% 3 hr	283	345	339
2% 4 hr	284	343	336
2% 5 hr	277	343	336
4% 3 hr	284	346	340
4% 4 hr	287	346	341
4% 5 hr	291	349	345
6% 3 hr	292	352	352
6% 4 hr	294	350	348
6% 5 hr	293	350	350

Fibres with a higher onset temperature are preferable because it has higher heat resistance. These fibres will resist degradation during processing which involves

temperatures up to 200°C. Fibres treated with 6% NaOH solution for 4 hours has the highest T_{onset} at 294°C. The improvement in heat resistance can be attributed to the removal of hemicellulose and lignin and increased crystallinity as a result of the chemical treatment. Sgriccia et al. (2008) have reported that alkaline and bleaching treatments would increase the degree of crystallinity of natural fibres. The crystallinity of the fibres was increased simply due to the removal of the amorphous hemicellulose and lignin during the treatment process (Suryanto et al., 2014). Suryanto et al. suggested that due to amorphous hemicellulose having a lower molecular weight than cellulose, they are more susceptible to attacks by the NaOH solution and therefore easily removed during treatment. It was also observed that the thermal stability of the fibres improved with the increase of NaOH concentration. This improvement is because the solution with a higher NaOH concentration can remove more hemicellulose and lignin during the soaking process. Hemicellulose and lignin have lower thermal resistance than cellulose (Hossain et al., 2013; Shahinur et al., 2020). Thermal decomposition of hemicellulose and lignin occurs at a temperature range of 25°C - 290°C and 150°C - 420°C, respectively. A similar trend was observed for $T_{50\%}$ and DT_p.

4.1.4 XRD

X-ray diffractograms of the untreated and treated kenaf fibres are provided in Figure 4.6. The diffractograms were typical of semi-crystalline materials, displaying a broad amorphous hump and crystalline peaks. Cellulose 1 is the principal constituent of natural fibres, and its structure proposed by Arthur (1989) is illustrated in Figure 4.7.

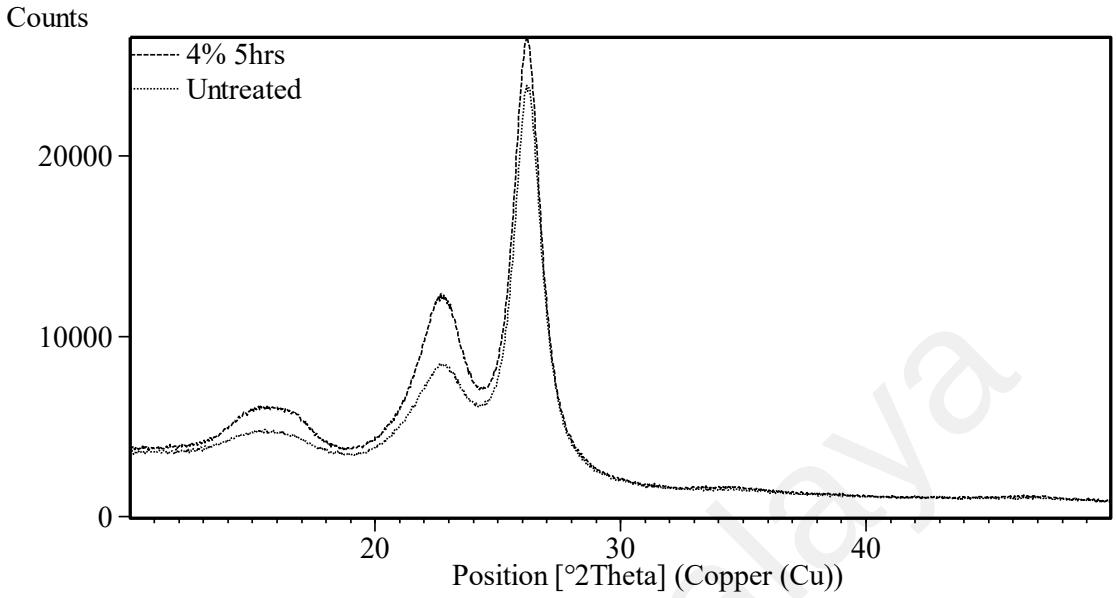

Figure 4.6: XRD diffractograms of untreated and treated kenaf fibres.

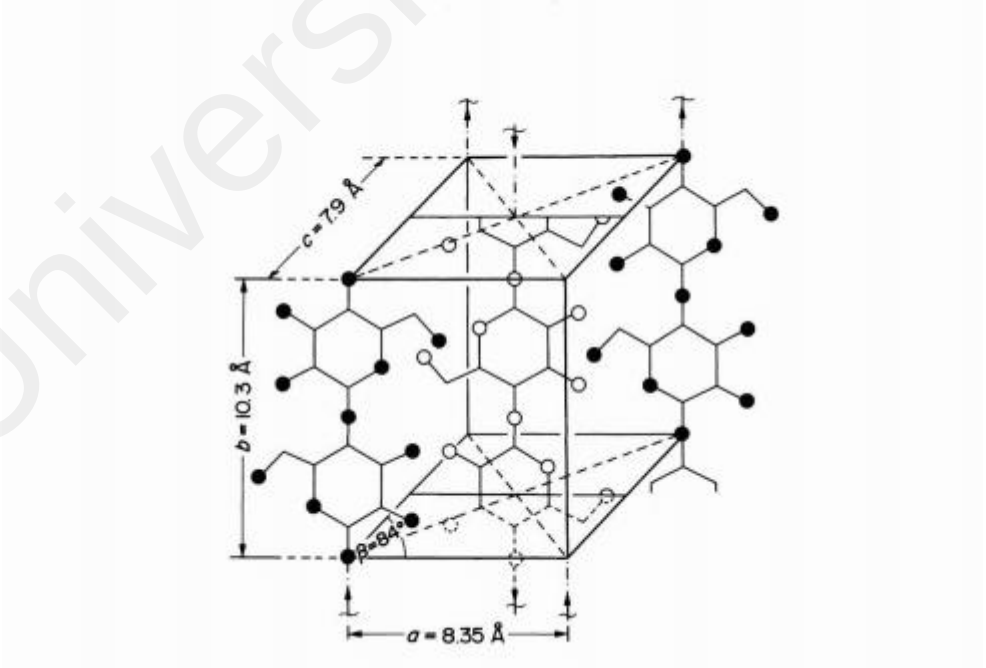

Figure 4.7: Crystalline unit cell of natural cellulose 1.

Three peaks typical to cellulose I were present at around 2θ = 16°, 23°, and 27° (Kargarzadeh et al., 2012; C. Wang et al., 2016). It was also observed that the intensity of the peaks was increased after the alkaline treatment producing sharper peaks. This observation indicates that the treatment effectively removed non-cellulosic amorphous components such as hemicellulose and lignin on the fibre's surface.

The CrI of the samples was calculated using the Highscore Plus software and is illustrated in Figure 4.8. It should be noted that the crystallinity value reported is not the actual crystallinity of the sample, but it is still helpful for comparison. Park et al. (2010) discussed that the method developed by Segal et al. (1959) helps compare relative differences between samples but should not be used to estimate the amount of crystalline and amorphous material in a cellulose sample. The researchers suggested that the Segal method underestimates the I_{am} value, resulting in overestimating the CrI. In addition, only the tallest peak was used in the calculation, putting too much emphasis on the contribution from one alignment of the crystal lattice.

Lastly, peaks in the cellulose diffraction spectrum are broad and vary considerably in their width, which could be affected by crystallite size (Garvey et al., 2005). A simple height comparison cannot be expected to provide a reasonable estimate of cellulose crystallinity. Nevertheless, the Segal method is quick and straightforward and is sufficient for this work.

The XRD diffractogram of untreated kenaf fibre and kenaf fibre treated with 4% NaOH for 5 hours illustrated in Figure 4.6 showed that all three major peaks attributed to cellulose 1 are still present, indicating that no alteration of the crystal structure has happened due to the low concentration and temperature used. It was found that treated kenaf has higher crystallinity when compared to untreated kenaf. For example, the

crystallinity for untreated kenaf and kenaf treated with 4% NaOH for 4 hours is 49.9% and 53.0%, respectively.

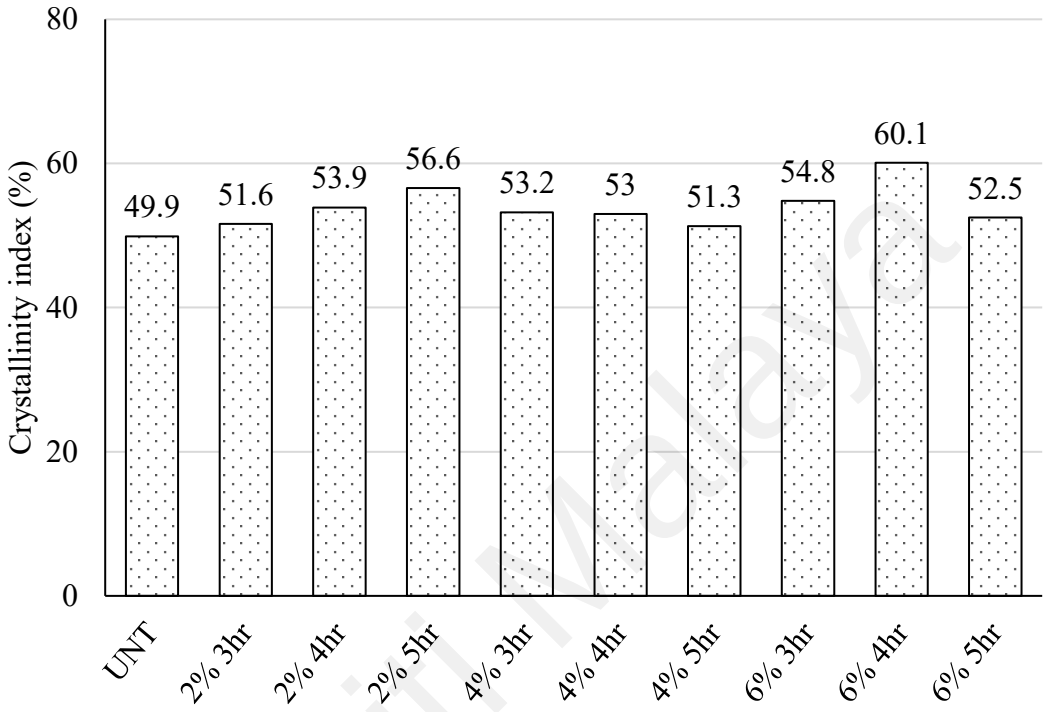

Figure 4.8: Relative crystallinity of treated and untreated fibres.

As illustrated in Figure 4.8, the crystallinity of the samples slightly increased with the increase in soak time. However, no clear trend was observed when the NaOH concentration was increased. Sri Aprilia et al. (2016) reported that the crystallinity of fibres extracted from kenaf slightly increased when the soaking time was increased from 1 to 2 hours. However, increasing the treatment time to 3 hours caused the crystallinity to decrease, possibly due to damages done to the crystalline region during the treatment.

4.1.5 Fibre diameter

The diameter of the fibres was measured using a Leco image analyser. A minimum of 80 fibres were measured. Each fibre was measured at ten different points, and the average was recorded. The values were then tabulated and presented in histogram form, as shown in Figure 4.9.

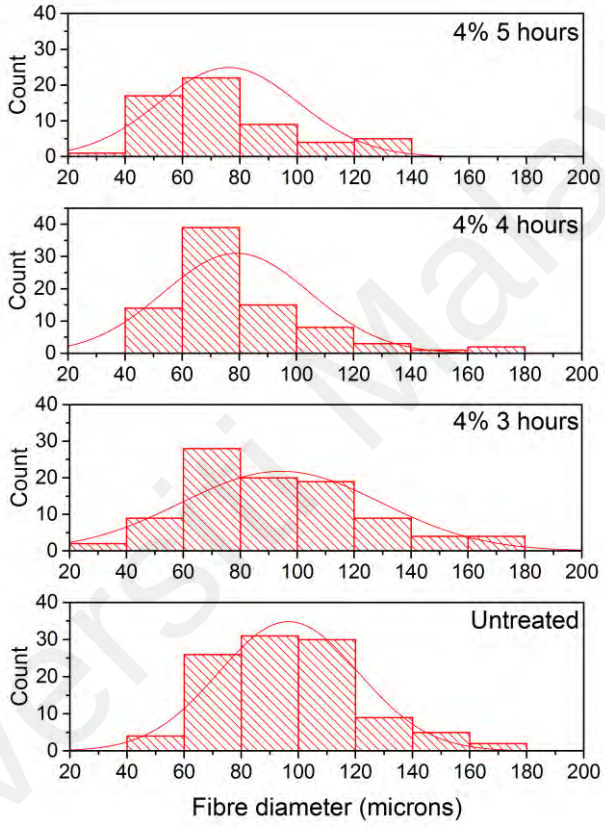

Figure 4.9: Histogram of kenaf fibre diameter.

From the histogram, it can be observed that the diameter has a normal bell-shaped distribution. For untreated fibres, the highest population is observed in 90 to 110 µm. However, for treated fibres, most of the population is observed in the range of 70 – 90 µm, indicating a reduction in diameter. The mean diameter of the fibre decreases after

alkali treatment. The number-average (D_n) and weight-average (D_w) of the fibre diameter were calculated and presented in Table 4.3.

Table 4.3: D_n and D_w for untreated and treated kenaf.

Sample	D_n (µm)	D_w (µm)
Untreated	110	110
4% 3 hr	100	110
4% 4 hr	90	100
4% 5 hr	80	90

The mean diameter was reduced from 110 µm for untreated fibres to 80 µm for fibres treated with 4% NaOH for 5 hours. The alkali treatment breaks the hydrogen bonds between the hydroxyl groups of the cellulose, hemicellulose, and lignin, leading to the breakdown of fibre bundles into smaller fibres (Roy et al., 2012). This observation is consistent with the results obtained from the chemical composition analysis, where the content of hemicellulose and lignin in the kenaf fibres were reduced post-treatment. The reduction in fibre diameter is favourable because it will increase the effective surface area (Krishnaiah et al., 2017). Theoretically, fibres with smaller diameters will have lower critical fibre length, the minimum length at which the fibres would effectively reinforce the matrix (Thomason et al., 1996).

4.1.6 Single fibre tensile test

The tensile properties of the fibre will be one of the more important factors when deciding the optimal treatment. The treatment must be effective enough that the surface of the fibres will be cleaned but not to the point of damaging the fibres. Theoretically, damaged fibres would have lower mechanical properties compared to undamaged fibres. A stress-strain curve was obtained from the single fibre test, and the tensile properties of the fibres were extracted from it. The stress-strain curves for different natural and

synthetic fibres were reported by Vistal & Retulainen (2014) and are illustrated in Figure 4.10.

A stress-strain curve for a material describes the relationship between stress and strain. During tensile testing, tension was applied gradually onto the sample until failure. The elongation of the gauge section was recorded against the applied force. Elongation measurement was used to calculate the tensile strain, ε, using the following equation:

$$\varepsilon = \frac{\Delta L}{L_0} = \frac{L - L_0}{L_0} \quad (4.1)$$

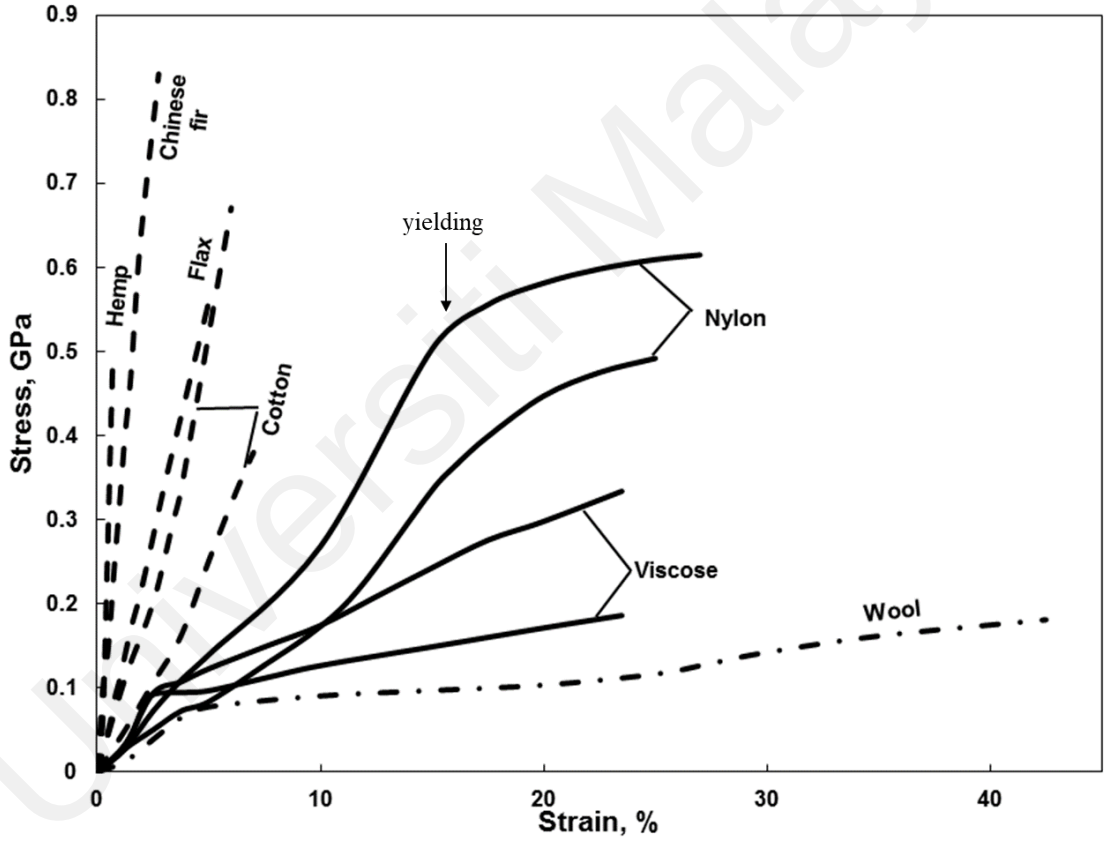

Figure 4.10: The stress-strain curves of different natural and synthetic fibres (Vishtal & Retulainen, 2014).

where ΔL is the gauge length change, L_0 is the initial gauge length, and L is the final length. On the other hand, stress, σ, is calculated using the following equation:

$$\sigma = \frac{F}{A} \tag{4.2}$$

where F is the tensile force, and A is the nominal cross-section of the specimen. The machine constantly calculates these values during the experiment and plots the stress-strain curves, as seen in Figure 4.10.

Young's modulus is measured by determining the slope of the stress-strain curve in the linear region, typically at very low strain values. Materials with steeper stress-strain curves would exhibit greater Young's modulus values. The tensile strength is determined by the greatest load on the stress-strain curve. The ductility of the fibres can also be determined by studying the stress-strain curves. Ductile fibres such as Nylon, viscose and wool exhibit yielding and strain hardening due to plastic deformation. On the other hand, brittle fibres such as kenaf, hemp and flex do not exhibit any yielding. The stress-strain curve ends at the highest load because the fibre breaks immediately. The Young's modulus and tensile strength of the kenaf fibres measured in this work are illustrated in Figure 4.11.

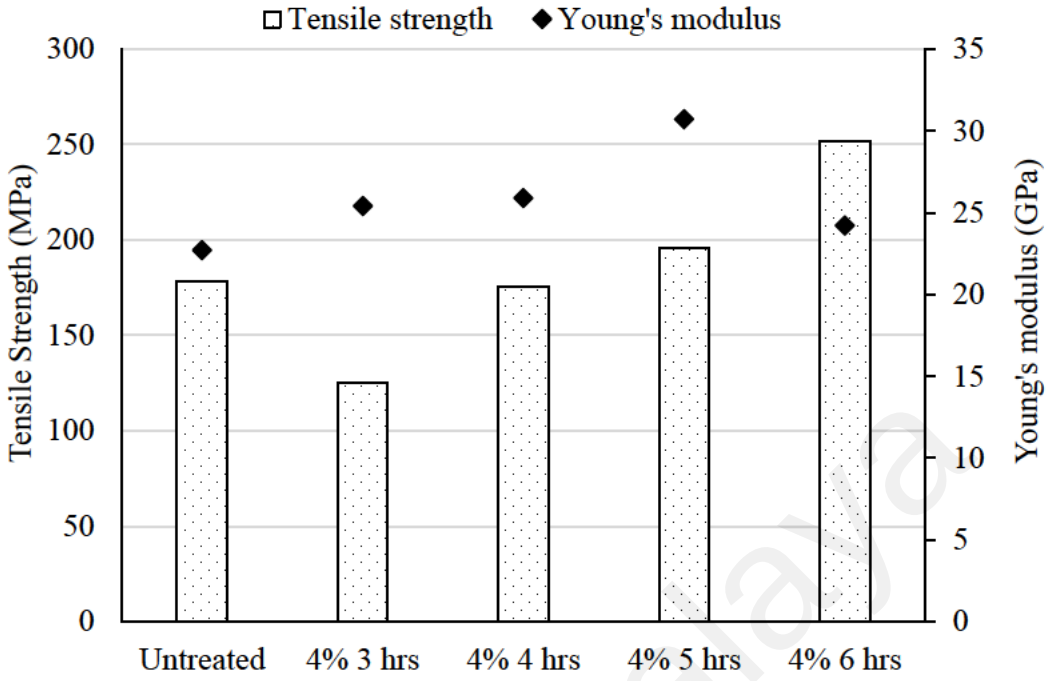

Figure 4.11: Tensile properties of untreated and treated kenaf fibres.

In general, the treated fibres have a higher modulus than untreated fibres, which indicates that treated fibres are stiffer when compared to untreated fibres. Kargarzadeh et al. (2012) reported that NaOH treatment would increase cellulose crystallinity through modification of the cellulose. In addition, amorphous lignin was removed from the fibre, thus increasing the overall fibre crystallinity. As the fibres become increasingly crystalline, their stiffness also increases. On the other hand, it was found that the modulus increase is unaffected by the condition of the fibre's surface. Even though the fibres treated with 4% NaOH for 3 hours are not thoroughly cleaned, the modulus value recorded is still higher (25.4 GPa) when compared to the untreated fibres (22.7 GPa). Increasing soak time to 6 hours caused the modulus to decrease to 24.2 GPa.

For tensile strength, the treated kenaf fibre exhibited lower tensile strength when compared to the untreated fibre. However, a comparison among the treated fibre found that the tensile strength increases as the soaking time increases. Some researchers

suggested that the tensile strength increases after NaOH treatment due to the increased uniformity of the fibre after the impurities were removed (Asim et al., 2016). The initial reduction can be due to the ineffectiveness of the treatment, leaving the fibre in an irregular structure due to impurities still present on the surface of the fibres, as observed in Figure 4.2. These irregularities can form stress concentration areas on the fibres, leading to premature failure, resulting in the treated fibre having lower tensile strength than untreated fibres. When the kenaf fibres are soaked for a longer duration, the fibres become more uniform, improving their strength in the process. In order to get the best possible fibres in terms of tensile strength, the lignin and hemicellulose must be entirely removed, leaving only cellulose. Unfortunately, the method employed in this study was unable to achieve complete removal of hemicellulose and lignin.

In order to better understand the data obtained from single fibre testing, Weibull analysis was performed. The Weibull plots for the treated and untreated fibres were plotted in Figure 4.12. At higher stress, the plot exhibits a linear shape. However, deviations from the line were observed at lower stresses, especially for fibres treated for more than 3 hours. The deviation is because weaker fibres tended to fail prematurely and were not tested during the preparation of the samples, although the selection was made at random. This premature failure results in a bias in the lower stress region and must be considered later when selecting the optimal treatment.

In order to study the Weibull parameters, the plot was linearly fitted and analysed. The corresponding Weibull parameters, m and σ_o, are tabulated in Table 4. The Weibull modulus, m, describes the variability in measured material strength of brittle materials. A higher m value would indicate that the measurement slightly varies from sample to

sample. The slight variation can be due to the samples having evenly distributed flaws throughout the sample instead of flaws clustered inconsistently.

From Table 4.4, it can be observed that the m value increases as the treatment time increases, from 1.87 to 2.79 for samples treated for 3 and 4 hours, respectively. However, soak time of 5 hours caused the m value to decrease. This observation may indicate that the alkaline solution has started to erode the cellulose fibrils with prolonged soaking time, introducing new flaws into the system, reducing the Weibull modulus. In order to support this explanation, Weibull analysis of kenaf fibres treated at 4% NaOH concentration for six hours was done. m for fibres treated for 6 hours at 4% concentration was further reduced to 1.67. The majority of the fibres had prematurely failed even before the tensile load was applied.

Table 4.4: Weibull parameters of tested fibres.

Sample	m	σ_0 (MPa)	R^2
Untreated	1.58	210.2	0.91
4% 3hr	1.87	138.2	0.97
4% 4hr	2.79	195.7	0.96
4% 5hr	2.64	219.0	0.92
4% 6hr	1.67	301.7	0.97

The characteristic strength, σ , also exhibited a similar trend as observed earlier. The strength of the fibre increases with increasing soak time. σ increases from 138.2 MPa to 219.0 MPa when the soak time increases from three to five hours. Although fibres treated for six hours exhibited the highest σ , it must be brought to attention that this value could be inaccurate because most of the lower strength fibres have prematurely broken, and its tensile properties were not measured.

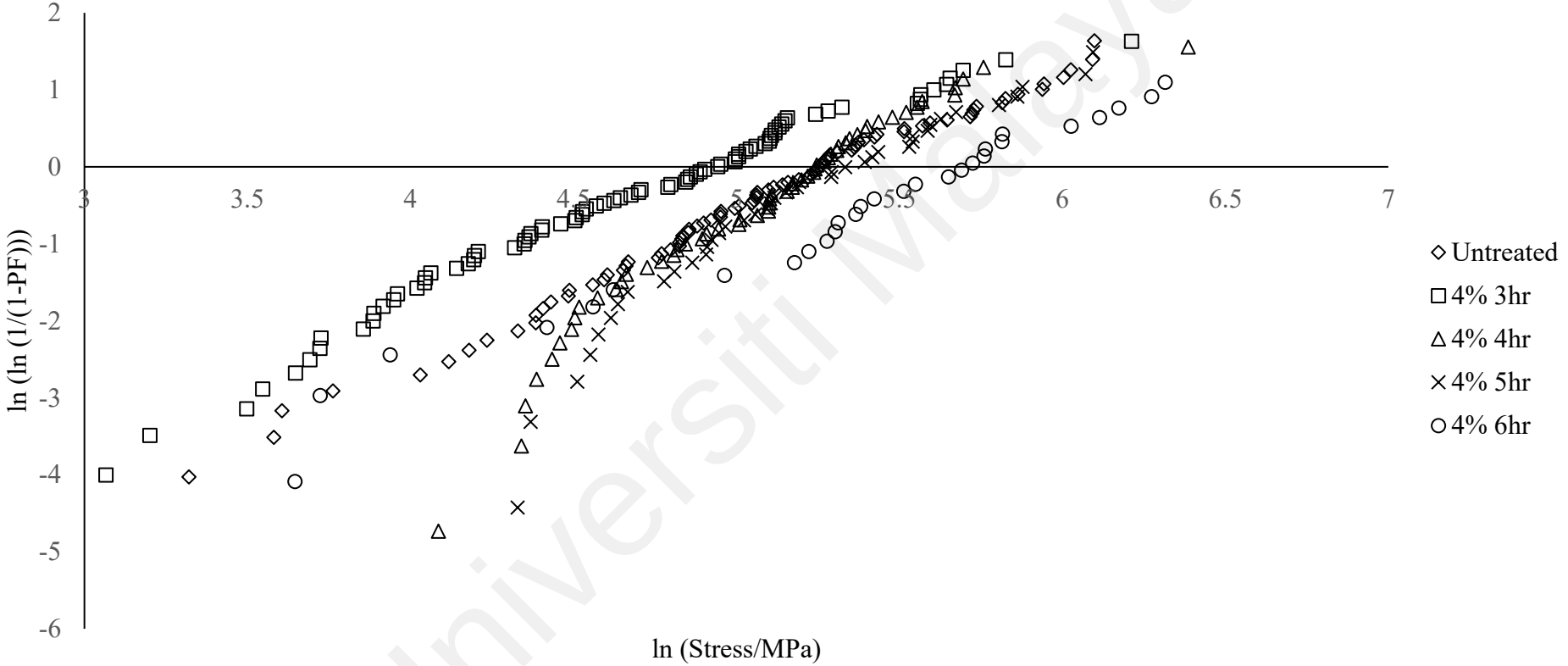

Figure 4.12: Weibull plot for untreated and treated kenaf fibres.

4.2 Kenaf fibre composite properties

Kenaf reinforced PHB composites were prepared using alkali-treated and untreated kenaf fibres. The alkali treatment parameter selected was immersion in 4% NaOH for four hours. The properties of the specimens were characterised immediately for specimens subjected to dry as moulded condition.

4.2.1 Thermal properties

The thermal properties of the composite were studied using DSC and TGA. TGA would yield information critical in understanding the thermal resistance of the material. On the other hand, DSC provides an understanding of the composite's crystallinity and melting behaviour.

4.2.1.1 TGA

The thermal degradation behaviour of the composites and the influence of fibre surface treatment was studied using TGA. The TGA curve of PHB and the treated kenaf composites are provided in Figure 4.14.

The PHB exhibited a single step degradation between 240°C and 320°C. The sharp incline suggested that the degradation rapidly occurred. In contrast, the composite displayed two-step degradation. The first step was similar to pure PHB, containing a sharp incline, occurring between 230°C and 320°C, and it was attributed to the degradation of the matrix. The second step occurred over a wider range, between 320°C and 600°C. The second transition was more prominent in the samples with a higher fibre content and was attributed to the degradation of kenaf fibres. The onset temperature (T_{onset}), $T_{50\%}$, and derivative peak temperature (DT_p) were calculated from the curve and tabulated in Table 4.5.

Table 4.5*:* Onset temperature (T_{onset}), $T_{50\%}$, and derivative peak temperature (DT_p) for kenaf reinforced composites.

Sample	T_{onset} (°C)	$T_{50\%}$ (°C)	DT_p (°C)
PHB	298.1	310.0	314.2
UT5	286.2	297.3	300.8
UT10	288.2	296.7	299.5
UT20	279.6	288.0	289.7
CT5	284.3	296.4	298.6
CT10	279.8	292.2	295.0
CT20	273.5	283.7	284.6

PHB – polyhydroxybutyrate; UT – untreated fibre composite; CT – alkali-treated fibre composite

The thermal degradation mechanism of PHB has been studied and is suggested to be primarily a random chain scission process by a β-elimination reaction via a six-membered cyclic transition state (Doi et al., 1990; Grassie et al., 1984; Xiang et al., 2016). Activation energies between 109 ± 13 kJ mol^{-1} for PHB have been reported (Mitomo & Ota, 1991). PHB thermal decomposition produces crotonic acid via β-elimination (Ariffin et al., 2008). Bordes et al. (2009) suggested the mechanism of thermal degradation for PHB, illustrated in Figure 4.13.

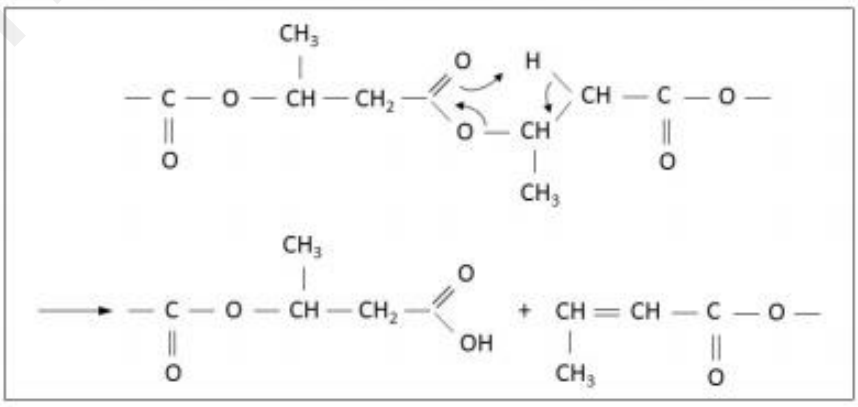

Figure 4.13: Thermal degradation mechanism of PHB.

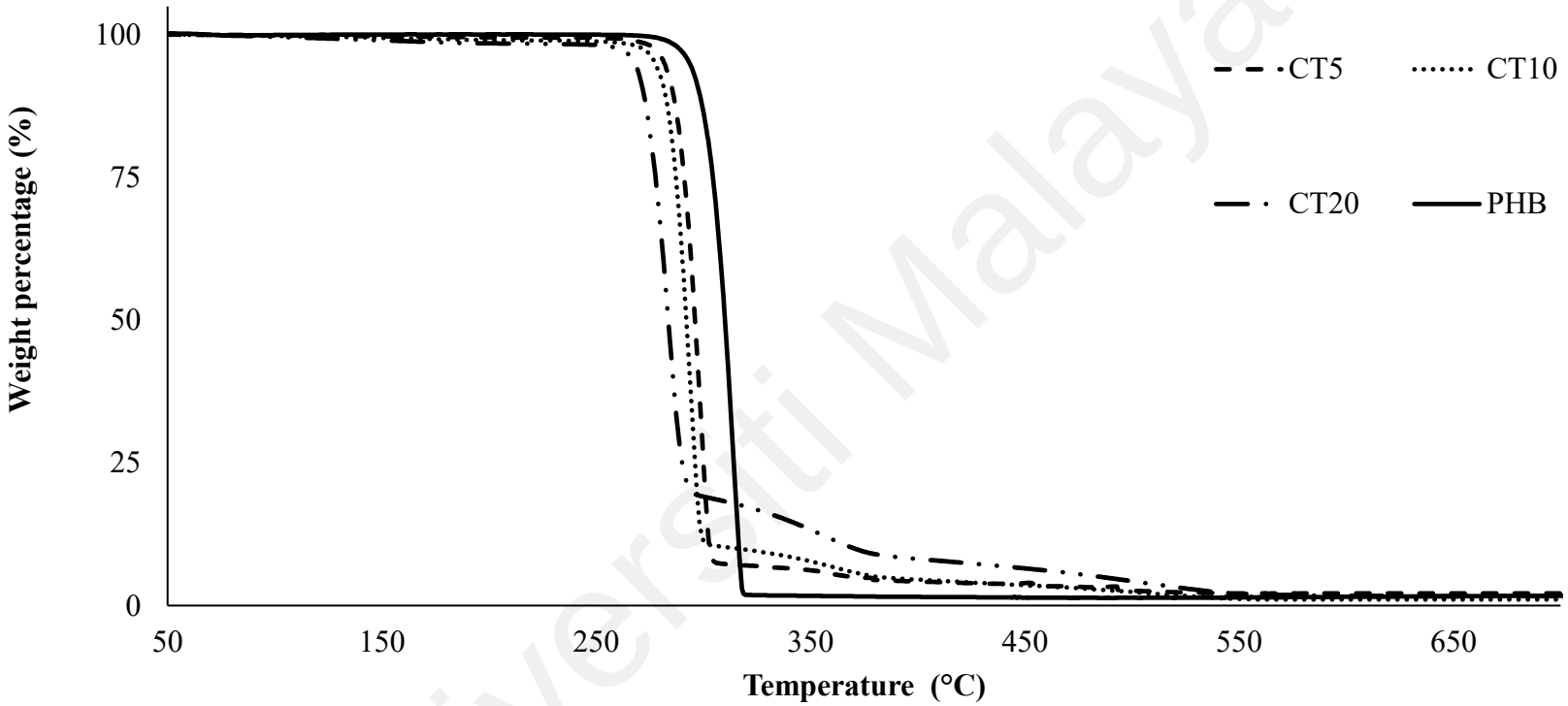

Figure 4.14 TGA curve for PHB and treated kenaf composites.

Significant quantities of PHB oligomers and small quantities of isocrotonic acid were also evolved on heating the polymer to around 300°C. Secondary products such as propylene, ketene, CO_2, and acetaldehyde were also formed by the further decomposition of the primary products. Conventional thermal stabilisers have been shown to have little effect in preventing thermal degradation of PHB (Asrar & Gruys, 2005). The thermal degradation mechanism of PHB-HV copolymers has been reported to be similar to that for PHB, with similar activation energy and degradation kinetics (Doi et al., 1990).

The thermogram for kenaf reinforced PHB composites in Figure 4.14 exhibit a two-step degradation. The first transition is a sharp weight reduction between 250°C - 300°C. This degradation step can be attributed to the thermal degradation of PHB and cellulose. At this temperature range, the pyrolysates' volatilisation was reported, which contributes to the reduction of the sample weight (Mitomo & Ota, 1991). There is a correlation between weight reduction and fibre loading. For example, the weight reduction occurring for CT10 and CT20 is 89% and 81%, respectively. In addition, neat PHB decomposes entirely, leaving almost no residue. This observation indicates that PHB fully decomposed within that temperature range, leaving only residues from incomplete thermal decomposition of kenaf fibres. The second transition step is more gradual and similar to the second degradation transition observed in kenaf fibre samples (Figure 4.4)

In general, kenaf-reinforced PHB composites, regardless of the treatment, had lower thermal stability compared to pure PHB. For example, the T_{onset} for PHB, UT20, and CT20 were 298.1°C, 279.6°C, and 273.5°C, respectively. A lower onset temperature indicated that the material began to degrade at a lower temperature. A similar trend was observed for $T_{50\%}$ and DT_p. During thermal processing of PHB, chain-end condensation leads to an increase in the molecular weight, and thermal degradation leads to a decrease in molecular weight concurrently. Since each thermal degradation event produces a

carboxyl and a crotonate chain end, the carboxyl group concentration increases significantly with time. At the same time, chain-end condensations are minimised, leading to a reduction in the molecular weight. It is reported that an increase in the hydroxy termination in PHB results in improved thermal stability by prolonging the condensation and delaying the degradation reaction (Asrar et al., 2000). Vahabi et al. (2019) has reported that the presence of lignin causes PHB to start to decompose at a lower temperature compared to neat PHB thermally. When subjected to Pyrolysis Combustion Flow Calorimeter analysis, the researchers reported that PHB samples containing lignin exhibited peak thermal decomposition 60°C lower than neat PHB (~300°C).

The composite's thermal stability decreased with increasing kenaf fibre content for untreated and treated fibres. In addition, it was observed that the thermal stability of untreated kenaf-reinforced composites is higher than their treated counterparts. It was proven that the alkali treatment had stripped the fibres of its lignin outer layer (Hassan et al., 2018). It could be possible that an interaction between the exposed cellulose portion of the treated kenaf fibres and PHB or its decomposition byproducts, such as crotonic acid, at elevated temperatures, led to lower thermal stability. In comparison, the lignin and hemicellulose present on untreated kenaf fibres could act as a protective layer against these chemicals. Further study is required to understand the phenomenon better.

4.2.1.2 DSC

Information obtained through DSC would improve the understanding of the phase changes (e.g., melting) that the composite went through in the temperature range studied. The mechanical properties of the composite were influenced by the molecular structure of the matrix (crystalline structure, orientation of amorphous regions), especially the

degree of crystallinity. The DSC thermogram for the PHB and treated kenaf composites is provided in Figure 4.15.

Important parameters that were studied, such as melting temperatures (T_m), enthalpy heat of melting (ΔH_m), and the degree of crystallinity (X_c), for the composites are given in Table 4.6. The X_c was calculated using the following equation,

$$X_c = \frac{\Delta H_m}{\Delta H_m *} \times 100 \quad (4.3)$$

where ΔH_m* is the enthalpy heat of fusion for an 'ideally' fully crystalline PHB, taken as 146 J/g (Barham et al., 1984). The values provided in the table have been normalised according to the actual PHB content in the composite.

The thermogram obtained from DSC showed a single endothermic peak attributed to the melting of PHB. As shown in the table, the addition of kenaf fibres slightly reduced the melting temperature of PHB. For example, the T_m for neat PHB and UT5 were 175.1°C and 166.1°C, respectively. Melting temperature is influenced by the intermolecular forces and the packing of the crystals. If the crystal is closely packed, more intermolecular forces will hold the crystals together. These minor bonds need to be broken to melt, hence a higher T_m value. However, the presence of kenaf fibres in the composite disrupted the crystal packing, reducing the intermolecular bonds and thus lowering the T_m. In contrast, when the fibre weight fraction was increased, no clear trend regarding the T_m was observed regardless of the fibre type used.

Mousavioun et al. (2013) studied the effect of lignin on the thermal properties of PHB/lignin blends. The researchers reported that lignin and PHB are miscible up to 40% lignin content. In addition, lignin has a plasticizing effect on PHB, increasing its glass transition temperature (T_g) and reducing T_m. This effect is only observed at lower lignin content. The blend is no longer miscible above 40% lignin content, resulting in two

separate $T_{g\ and}$ T_m peaks observed. In this work, it has been shown that untreated kenaf contains a higher amount of lignin compared to alkali-treated kenaf fibres (Table 4.1). This relatively higher lignin content can contribute to the relatively low T_m observed in untreated kenaf PHB composites compared to its alkali-treated counterpart.

Table 4.6 Melting temperature (T_m), enthalpy of fusion (ΔH_m), and degree of crystallinity (X_c) for kenaf reinforced PHB composites.

Sample	T_m (°C)	ΔH_m (%)	X_c (%)
PHB	175.1	73.9	50.6
UT5	166.1	78.3	56.4
UT10	169.0	71.2	54.2
UT20	169.0	63.3	54.2
CT5	172.7	61.9	44.7
CT10	172.3	63.5	48.4
CT20	169.4	60.2	51.5

The introduction of untreated kenaf fibres into PHB increased its X_c. For example, the X_c for neat PHB and UT5 was 50.6% and 56.4%, respectively. It has been reported that fibres can promote nucleation along the fibre matrix interface resulting in increased X_c (Yang et al., 2014). However, increasing the fibre weight fraction of untreated fibres from 5% to 20% caused the X_c to decrease from 56.4% to 54.2%. On the other hand, introducing alkali-treated kenaf fibres caused the X_c to be lower than neat PHB. For example, X_c for CT10 was 48.4%, lower than neat PHB (50.6%). Lower X_c indicated that the addition of treated kenaf fibres may have interfered with the crystallisation process of the PHB matrix.

Weihua et al. (2004) prepared a compression moulded lignin/PHB blend to study lignin's ability as a nucleating agent for PHB. The researchers reported that the spherulitic growth rate, the maximum spherulitic growth temperature, and the nucleation density were increased, indicating that lignin is a promising nucleating agent for PHB. This

behaviour explains the observation in this work, where X_c for untreated fibres is higher than treated fibres. In DSC analysis, the crystallinity of the polymer is the one being studied; therefore, the fact that treated fibre has higher crystallinity, as discussed earlier, is a non-factor. DSC measures phase changes and the fibres do not undergo any phase change in the temperature range tested.

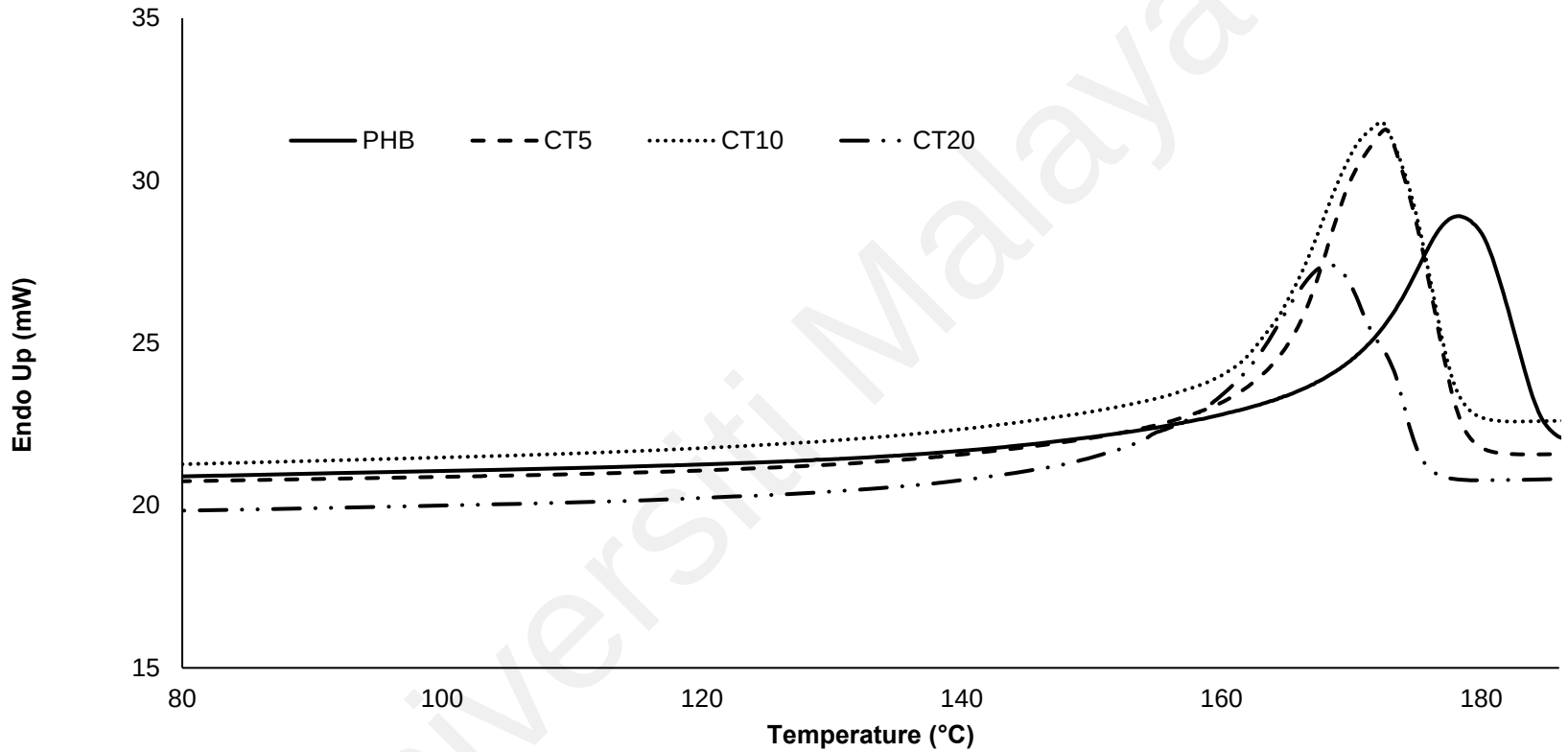

Figure 4.15: DSC thermogram for PHB and treated kenaf composites.

4.2.2 Rheology

The flow of composite melt is essential and can be influenced by temperature, pressure, screw speed, filler content, and die size. Information from rheology can reflect the internal structure and processability of the melt. Flow behaviour is important during compounding and injection moulding, especially to understand and optimise the mould filling process. Information, such as the storage modulus (G'), loss modulus (G''), and complex viscosity (η*), were obtained from a dynamic frequency sweep of the composite sample at constant amplitude and temperature. Figure 4.16 illustrates the complex viscosity curve as a function of angular frequency for the kenaf-reinforced PHB composites for treated and untreated fibres and different fibre loadings.

From Figure 4.16, it can be observed that for neat PHB, UT5, and CT5, the complex viscosity (η*) slightly increased with increasing angular frequency (ω). However, above ten rad/s, the melts exhibited Newtonian fluid behaviour. For UT10 and CT10, the melts exhibited Newtonian fluid behaviour throughout the tested ω range. However, for UT20 and CT20, the composite melts displayed a shear-thinning behaviour, where the η* decreased with increasing ω. These behaviours indicate the transformation from solid-like behaviour at lower ω to fluid-like behaviour at higher ω (Salleh et al., 2014). At higher fibre loading, the presence of fibres affected the normal melt flow and hindered the mobility of the polymer chain. In addition, the fibre-fibre collision compounded this effect. However, sufficient force was subjected to the fibres at a higher frequency, aligning the fibres with the flow direction and significantly improving flowability.

It was also observed that increasing the fibre content increased the η*. Composites reinforced with treated kenaf fibres also exhibited higher η* for all fibre loadings, indicating the fibre and matrix having improved interaction. Stronger interactions

between the fibre and matrix obstruct the flow of the matrix, hence increasing the viscosity (Chun et al., 2015).

The storage and loss modulus for neat PHB and all the composites are illustrated in Figure 4.17 and Figure 4.18. Both the storage modulus (G') and loss modulus (G") for neat PHB and all the composites increased with increasing ω. The G' of the composite melted at a lower ω and was heavily influenced by the kenaf fibre content. The composite melt exhibited a plateau at a lower ω, and the magnitude of the plateau increased with increasing kenaf fibre content. The increase was attributed to the increasing rigidity of the melt due to the addition of fibres. The G" also displayed a similar trend; however, the plateau was only visible in composites with 20% fibre loading. At 20% fibre loading, the melt behaves as a solid at lower angular frequencies. The high content of fillers in the melt requires more force before the material can flow. At lower fibre loading (5% and 10%), the melt behaved as a Maxwell fluid, typical for thermoplastic melts. For both G' and G", the CT composites exhibited higher values than their UT counterpart.

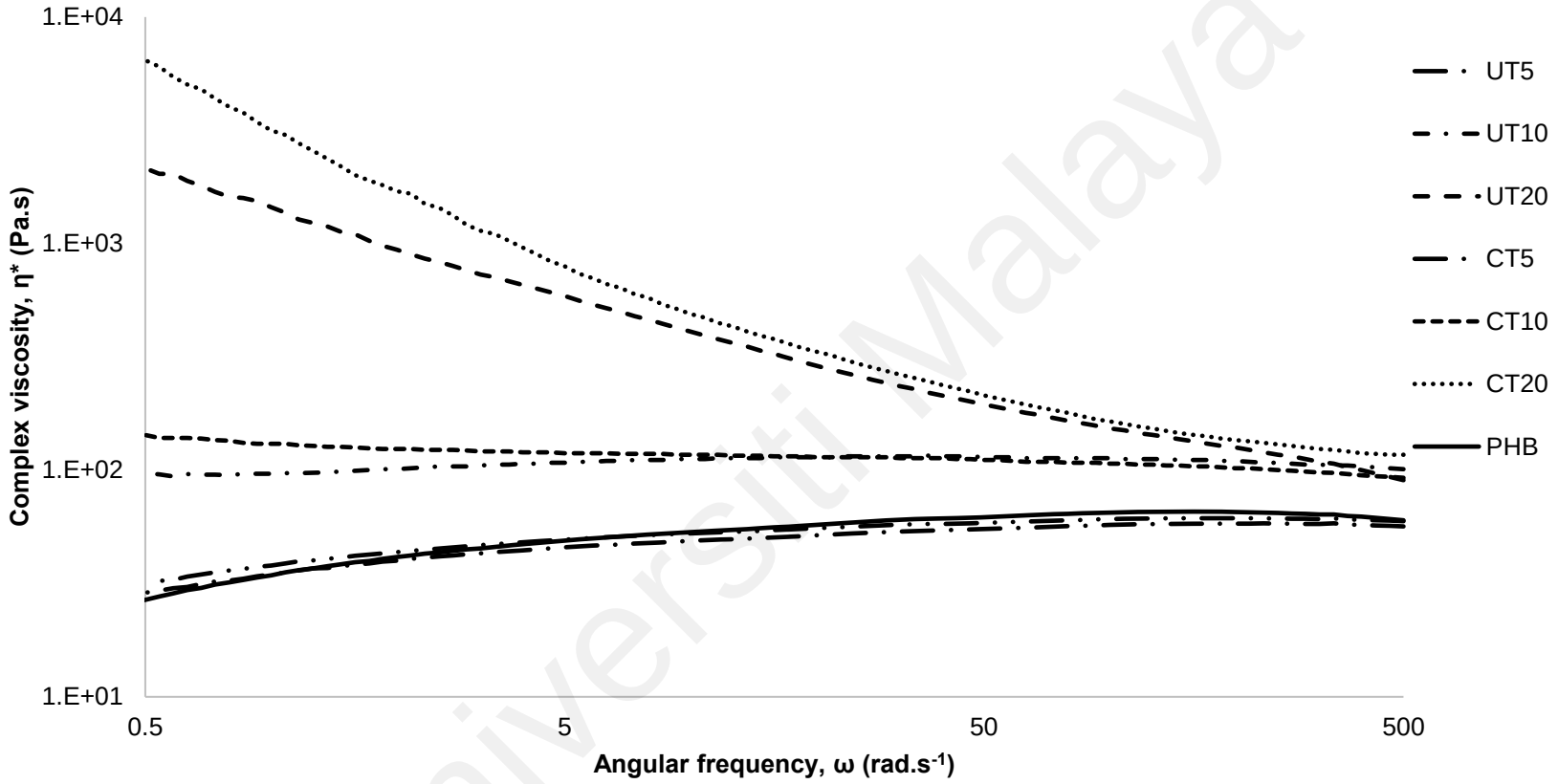

Figure 4.16 Complex viscosity-angular frequency behaviour of untreated and treated kenaf PHB composites at three different fibre loadings.

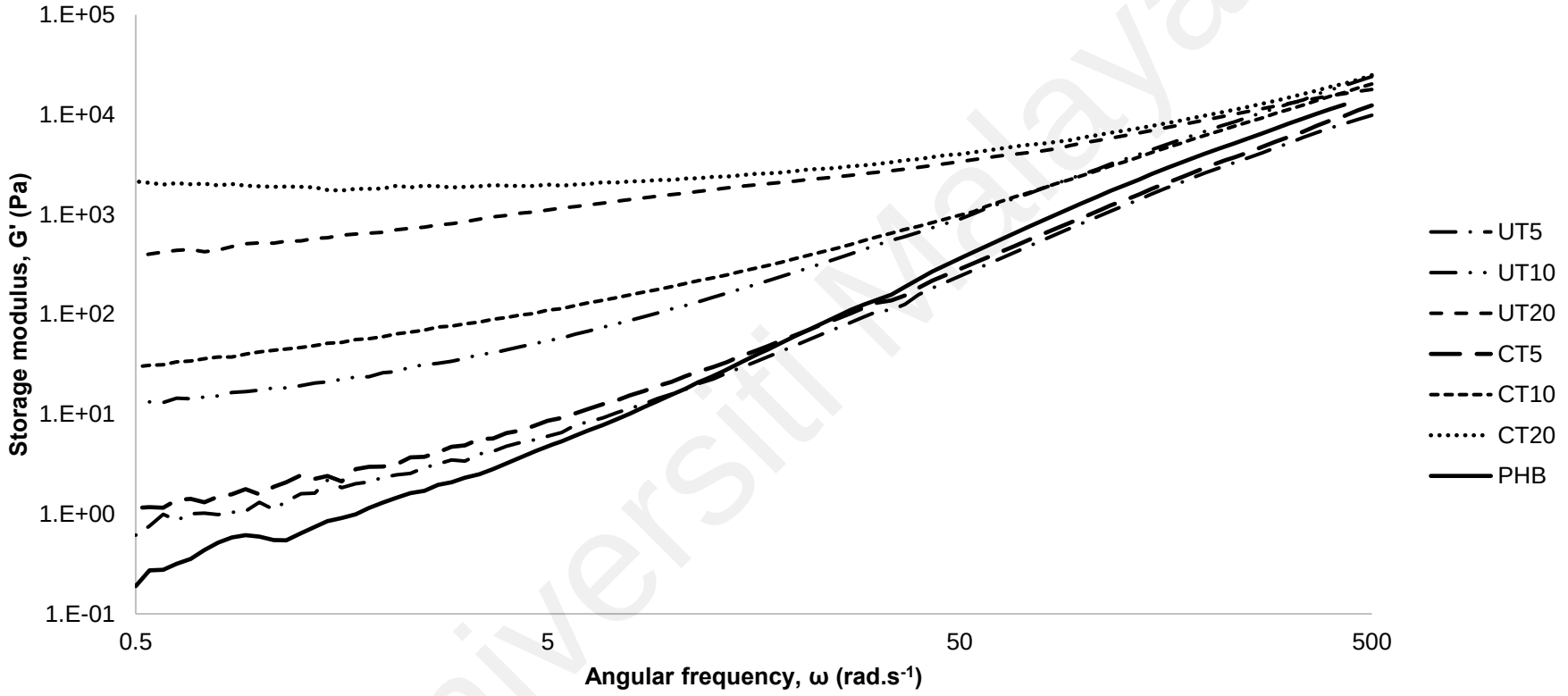

Figure 4.17 Storage modulus-angular frequency behaviour of untreated and treated kenaf PHB composites at three different fibre loadings.

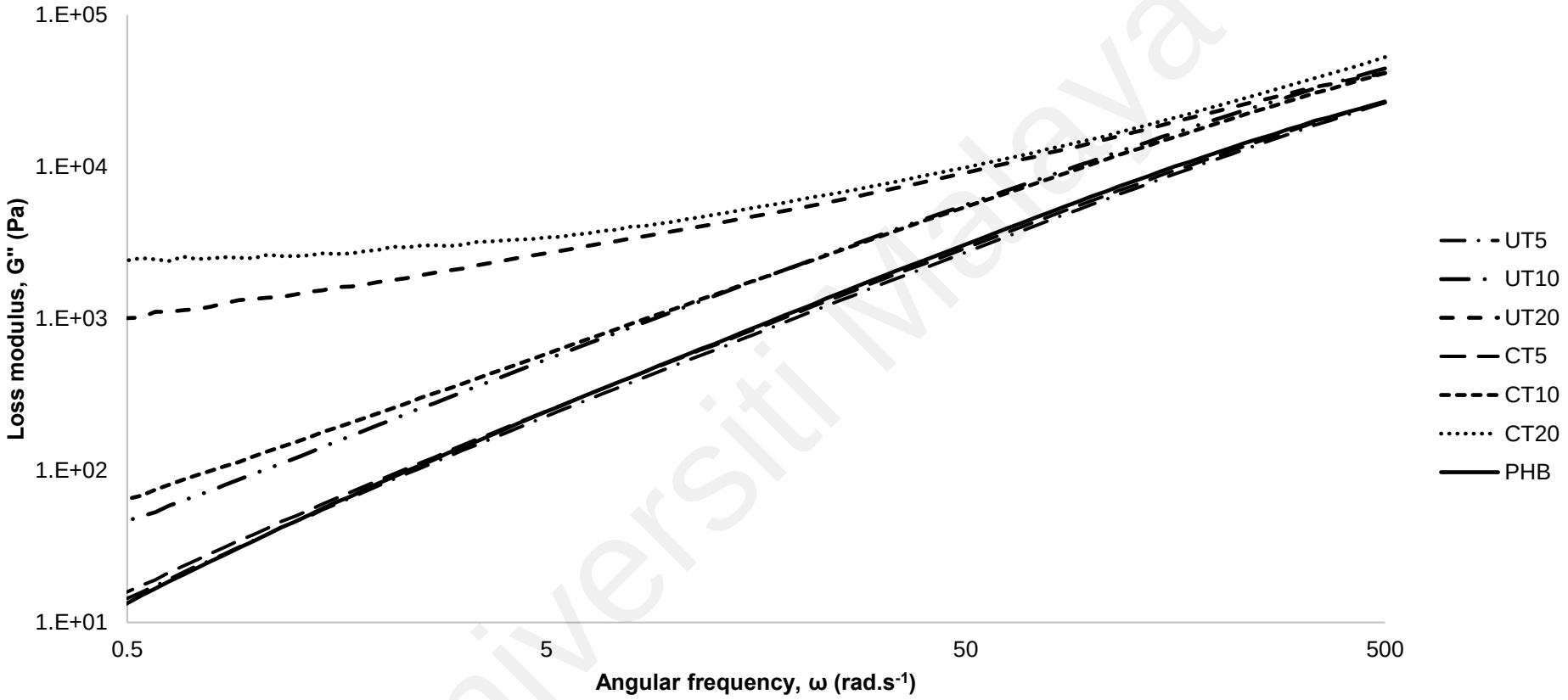

Figure 4.18 Loss modulus-angular frequency behaviour of untreated and treated kenaf PHB composites at three different fibre loadings

4.2.3 Mechanical properties

4.2.3.1 Tensile Properties

Young's modulus, E, is a measurement of the tensile stiffness of a solid material. It defines the relationship between tensile stress, σ and axial strain, ε in the linear elastic region. It is calculated using (4.4).

$$E = \frac{\sigma}{\varepsilon} \tag{4.4}$$

Stiffness is the ability of a material to resist deformation when force is applied to it. Materials with lower stiffness will undergo deformation when subjected to tensile strain. Elongation of the specimen and necking can be observed due to the deformation. On the other hand, tensile strength is the maximum stress applied to the material before it irreversibly deforms. For brittle material, tensile strength can be measured at the point of fracture, observed as a sharp drop in the stress vs strain curves at the point of failure. Refer to Figure 4.19. If a material undergoes ductile failure, a gradual decline would be observed instead.

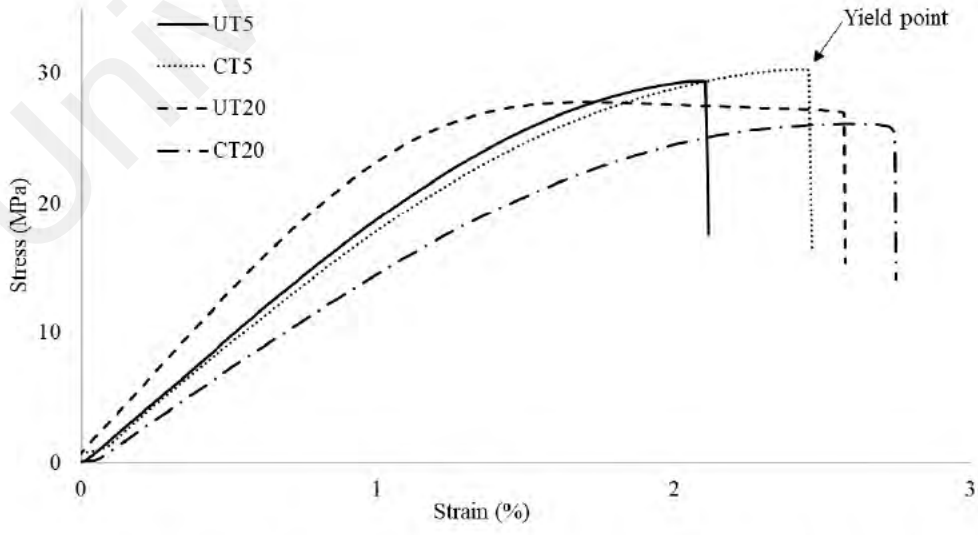

Figure 4.19: Stress vs strain diagram for selected specimens.

Tensile strain measures the deformation of an object under tensile stress and is defined as the fractional change of the specimen's length when it is subjected to tensile stress. E is calculated using the following equation:

$$\varepsilon = \frac{\Delta L}{L_0} \tag{4.5}$$

where ΔL is the increase in length of the specimen and L_0 is the initial length. The untreated and treated kenaf-reinforced PHB composites were tested, and Young's modulus, tensile strength and tensile strain of untreated and treated kenaf composites are listed in Table 4.7 and illustrated in Figure 4.20.

Table 4.7: Young's modulus, tensile strength and tensile strain for kenaf/PHB composites.

	Young's modulus (GPa)	**Tensile strength (MPa)**	**Tensile strain (%)**
PHB	1.95	35.6	4.1
UT5	2.12	32.1	2.9
UT10	2.21	31.4	2.7
UT20	2.68	31.3	2.3
CT5	1.97	30.0	2.8
CT10	2.12	27.4	2.2
CT20	2.36	26.3	1.9

The Young's modulus and tensile strength of neat PHB were recorded at 1.95 GPa and 35.6 MPa, respectively. The Young's modulus increased with the addition of treated and untreated kenaf. For example, Young's modulus for UT10 and CT10 was 2.21 GPa and 2.12 GPa, respectively. This increase indicated that incorporating kenaf fibre into the PHB increased its stiffness. Expectedly, the tensile strain was reduced for both specimens. This reduction is because a stiffer material will deform less.

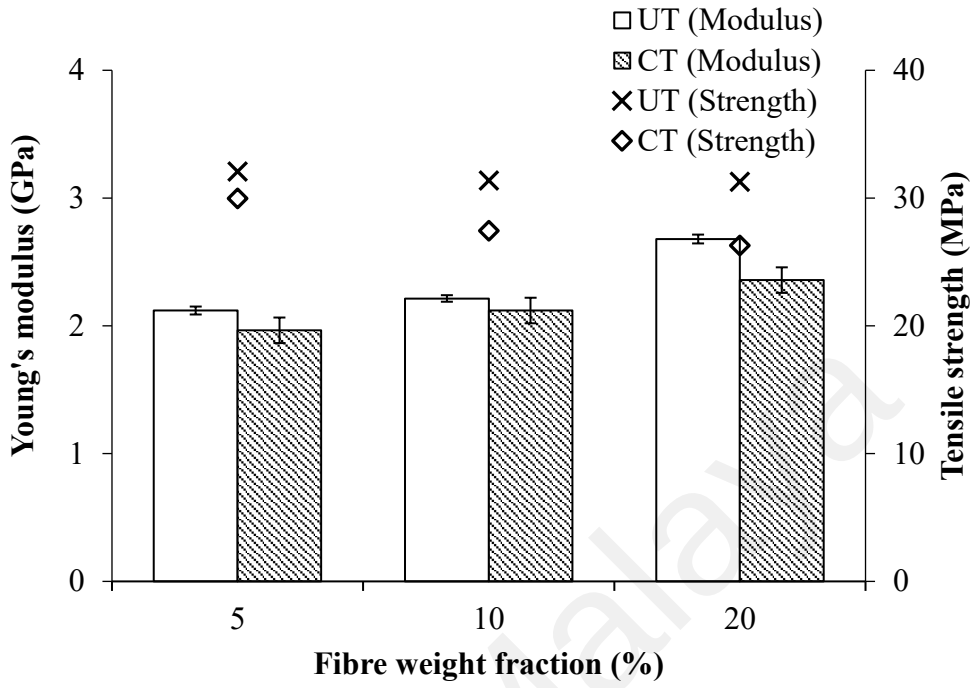

Figure 4.20. Young's modulus and tensile strength of kenaf-reinforced PHB composites.

The effect of fibre content on Young's modulus was studied. Increasing the fibre content increased Young's modulus for both the treated and untreated kenaf-reinforced composites. For example, Young's modulus for CT increased from 1.97 GPa to 2.36 GPa when the fibre content was increased from 5% to 20%. A similar observation was reported by Ibrahim et al. (2009). The researchers found that increasing the fibre content increased the tensile modulus to a certain optimal fibre loading. As the fibre was further increased beyond the optimal value, the modulus decreased due to poor wettability resulting in lower stiffness.

Fibre surface treatment is expected to improve the mechanical properties of the composites. In theory, the surface treatment is expected to produce a cleaner and rougher surface where the matrix and fibre can bind and interlock, producing composites with

superior mechanical properties from their untreated counterpart (Fiore et al., 2015). However, in this study, it was found that the modulus for composites prepared with treated kenaf fibres had a lower modulus compared to the composites prepared with untreated fibres. The modulus for UT20 and CT20 was 2.68 GPa and 2.36 GPa, respectively. There were several explanations for this observation. Firstly, from the DSC, it was found that the crystallinity of the composites prepared with the treated fibres was lower than the composites prepared with the untreated fibres. Materials with lower crystallinity are ductile and will record a lower stiffness during tensile testing. Another possibility was increased fibre breakage during processing. It was found from fibre characterisation that surface-treated kenaf was more crystalline and brittle compared to untreated kenaf. This increased brittleness may have caused the fibre to break more during processing due to the fibre-matrix, fibre-fibre, and fibre-machinery interactions. Increased fibre breakage would result in shorter fibres, which are less efficient at reinforcing the composites due to the increased fibre ends (Hassan et al., 2018). The treated fibre surface was also rougher, which led to greater fibre-fibre friction.

The tensile strength of the composite was lower than the neat PHB. For example, the tensile strength for neat UT10 and CT10 were 31.37 MPa and 27.44 MPa, respectively, which were lower than the tensile strength of neat PHB (35.6 MPa). Due to the introduction of kenaf fibres, the composites became less ductile as the fibres constrained the molecular rearrangement. The notching effect of the fibres is also crucial because considerable stress concentration is induced in the matrix at the fibre end and matrix flow constrained by adjacent fibres (Takahashi & Choi, 1991).

The effect of fibre loading on the tensile strength of the composite was studied. The tensile strength decreased with increasing fibre weight fraction for both the treated and untreated composites. For example, the tensile strength for CT decreased from 29.97

MPa to 26.28 MPa as the fibre weight fraction increased from 5% to 20%. The reduction in tensile strength was attributed to the increased fibre breakage during processing at higher fibre loading. It could have been due to a wetting problem at a higher fibre content. The modulus was not affected by these flaws due to the modulus being measured at a very low strain. In the lower strain region of the testing, the flaws discussed above have yet to manifest.

The fracture surface of the treated and untreated composites is illustrated in Figure 4.21. It was observed that there was no improvement regarding the fibre matrix adhesion. There was a clear separation between the fibre and the matrix (shown by arrows). The observation suggests that an alkali treatment alone is insufficient to improve the fibre matrix adhesion. Adding compatibilisers or functional groups onto the fibre surface is necessary to achieve better fibre-matrix adhesion. It can also be observed that plastic deformation is absent on the fracture surface, indicating that the material underwent brittle failure.

The stress vs strain curve supports this observation for selected specimens illustrated in Figure 4.19. Plastic deformation, such as necking, was not observed. The specimens abruptly break into two pieces at the point of failure.

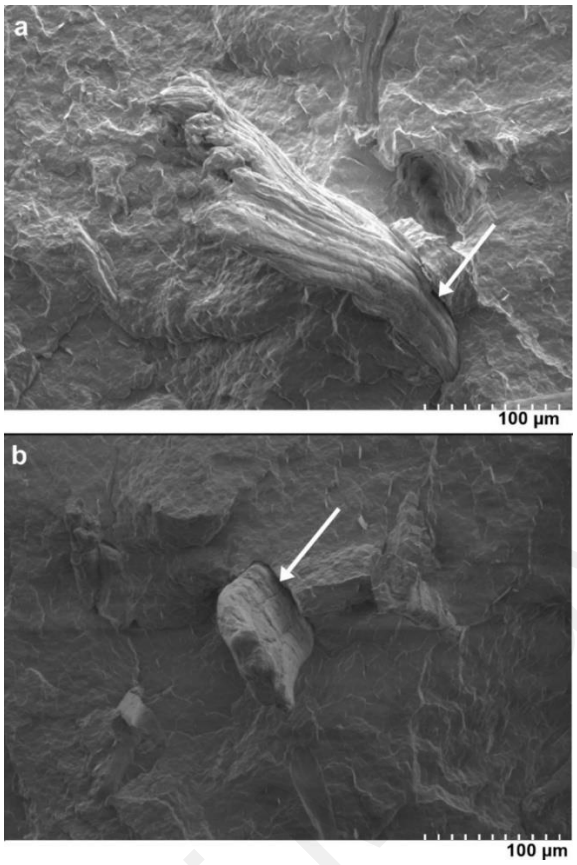

Figure 4.21 Fracture surface of UT5 (a) and CT5 (b) captured using FESEM at 1000 times magnification.

For tensile strain, the trend observed is according to expectation. Tensile strain for the kenaf reinforced PHB composites is lower than neat PHB. Generally, the inclusion of natural plant fibres into thermoplastics decreases the elongation at break but increases Young's modulus (Djafari Petroudy, 2017). The presence of fibres limits the ability of the polymer to rearrange under tensile stress. In addition, the notch effects of the fibre ends also served as stress concentrators in the system.

4.2.3.2 Flexural Properties

The flexural properties of the untreated and treated kenaf-reinforced PHB composites were tested under a three-point bending setup. The flexural properties describe the ability of the material to withstand bending, which is essential for load-

bearing applications. The stresses induced are a combination of tensile and compression stresses (Campo, 2008). Flexural modulus is the ratio of the stress and strain during deformation, calculated from the slope of the stress-strain curve generated during the testing (Hodgkinson, 2000). A material with a higher flexural modulus is harder to bend than a material with a lower flexural modulus. Flexural strength is denoted by the stress in the material just before the specimen yields in flexural testing. Typically, it is the highest point in the stress-strain generated during the flexural testing. Flexural displacement is the distance travelled by the cross-head in the test. The flexural modulus and flexural strength of kenaf-reinforced PHB composites are tabulated in Table 4.8.

Table 4.8: Flexural properties of kenaf/PHB composites.

	Flexural modulus (GPa)	Flexural strength (MPa)	Flexural displacement (mm/mm)
PHB	2.65	54.7	0.03
UT5	2.93	54.6	0.03
UT10	3.75	56.9	0.02
UT20	4.04	58.3	0.02
CT5	3.58	53.58	0.02
CT10	3.82	52.62	0.02
CT20	4.29	52.73	0.02

The incorporation of kenaf fibres into PHB improved its flexural modulus. Refer to Figure 4.22. The flexural modulus of neat PHB increased from 2.65 GPa to 2.93 GPa with the addition of only 5% w/w kenaf fibre. The improvement was even more significant when the treated kenaf was added at the same weight fraction (W_f) (3.58 GPa). Neat PHB tends to fail catastrophically during flexural testing, with the sample breaking into two big pieces with smaller pieces shattering from the larger pieces. However, this did not happen with the addition of kenaf fibres. As the fibre content further increased, the flexural modulus also increased. The flexural modulus for CT increased from 3.58 GPa to 4.29 GPa as the W_f increased from 5% to 20%.

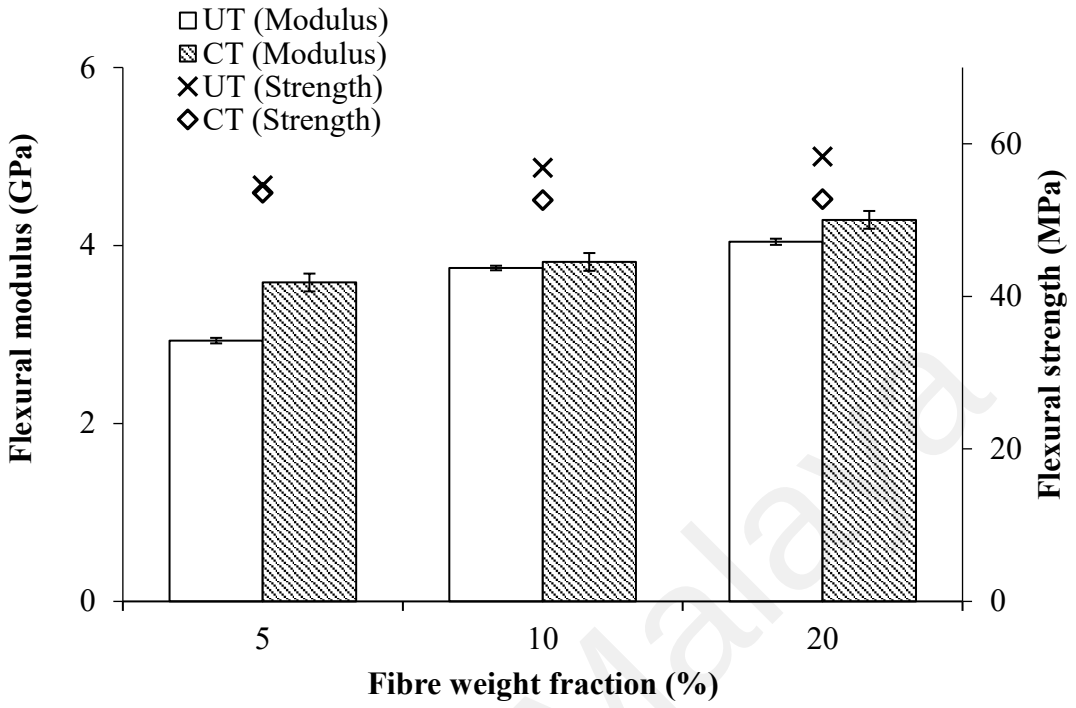

Figure 4.22 Flexural modulus and strength of kenaf-reinforced PHB composites.

The improvement for flexural properties was more noticeable compared to the improvement for tensile properties and was attributed to the nature of the injection moulded fibre-reinforced composites. In injection moulded specimens, the fibre orientation near the mould will align according to the flow direction of the polymer melt (Darlington & Mcginley, 1975). In contrast, the fibre in the middle section would be randomly aligned perpendicularly to the flow direction. Refer to Figure 4.23.

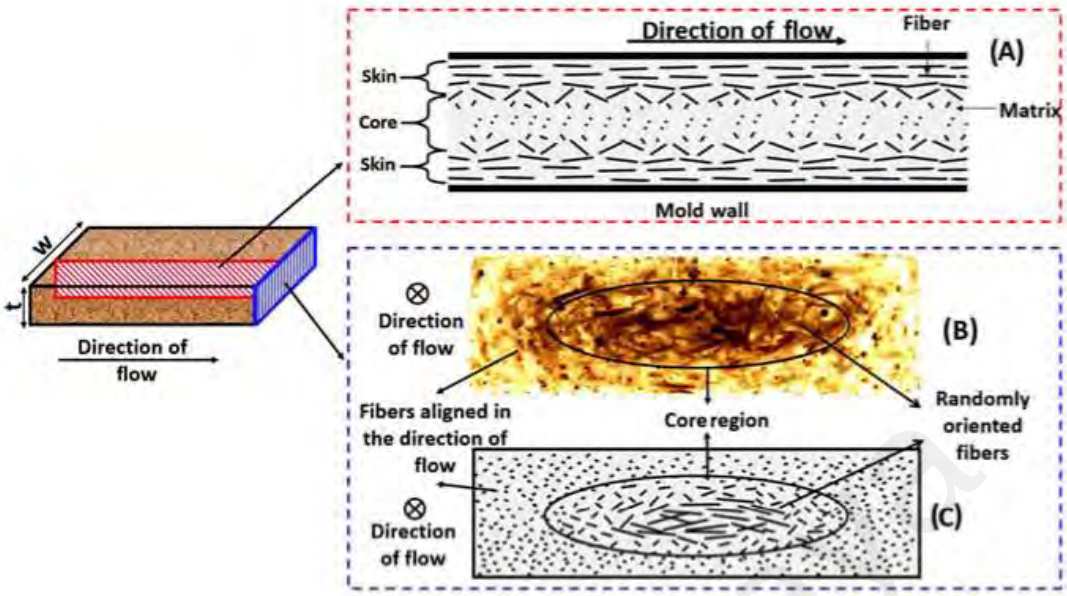

Figure 4.23: Fibre orientation in injection moulded fibre reinforced composites. (Singh & Chaitanya, 2015).

Similar fibre orientation was observed in this study and is illustrated in Figure 4.24, where the fibres in the bottom right corner are more aligned to the melt flow (moving away from the reader) while the fibres in the top left corner were perpendicularly oriented to the melt flow direction. In tensile, these variations in fibre orientation would result in a poorer reinforcement effect because the strain applied was uniform across the sample. However, for flexural testing, only the outermost layer (top and bottom) experienced the full force of the testing. Because the fibres in these regions were more oriented than the fibres in the central region, the exhibited flexural properties were also higher.

The flexural strength of the neat PHB increased with the incorporation of kenaf fibres, from 54.7 MPa to 58.3 MPa (UT20). For untreated kenaf fibres, increasing the W_f improved the flexural strength of the composite. For example, the flexural strength improved from 54.6 MPa to 58.3 MPa when the W_f increased from 5% to 20%. UT also

exhibited slightly higher flexural strength than CT at a similar fibre loading. For example, the flexural strength for UT10 and CT10 was 56.9 MPa and 52.6 MPa, respectively.

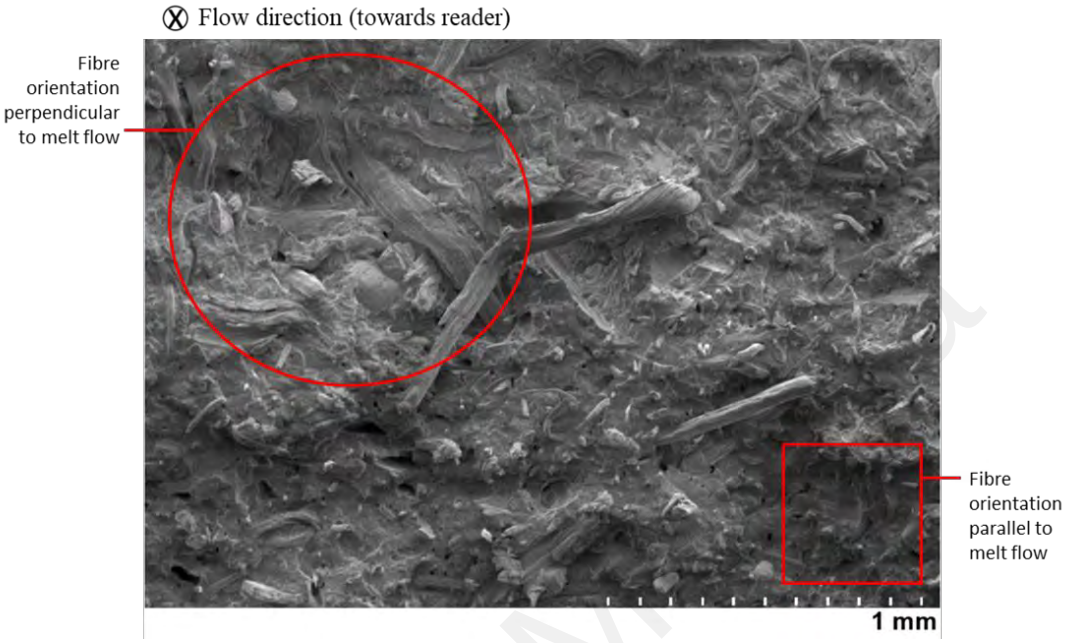

Figure 4.24 Fracture surface of UT20 at 50 times magnification.

Flexural displacement exhibited different trends for treated, and untreated kenaf reinforced composites. For untreated kenaf composites, at 5% fibre loading, the flexural displacement is similar to neat PHB. The flexural displacement for UT5 and neat PHB is 0.03 mm/mm. However, as the fibre loading was increased to 10% and 20%, the flexural displacement decreased to 0.02 mm/mm. However, for the treated kenaf composites, the flexural displacement for all the samples regardless of fibre loading is lower than neat PHB at 0.02 mm/mm. As the fibre content was further increased to 10% and 20%, the mobility of the polymer chains was hindered physically by the fibres present.

4.2.3.3 Impact properties of the composite

Fracture energy (W) and peak load (P) were obtained from the impact test and were used to calculate the critical strain energy release rate (G_c) and critical stress intensity factor (K_c) (Hassan et al., 2011). Impact tests produced energy vs time graphs for each tested specimen. Two essential parameters were extracted from these graphs, fracture energy (W) and peak load (P). Fracture energy or work of fracture can be defined as total work required to fracture the sample, per unit area of new surface produced or the total amount of energy dissipated during crack growth (Folkes, 1979). Fracture energy is obtained by calculating the area under the graph before sample fracture. The relationship between W and the critical strain energy release rate (G_c) and specimen geometry function (BDΦ) is given by,

$$W = G_c BD\Phi \tag{4.6}$$

where B and D are the width and depth of the specimen, respectively. A correction factor, Φ, is given by,

$$\phi = \frac{1}{2}\left(\frac{a}{D}\right) + \frac{1}{18\pi}\left(\frac{S}{D}\right)\frac{1}{\left(\frac{a}{D}\right)} \tag{4.7}$$

where a and S are notch depth (crack length) and the specimens support span.

The peak load was obtained from the highest point in the graph prior to fracture. G_c is the total energy absorbed by the test specimen divided by its net cross section area. It is used to measure the energy required for crack initiation. K_c is a function of loading, crack size, and structural geometry. K_c indicates the resistance of the material to unstable crack growth. The relationship between the critical stress intensity factor (K_c) with

nominal fracture stress (σ), a geometry correction factor (Y) and a notch or crack length (a) is given by,

$$\sigma Y = \frac{K_c}{\sqrt{a}} \tag{4.8}$$

In three-point bend test, σ is given by simple bending theory as,

$$\sigma = \frac{6PS}{4BD^2} \tag{4.9}$$

For the three-point bend test specimen, where S/D is equal to 4, Y is given by,

$$Y = 1.93 - 3.07\left(\frac{a}{D}\right) + 14.53\left(\frac{a}{D}\right)^2 - 25.11\left(\frac{a}{D}\right)^3 + 25.80\left(\frac{a}{D}\right)^4 \tag{4.10}$$

When the stress in the material exceeds K_c, the crack will propagate. These four essential values for understanding the impact properties of the composites are reported in Table 4.9.

Table 4.9: Impact properties of kenaf reinforced PHB composites.

	W (mJ)	**P (N)**	**G_c (kJm^{-2})**	**K_c ($MPam^{-½}$)**
PHB	100	436	3.1	3.2
UT5	90	406	2.7	2.9
UT10	95	415	2.9	3.0
UT20	111	452	3.4	3.3
CT5	89	343	2.7	2.3
CT10	95	350	3.0	2.6
CT20	122	395	3.8	2.9

For both untreated and treated kenaf composites, increasing the fibre content increases W and P. For example, W for CT5, CT10 and CT20 are 89, 95 and 122 mJ, respectively. Similar trends were observed for G_c and K_c. The increase can be attributed to the simple fact that more fibres are present in the specimens with higher fibre content. The fibres are expected to absorb the energy through mechanical friction and fibre debonding, contributing to the increased energy needed during fracture (Manshor et al., 2014). It is also observed that the impact properties only exceed the properties of neat PHB at 20% fibre loading for UT composites. This observation is expected to be due to the notching effect of the reinforcing fibres being more dominant at lower fibre loading, reducing the impact properties of the composites compared to neat PHB (Hassan et al., 2004). A similar trend is observed for CT composites. However, P and K_c values for CT composites at 20% fibre loading remained lower than neat PHB.

When comparing CT and UT, it was found that CT has better W and G_c, especially at higher fibre loadings. For example, G_c for CT20 and UT20 are 3.8 and 3.4 kJm^{-2}, respectively. The improved impact properties might be due to the better distribution of kenaf fibres in the matrix than the untreated kenaf composites. Treated kenaf fibres interact better with the matrix, improving the fibres' dispersion during extrusion. Treated kenaf fibres also have a rougher surface, increasing mechanical friction during failure. The fibres' wetting was also significantly improved, reducing the presence of voids and fibre agglomeration in the system (Pickering et al., 2016). The presence of voids can reduce the energy required during fracture.

On the other hand, P and K_c values for UT composites are higher than CT composites. For example, K_c for CT20 and UT20 are 2.9 and 3.3 $MPam^{-½}$, respectively. This increase could be attributed to the higher nucleation rate due to the lignin present, discussed previously in the DSC results (Table 4.6). A higher nucleation rate leads to the

formation of smaller spherulites. These smaller spherulites would contribute to crack bifurcation or branching, intrinsically improving the fracture toughness of the UT reinforced composites. Studies have shown that crack bifurcation can lead to retardation or arrest of crack propagation (Kazerani et al., 2010; Smith, 1968; Theocaris & Papadopoulos, 1986). A simple diagram showing crack bifurcation is illustrated in Figure 4.25.

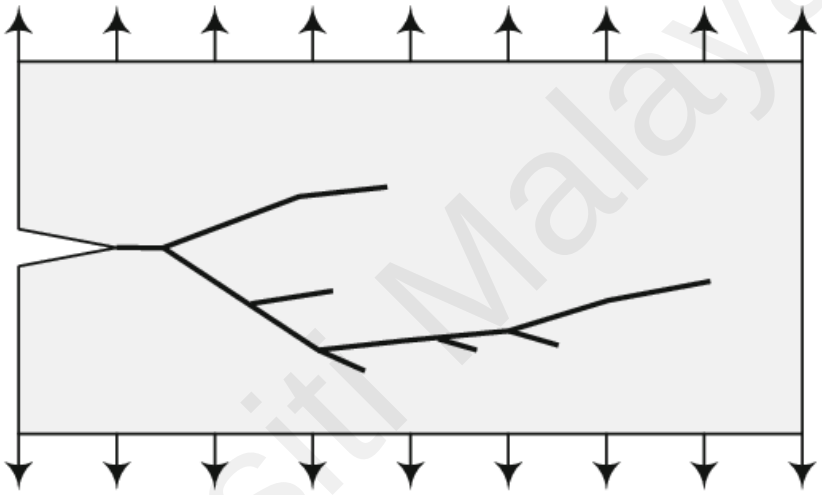

Figure 4.25: Crack bifurcation (Kazerani et al.,2010).

An important factor influencing the appearance of bifurcation is the state of adhesion between phases in composites. It has been shown that these mesophases play an essential role in advancing and attracting to themselves bifurcations, which are beneficial for the structure, since they constitute poles, splitting the strain energy at the crack tip into parts, thus blunting any tendencies of failure (Theocaris & Papadopoulos, 1986). Therefore, a composite with good interfacial adhesion and better mechanical interlocking would produce better impact properties.

4.3 Montmorillonite modified PHB

4.3.1 Dispersion of nanoclay

The dispersion of the nanoclay is a crucial aspect to be studied in a nanocomposite. FESEM-EDS mapping was used to verify the presence and the dispersion of clay in the system. Montmorillonite is an aluminosilicate, containing the elements Al and Si. Meanwhile, PHB consists of the elements C, H and O. The surface-modified MMT was treated with methyl, bis hydroxyethyl, octadecyl ammonium (elements N, C, H and O present). Therefore, mapping the element Al and Si should provide the necessary information regarding MMT dispersion. The EDS mapping for TCN modified PHB at 3, and 9 phr is illustrated in Figure 4.26.

The image shows that the nanoclay dispersion in the system with higher clay content (9 phr) is poorer than specimens with lower clay content. Hotspots of Al and Si are observed in the mapping image, indicating that agglomeration is present. Higher clay content increases the probability of clay-clay contact, thus increasing the occurrence of agglomeration. Agglomeration affects the properties of the composite poorly, especially the mechanical properties (Lim et al., 2017). It can also be observed that the dispersion of treated MMT (TCN3 and TCN9) is better compared to its untreated counterpart (PGV3 and PGV9). It is suggested that better dispersion results from better clay-matrix interaction between PHB and the treated clay.

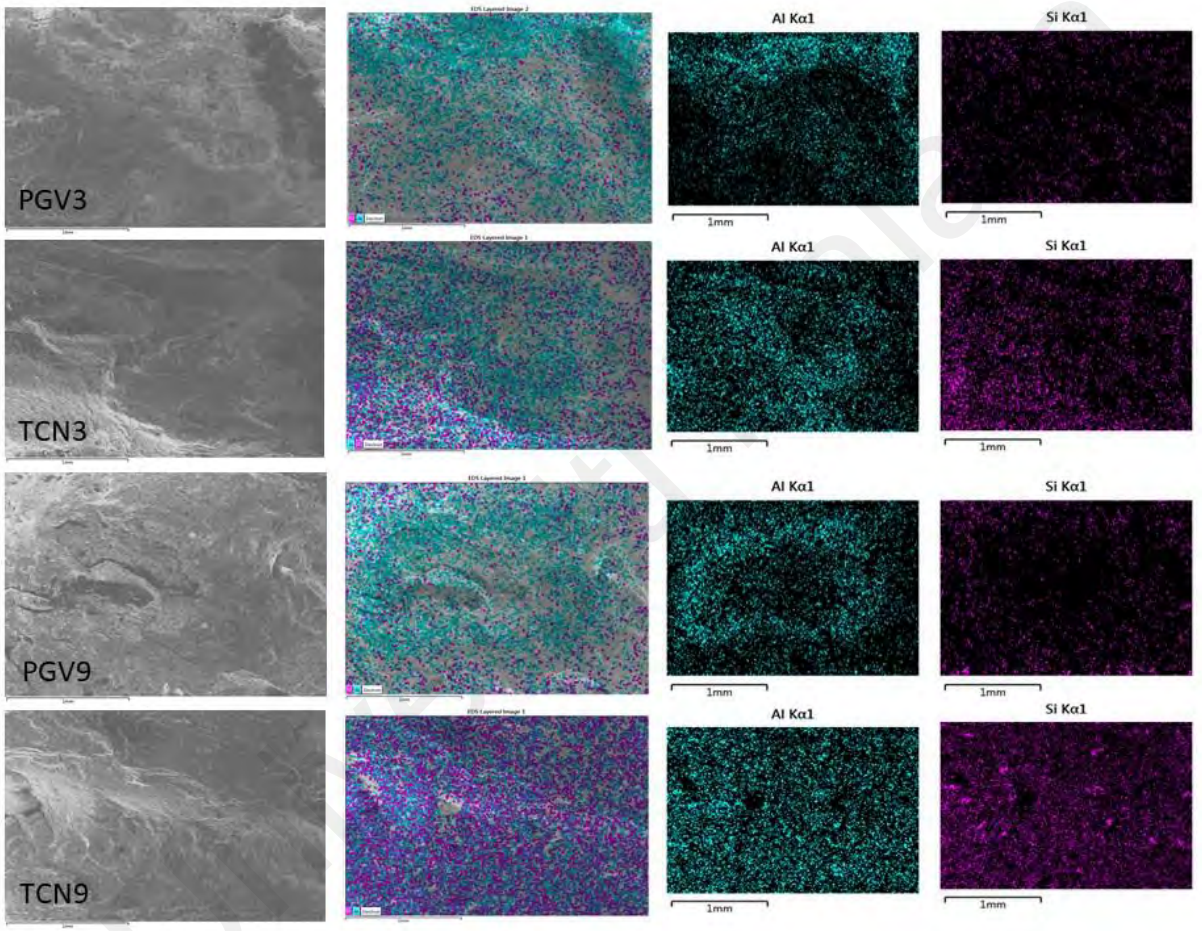

Figure 4.26: EDX mapping of treated and untreated MMT modified PHB.

The samples were further analysed with TEM to study the MMT nanoparticles' dispersion. The TEM images of PGV3 and TCN3 at 43k magnification are shown in Figure 4.27.

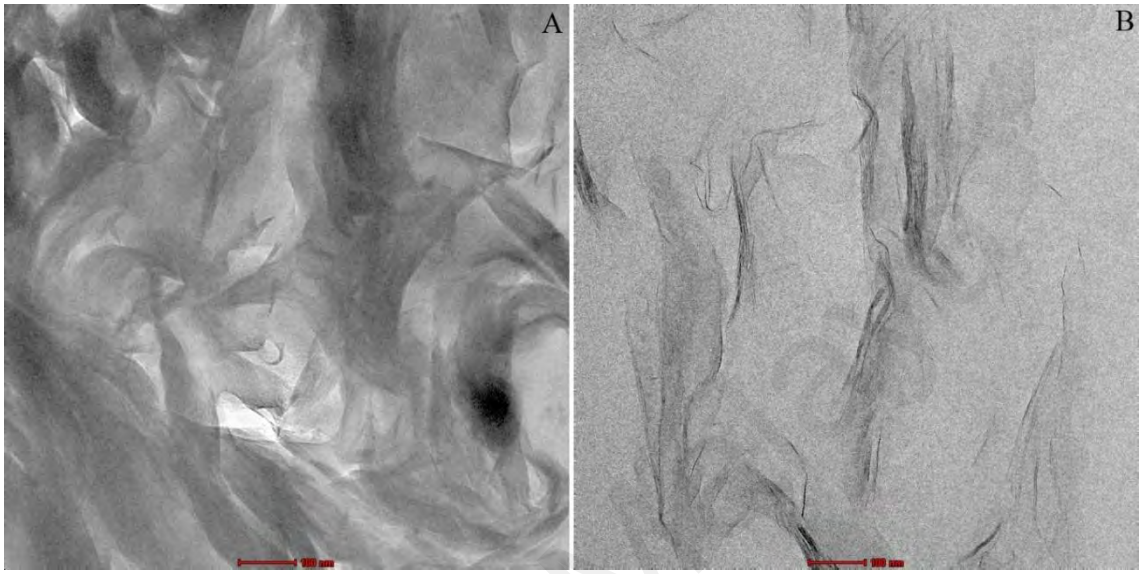

Figure 4.27: TEM image for untreated (A) and surface treated (B) MMT modified PHB at 43k magnification.

It can be seen that for PGV3, there is a severe agglomeration of the nanoclay. This agglomeration is due to the untreated clay having poor affinity to the resin. On the other hand, nanoparticles in TCN9 exhibit exfoliation, indicating good dispersion. The exfoliated layers can be observed in Figure 4.27. Exfoliation is only possible when the resin can penetrate and wet the interlayers of the nanoclay structure. The surface of untreated MMT is hydrophilic, while the surface of treated MMT is more hydrophobic, which allows the molten polymer to wet the treated clay more effectively.

In addition to increasing the hydrophobicity of the MMT, surface treatment of MMT also showed increased interlayer spacing (Liu & Wu, 2001). The increase in spacing allows the polymer melt to penetrate deeper into the MMT layered structure,

further facilitating the intercalation process. A schematic representation of the MMT treatment process and the increased interlayer distance is illustrated in Figure 4.28.

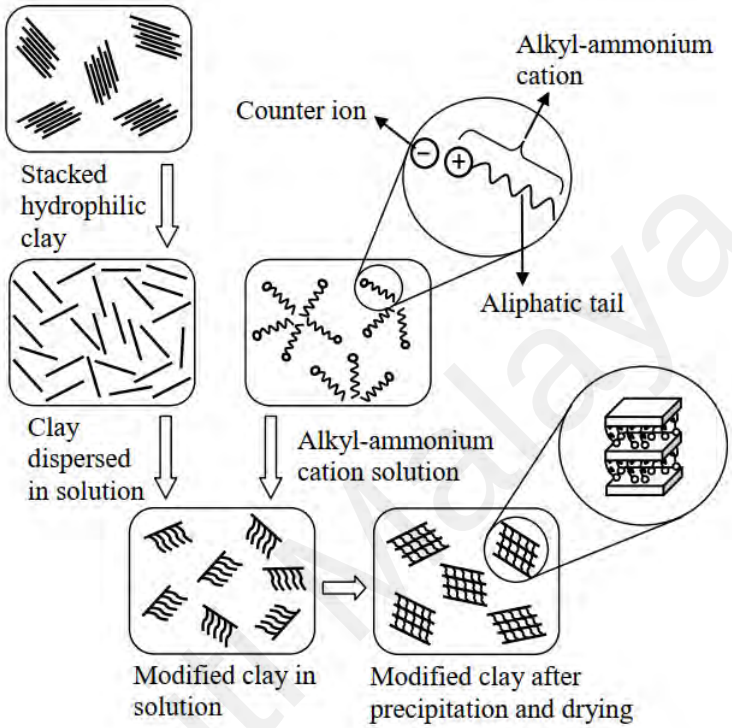

Figure 4.28: Schematic representation of clay surface treatment (Liu & Wu, 2001).

Although the modified MMT exhibited better exfoliation than untreated MMT, there are still stacks of unexfoliated MMT scattered consistently throughout the composite, as illustrated in Figure 4.29. The observation might indicate that even though processing was done at relatively higher RPM, the shear generated was insufficient to exfoliate most of the clay stacks thoroughly. The Brabender twin-screw extruder used in this study can reach a maximum screw speed of 1200 RPM. However, in preliminary testing done prior to the main research, it was determined that 200 RPM was the maximum screw speed that could be used for the current setup. When the RPM was increased further, due to the sticky nature of the PHB melt, it was impossible to produce

continuous extrudates even with an additional cooling setup, resulting in excessive amounts of wastage.

Figure 4.29: TEM image for TCN3 composites at 97,000 times magnification.

4.3.2 Thermal properties

4.3.2.1 Thermogravimetric Analysis (TGA)

The effect of clay content and surface treatment on the thermal stability of MMT modified PHB was studied using TGA. The TGA curves for TCN modified PHB are provided in Figure 4.30.

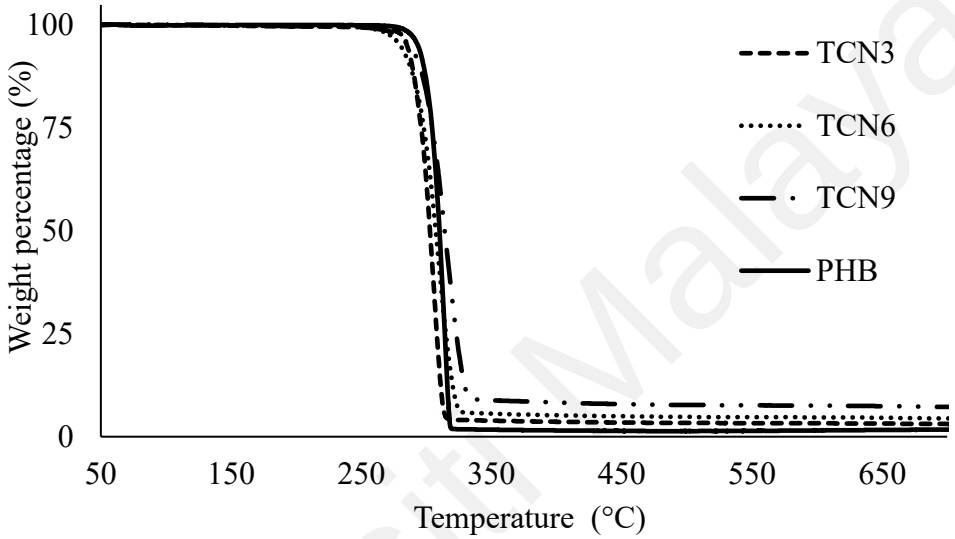

Figure 4.30 TGA curve of MMT modified PHB.

The modified composites exhibited a single degradation step, between 240°C - 400°C. The degradation occurs rapidly, evident by the sharp decline of the curve. It can be attributed to the degradation of the matrix, PHB. An in-depth study of the thermal degradation kinetics of MMT modified PHB by Achilias et al. (2011) found that the activation energy does not vary significantly with the degree of degradation, indicating a one-step degradation with similar values for pure PHB and all nanocomposites. The kinetic rate constant was also found to decrease with the amount of the MMT up to 3 wt%. However, once MMT content exceeded 10%, the kinetic rate constant was higher than neat PHB.

There is also a small amount of residue left, and the amount is higher for samples with more MMT added. For example, the residue for TCN3, TCN6 and TCN9 is 4.1%, 5.6% and 8.8%, respectively. It can be concluded that MMT did not degrade within the tested temperature range and under an inert environment. It was reported that the organic component of organically treated montmorillonite would degrade between 200°C to 500°C (Wang et al., 2016; Xie et al., 2001). However, weight loss due to these organic components was not detected due to their low content in the nanocomposite.

The onset temperature (T_{onset}), 50% degradation temperature ($T_{50\%}$) and derivative peak temperature (DT_p) extracted from Figure 4.30 were tabulated in Table 4.10.

Table 4.10. T_{onset}, $T_{50\%}$ and DT_p for MMT modified PHB.

Sample	T_{onset} (°C)	$T_{50\%}$ (°C)	DT_p (°C)
PHB	298.1	310.0	314.2
PGV3	289.1	301.8	306.6
PGV6	291.1	301.9	305.2
PGV9	290.0	299.1	302.6
TCN3	287.7	302.9	305.8
TCN6	291.9	307.0	309.3
TCN9	296.0	314.0	314.8

In general, the modified PHB exhibited lower T_{onset}, $T_{50\%}$ and DT_p compared to neat PHB. The T_{onset} for neat PHB is 298.1°C, while for PHB modified with 3 phr TCN is 287.7°C, which indicates that modified PHB will begin to degrade at a lower temperature. TCN3 exhibited the lowest thermal properties of all the MMT/PHB composites.

It has been reported that the presence of surfactants, in this case, the alkylammonium tallow used to treat the MMT surface, influenced the thermal degradation process (Bordes et al., 2009). At lower clay content, the shielding effect

offered by MMT is more negligible. Therefore, the thermal degradation is more impacted by the presence of the surfactants. The researchers also suggested that the surfactants could decompose according to the Hoffman elimination or a nucleophilic attack of the ammonium counter-ion, generally the chloride ion, on the ammonium. The decomposition products, amines or acidic protons, would enhance the random chain scission reaction of PHB. The reaction scheme is illustrated in Figure 4.31.

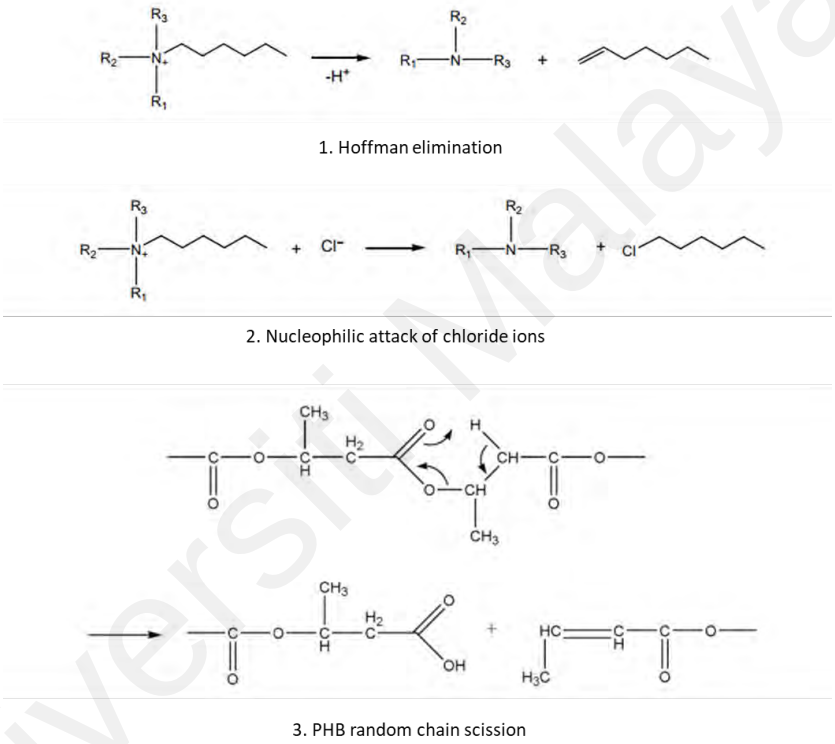

Figure 4.31: Reaction scheme for surfactant degradation and effect on PHB.

No clear trend regarding the thermal properties was observed for PGV as the clay content was increased from 3 phr to 6 phr. However, as the clay content was further increased to 9 phr, the thermal properties were reduced. Fitaroni et al. (2015) has suggested that organoclays typically have a degrading influence in the initial degradation steps at temperatures below 210°C and act as a stabiliser above 210°C. The researchers

reported that the stabilising effects were due to the delayed permeation of gases from participating in the oxidative reactions. However, since PGV9 exhibited various serious agglomerations, there is also a possibility that a large number of voids could also be present, although they were not observed in the SEM images. The presence of this void could provide a relatively more straightforward passage for the gases to participate in the degradation reaction, hence reducing the thermal stability.

For TCN, increasing the clay content causes the T_{onset}, $T_{50\%}$ and DT_p to increase. For example, T_{onset} increased by 9°C when clay content was increased from 3 to 9 phr. Salehabadi et al. (2014) has reported that increasing MMT content in PHB/MMT composites would result in a heat-shielding effect by the MMT nanoparticles. The nanoparticles would form a barrier that inhibits heat transfer to the polymer melt. For the shielding effect to be effective, MMT must be well dispersed in the matrix, which explains why the treated MMT composites exhibited better thermal stability at 6 and 9 phr than their untreated counterpart. Maiti et al. (2007) also attributed the thermal stability improvement to the ability of the clay to be a better mass transport barrier.

In contrast, Ollier et al. (2018) reported that increasing bentonite content in the composite decreased thermal stability. This trend was attributed to aluminium Lewis acid sites in the silicate layers, which could promote the thermal degradation of polyesters by catalysing the hydrolysis of ester linkages. The researchers suggested that bentonite's catalysing effect is more dominant at higher clay loading. The researchers also highlighted that the addition of nanoclay did not modify the degradation mechanism of PHB in the composite.

4.3.2.2 Differential Scanning Calorimetry (DSC)

The phase changes undergone by the material can be better understood through the information obtained from DSC analysis. The addition of clay particles was expected to disrupt or alter the crystallisation behaviour of PHB. As a result, the material's mechanical properties can also be altered as it is influenced by the molecular structure and arrangement of the matrix (crystalline structure, orientation of amorphous regions), especially the degree of crystallinity. The DSC curves of the samples are given in Figure 4.32. Melting temperatures, enthalpy heat of melting (ΔH_m) and the degree of crystallinity (X_c) for the composites were obtained from the curve and tabulated in Table 4.11.

Table 4.11. T_m, ΔH_m and X_c for MMT modified PHB.

Sample	T_m (°C)	ΔH_m (J/g)	X_c (%)
PHB	175.1	73.9	50.6
PGV3	172.3	76.1	52.1
PGV6	172.9	67.7	46.4
PGV9	169.4	73.8	50.6
TCN3	171.4	74.2	50.8
TCN6	170.8	65.5	44.9
TCN9	170.9	63.5	43.5

In general, the modification of PHB using both treated and untreated clays reduced the T_m of the material. For example, the T_m for neat PHB and TCN3 are 175.1°C and 171.4°C, respectively. T_m was significantly reduced for PGV/PHB composites when the clay content was increased to 9 phr. For treated clay modified PHB, no significant change in T_m was observed when the amount of clay was increased. This reduction is due to the restricted polymer chain mobility in the presence of fillers (Jimenez et al., 1997; Ogata et al., 1997). In addition, the level of penetration of the polymer into the MMT stacks also affected the composites' T_m. Polymer crystals formation on the surface of

intercalated MMT tends to be smaller, resulting in lower T_m. Lowering the T_m can benefit processing as there is a larger buffer zone between the polymer melting and before thermal degradation begins.

The addition of clay also causes X_c to decrease, especially at higher clay content. X_c for neat PHB and TCN9 are 50.6% and 43.5%, respectively. Bordes et al. (2008) suggested that although the presence of clay increases the nucleation rate of PHB, it also causes imperfection in the crystal structure, reducing its melting temperature. Hong and Huang (2015) also reported that the presence of silica accelerates the crystallisation process of the matrix. However, it is suggested that more agglomeration was observed at higher clay content due to the increased number of clay particles in the system. The presence of agglomeration would hinder the crystallisation process hence reducing X_c.

This suggestion is consistent with the observation in this study. For example, in TCN/PHB composites, X_c was reduced from 50.8% to 43.5% as the clay content was increased from 3 to 9 phr. A similar trend was observed for PGV/PHB composites. Jimenez et al. (1997) reported that a small amount of nanoclay in the polymer blend accelerated the crystallisation process. However, large quantities of the nanoclay would hinder the crystallisation process instead. The crystallisation rate is determined by two processes; nucleation and diffusion (Fatou, 1984). A smaller amount of nanoclay increases nucleation by acting as nucleation sites. However, excessive nanoclays hinder the transportation of polymer segments in the diffusion process. Mohamed El-Hadi (2014) reported that nanoclay serves as a nucleating agent in the PHB matrix. Analysis using polarized optical microscopy has shown that the spherulite sizes have become smaller, and the nuclei density was increased. However, the researchers highlighted that

the nanoclay was well dispersed in the matrix. Therefore, it is crucial to optimise the nanoclay content to get higher nucleation without hindering the diffusion step.

As discussed in section 4.3.1, the organomodified MMT TCN has a better affinity with the PHB matrix, resulting in better interaction. Exfoliation and intercalation of MMT stacks were observed. As explained earlier, MMT composites with exfoliated MMT tend to produce composites with lower T_m. Comparing PGV and TCN composites prepared in this study, PHB/TCN composites exhibited lower T_m. Xc reduction due to increasing clay content is more visible in TCN than PGV. This difference could be due to better interaction between the nanoclay and PHB, making the polymer chain transfer even harder than its untreated counterpart.

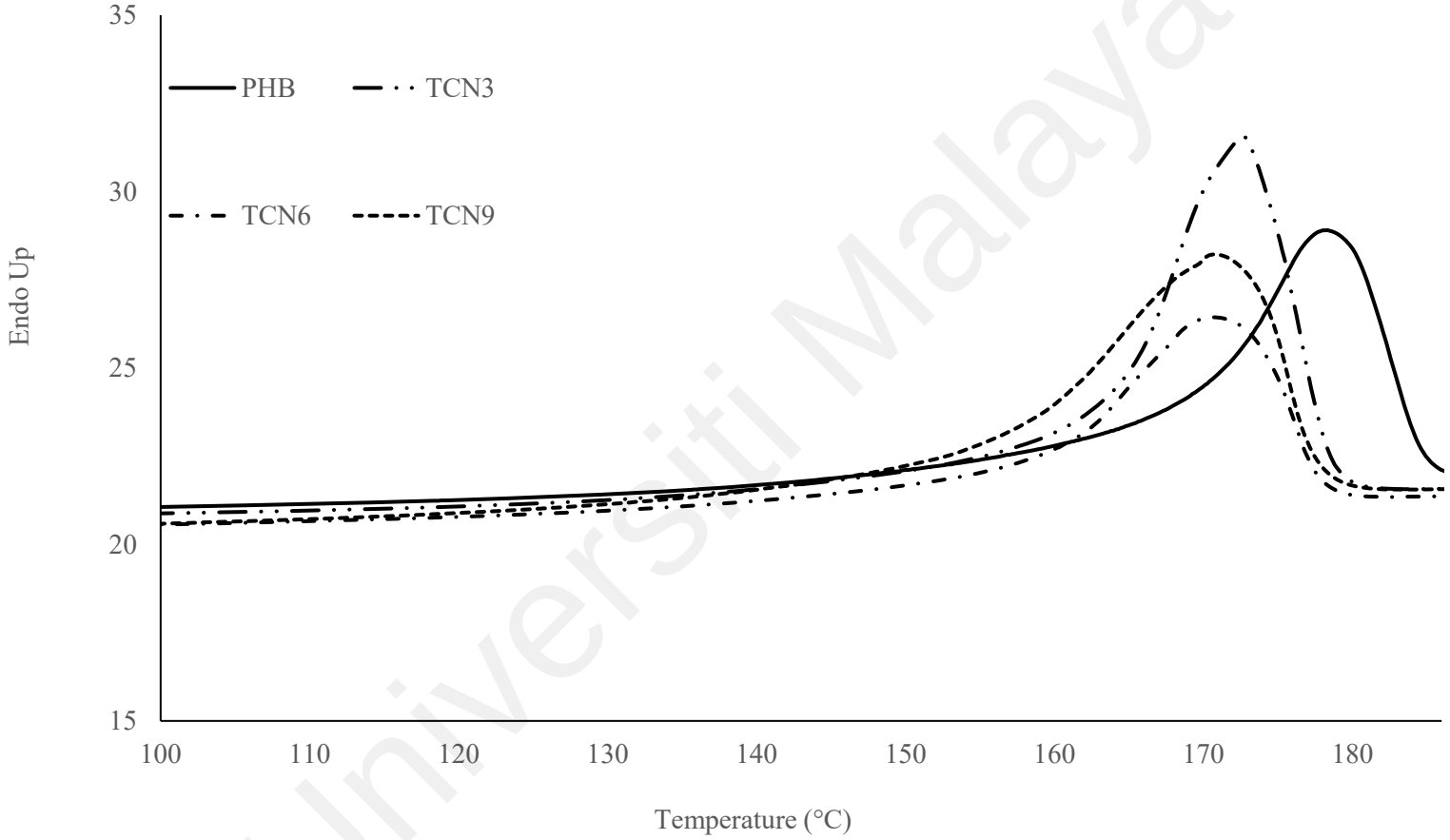

Figure 4.32 DSC curve of MMT modified PHB.

4.3.3 Rheology

Information from rheology can provide insight into the composites' internal structure and processability. The complex viscosity curve as a function of angular frequency for clay modified PHB is illustrated in Figure 4.33. From the figure, it can be observed that there are two different melt behaviours in the display. Complex viscosity (η*) for neat PHB and PGV samples increases slightly with increased angular frequency (ω). However, above 10 rad s^{-1}, the melts exhibited Newtonian fluid behaviour.

On the other hand, TCN samples exhibited shear thinning behaviour. Shear-thinning indicates that the melt initially behaves solid-like at lower ω and fluid-like behaviour at higher ω (Salleh et al., 2014). This difference in behaviour at lower angular frequencies between PGV and TCN samples indicates that compatibility between the matrix and the treated MMT is significantly better than the untreated MMT. It was also observed that increasing the nanoclay content increases the η*. Composites reinforced with treated nanoclay also exhibited higher η* for all nanoclay content, indicating the nanoclay and matrix having improved interaction. Viscoelastic properties such as the percolation threshold are susceptible to how the nanofillers are dispersed. The percolation threshold corresponding to the onset of solid-like behaviour can be observed at lower filler concentrations. The clay dispersion improves, the interaction between the nanofiller and the matrix is more substantial, or the filler aspect ratio is more prominent in treated clay composites than untreated clay composites (Thankappan et al., 2018). It was found that nanocomposites tend to form 3D networks through macroscopic interaction and that for a homogenous dispersion system, relatively lower filler loading may cause the 3D network and the composite system to exhibit solid-like behaviour (Jiang et al., 2016).

The storage and loss modulus for neat PHB and all the composites are illustrated in Figure 4.34 and Figure 4.35. Both storage modulus (G') and loss modulus (G") for neat PHB and all the composites increases with increasing ω. G' of the composite melts at lower ω is heavily influenced by the nanoclay content. The composite melt exhibited plateau at lower ω, and the magnitude of the plateau increases with increasing nanoclay content. The increase can be attributed to the increasing rigidity of the melt due to the addition of the nanoclay. G" also displayed a similar trend observed in G'. However, the plateau is only visible in TCN9. The melt behaves as a Maxwell fluid, which is typical for thermoplastic melts. The rheological behaviour of nanocomposites with treated MMT shows a gradual deviation of the G' slope at lower frequencies indicating a pseudo-solid-like property. This behaviour is a characteristic for the formation of clay mineral network-like structures that can reduce the mobility of the polymer chain in the melt and can be attributed to the percolation of the fillers (Issaadi et al., 2015). As stated earlier, it is more challenging to get good dispersion of the untreated nanoclay compared to its treated counterpart. Wang et al. (2016) reported that due to superior dispersion of surface treated carbon nanotubes (CNT), the rheological percolation was observed at lower filler concentration than untreated CNTs. Arrigo et al. (2017) also observed a similar phenomenon. The researchers reported that due to better interaction between the -OH modified CNTs and poly(styrene-butadiene-styrene) (SBS), the nanocomposites prepared using the treated CNT have higher viscosity and improved storage modulus.

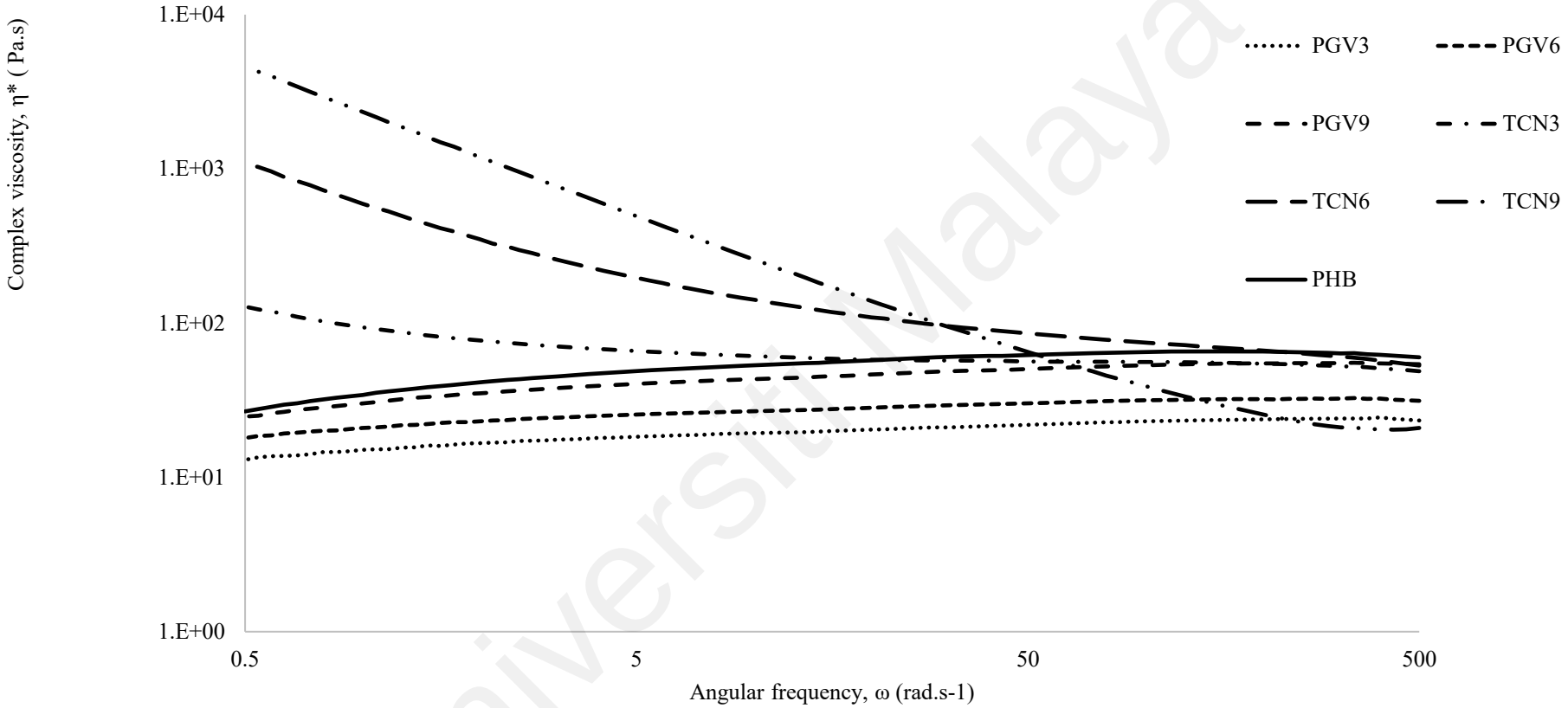

Figure 4.33 Complex viscosity of MMT modified PHB.

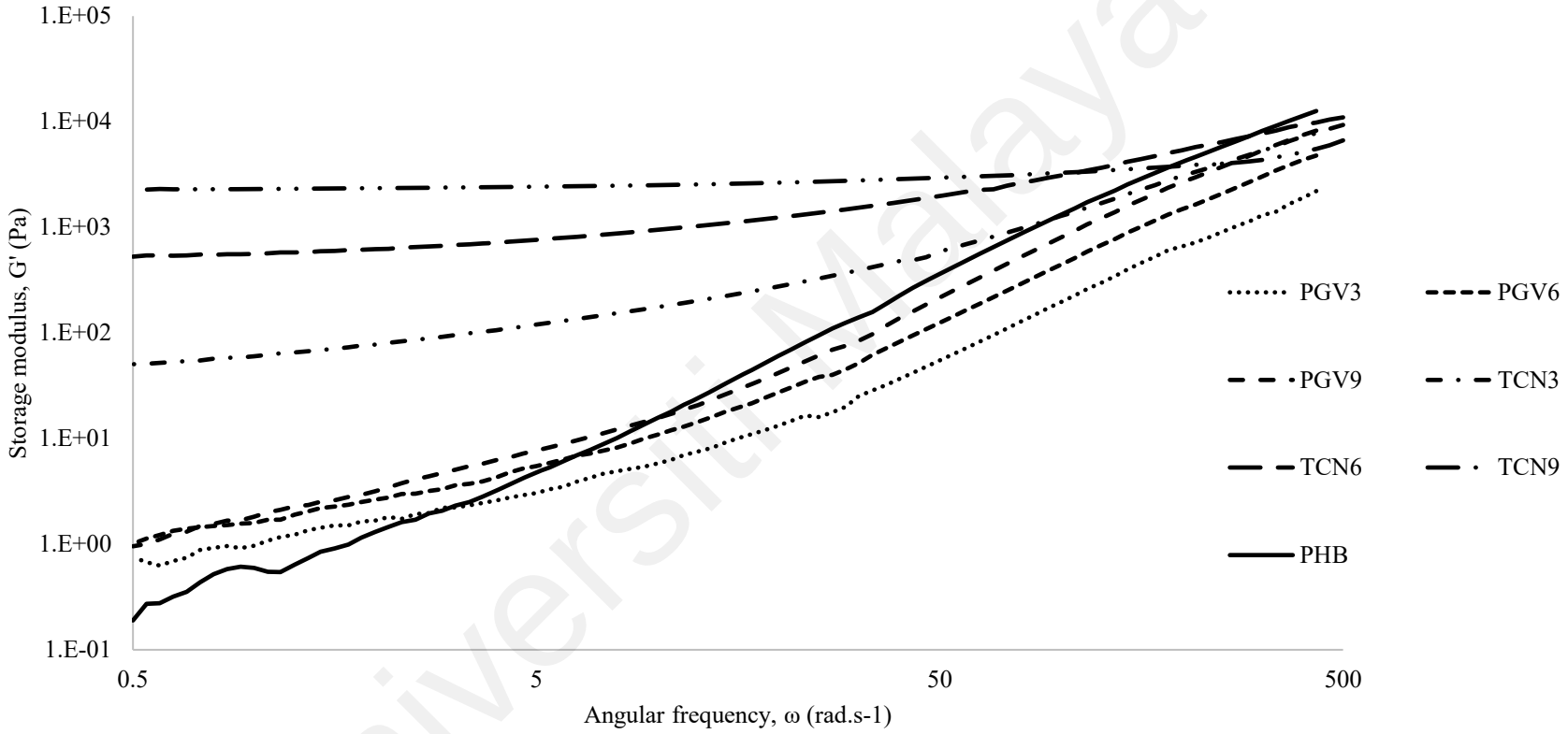

Figure 4.34 Storage modulus of MMT modified PHB.

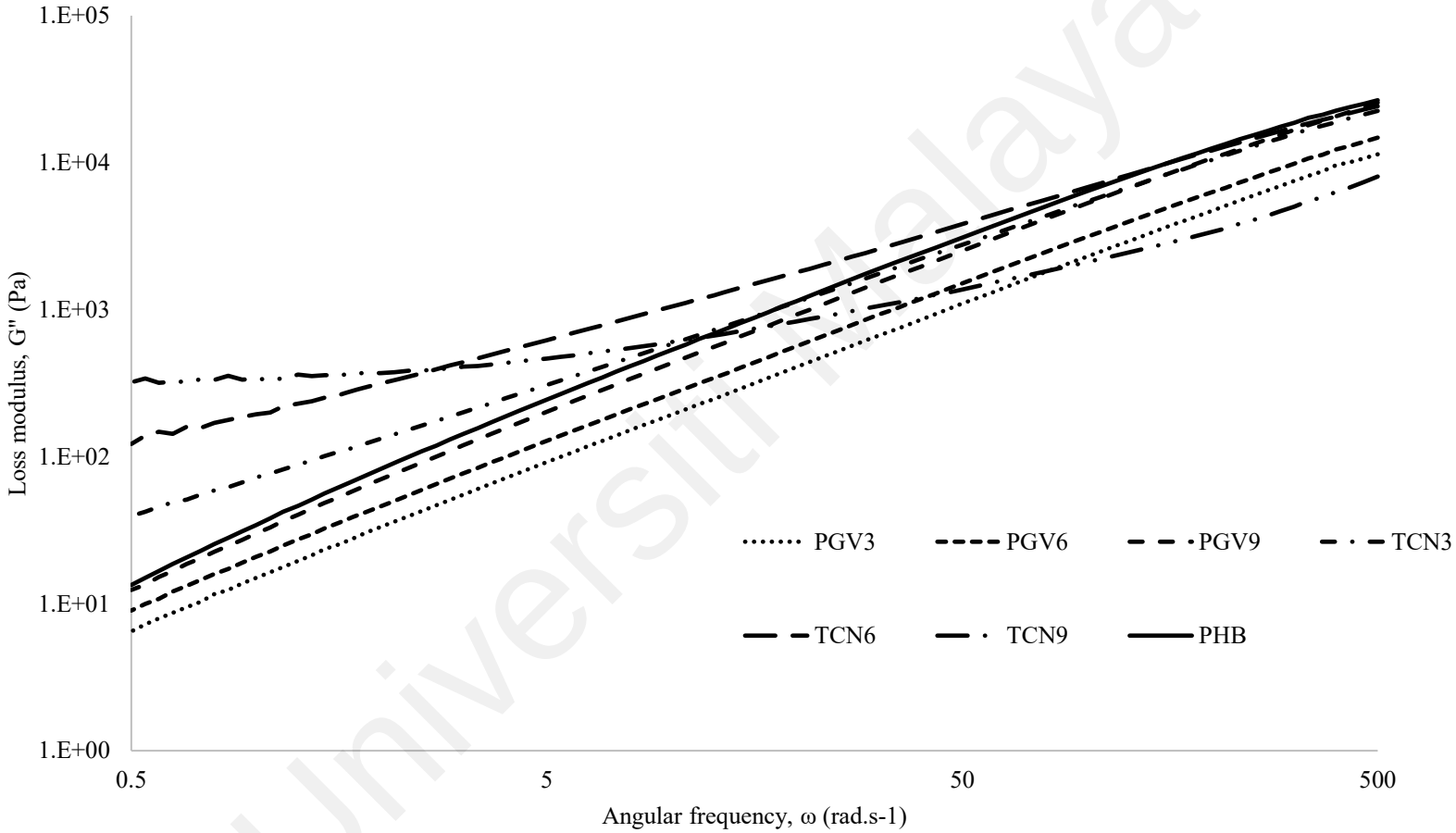

Figure 4.35 Loss modulus of MMT modified PHB.

4.3.4 Mechanical properties

4.3.4.1 Tensile properties

The tensile properties of the untreated and treated MMT modified PHB composites are tabulated in Table 4.12.

Table 4.12. Tensile properties of MMT modified PHB.

Sample	Young's modulus (GPa)	Tensile strength (MPa)	Elongation at break (%)
PHB	1.95	35.60	4.14
PGV3	1.96	29.08	1.91
PGV6	2.00	29.16	1.97
PGV9	1.98	30.62	2.33
TCN3	2.22	31.22	1.83
TCN6	2.33	28.82	1.45
TCN9	2.50	26.40	1.23

Young's modulus of PHB increased with the incorporation of treated and untreated MMT. Surface treated MMT offer more significant improvement compared to untreated MMT. For example, Young's modulus for PGV6 and TCN6 is 2.00 GPa and 2.33 GPa, respectively. This increase translates to a 3% and 19% improvement for PGV6 TCN6, respectively. MMT acts as mechanical reinforcement to the PHB matrix, reducing the flexibility of the matrix (Cyras et al., 2008). The reinforcement is even more effective when the interfacial interaction between matrix and MMT is better (de Moraes et al., 2011). The effect of clay content on Young's modulus was studied. Increasing the clay content increased Young's modulus for both the treated and untreated MMT modified composites. For example, Young's modulus for TCN increased from 2.22 GPa to 2.50 GPa when the clay content was increased from 3 phr to 9 phr. However, for PGV, further increase of clay content from 6 phr to 9 phr caused the modulus to decrease slightly, from 2.00 GPa to 1.98 GPa. Several researchers have also reported similar observations.

Jalalvandi et al. (2013) reported that, at lower MMT concentration, the formation of exfoliated structure contributes to higher tensile modulus. However, the researchers also reported that once the MMT loading exceeds the optimal level, the MMT particles were poorly distributed across the matrix and there was higher probability of MMT particles agglomeration. Agglomeration leads to the formation of segregated regions, which impart weaker lines between the MMT and the matrix. As a result, the sample breaks easily when subjected to stress. Similar trends were also reported by Liang et al. (2003) in their study of polyimide/MMT composites. When MMT content was below 3 wt%, the Young's modulus was increased with the increase in the MMT content. The increase in the modulus may be caused by the linear increase in the number of exfoliated MMT sheets at a lower MMT content. When the MMT content was further increased, the Young's modulus of the nanocomposite films levelled off or decreased slightly. This phenomenon may be caused by the aggregation of MMT in the matrix when the MMT content was high.

The tensile strength of the composite was lower than the neat PHB. For example, the tensile strength for PGV6 and TCN6 is 29.16 MPa and 28.82 MPa, respectively, which were lower than the tensile strength of neat PHB (35.6 MPa). The dispersion of the MMT was not optimal, resulting in a notching effect, which is typically seen in composites with a lower number of reinforcing components. During the study, parameters such as temperature and screw speed were optimised to have the best possible dispersion. However, the screw profile of the extruder can also play a part in the dispersion of the nanoclay. Better dispersion is possible with customised screw profiles explicitly designed to process PHB. Botana et al. (2010) reported that the introduction of modified mmt did not improve the tensile strength of the composite.

On the other hand, Bordes et al. (2008) reported a 15% tensile increase in a similar PHB/mmt system. Pavlidou & Papaspyrides (2008) highlighted that the intercalation/exfoliation ratio is the main factor responsible for improving mechanical properties. The researchers proposed that exfoliated particles are responsible for improving stiffness, while intercalated play a minor role.

The effect of MMT content on the tensile strength of the composite was studied. Tensile strength was not significantly affected by increasing the untreated MMT content. However, increasing the treated MMT content reduced the tensile strength of the composite. The tensile strength was reduced by 15% when treated clay content was increased from 3 phr to 9 phr. Arjmandi et al. (2015) reported similar observations in their PLA/CNW/MMT nanocomposites study. The researchers suggested that the decrease in tensile strength is due to agglomeration present in the system. As the nanoclay content increases, the probability of agglomeration also increases. From the TEM images in Figure 4.36, it was observed that at higher MMT content of 9 phr, more agglomerates of MMT were present compared to samples with 3 phr clay content.

Figure 4.36: TEM images for TCN3 (A) and TCN9 (B) at 43000 magnification.

The elongation at break of the composites is lower than neat PHB. For example, the elongation at break for PGV3 composite is 1.91% lower than the value for neat PHB (4.14%). A similar trend is observed for the treated MMT composites. This observation is expected since materials with higher modulus will resist deformation, resulting in lower elongation. When the clay content in the composite was increased, treated and untreated clay composite exhibited contrasting trends. For untreated clay reinforced composites, increasing the clay content from 3 phr to 9 phr causes the elongation at break to increase from 1.91% to 2.33%. On the other hand, increasing the clay content in treated clay composites causes the elongation at break to decrease from 1.83% (3 phr) to 1.23% (9 phr). The trend observed for elongation at break correlates with the trend observed for E.

4.3.4.2 Flexural properties

The flexural properties of the untreated and treated MMT-modified PHB composites were tested under a three-point bending setup. The flexural properties are essential to study as it describes the ability of the material to support the weight. Flexural modulus and flexural strength of MMT-modified PHB composites are compiled in Table 4.13.

Table 4.13. Flexural properties of MMT modified PHB.

Sample	Flexural modulus (GPa)	Flexural strength (MPa)	Flexural displacement (mm/mm)
PHB	2.65	54.70	0.03
PGV3	3.84	49.86	0.02
PGV6	3.64	49.67	0.02
PGV9	3.72	50.73	0.02
TCN3	3.87	48.58	0.02
TCN6	4.49	46.69	0.01
TCN9	4.62	40.56	0.01

Modification with MMT increases the flexural modulus of the system. The flexural modulus of neat PHB improved by 37% from 2.65 GPa to 3.64 GPa with 6 phr

untreated MMT. The improvement was even more significant (70%) when the treated MMT was added at the same clay content (4.49 GPa). The samples tend to fail catastrophically during flexural testing, with the sample breaking into two big pieces with smaller pieces shattering from the larger pieces. This behaviour may raise issues for designers planning to incorporate the material in their designs. However, it was found that the introduction of flexible fibres can mitigate this problem (Hassan et al., 2019).

The flexural modulus for TCN increased from 3.87 GPa to 4.62 GPa as the clay loading increased from 3 phr to 9 phr and overall was higher than the modulus for PGV composites at similar clay content. It was proposed that improved compatibility between treated MMT and the matrix allows for a high degree of intercalation or exfoliation of the nanoclay compared to untreated nanoclay (Chow et al., 2003; Modesti et al., 2005). The treated clay aggregates are smaller than untreated clay, and the silicate layers are better dispersed as the compatibility improves (Lertwimolnun & Vergnes, 2005).

The flexural strength of the MMT modified PHB is lesser than neat PHB. For example, the flexural strength for neat PHB is 54.70 MPa, while PGV3 is 49.86 MPa. A similar reduction is observed for TCN samples. Increasing the clay content reduces the flexural strength of the TCN samples. For example, the flexural strength reduced from 48.58 MPa to 40.56 MPa when the clay content increased from 3 phr to 9 phr. The flexural strength was relatively unchanged for untreated clay even when the clay loading was increased. It was reported that for MMT, optimal dispersion is usually achieved at relatively lower clay content (Kaynak et al., 2009). At higher clay concentrations, larger agglomerates and voids are present. These can act as a stress concentrator and causes the composite to fail prematurely.

Both PGV and TCN composites exhibited lower flexural displacement compared to neat PHB. Refer to Table 4.13. This reduction is expected as all the composites exhibited a higher modulus than neat PHB. For PGV, the flexural displacement remained constant as the clay content was increased. Increasing clay content in TCN composites from 3 phr to 9 phr causes the flexural displacement to decrease from 0.02 mm/mm to 0.1 mm/mm. As discussed earlier, the flexural modulus of the composites is higher than PHB and materials with higher modulus resist deformation more than materials with lower modulus. This behaviour is favourable if the material is used in similar load application situations such as beams.

4.3.4.3 Impact properties of the composite

Fracture energy (W) and peak load (P), critical strain energy release rate (G_c) and critical stress intensity factor (K_c) were calculated and reported in Table 4.14.

Table 4.14: Impact properties of MMT modified PHB composites.

	W (mJ)	P (N)	G_c (kJm^{-2})	K_c ($MPam^{-½}$)
PHB	100	436	3.1	3.2
PGV3	71	343	2.2	2.0
PGV6	69	326	2.1	2.4
PGV9	78	352	2.4	2.6
TCN3	63	309	1.9	2.3
TCN6	41	247	1.3	1.6
TCN9	32	237	1.0	1.8

For both untreated MMT modified PHB, increasing the clay content causes a mixed effect to W and P. For treated MMT modified PHB, increasing the clay content decreased W

and P, indicating poorer impact properties. For example, W for TCN3, TCN6 and TCN9 are 63 mJ, 41 mJ and 32 mJ, respectively. Similar trends were observed for G_c and K_c. The reduction observed in TCN modified PHB results from agglomeration at higher clay content. As observed previously, agglomeration may induce local stress concentration, resulting in reduced mechanical properties (Kusmono & Mohd Ishak, 2013).

The initial decrease of G_c for untreated MMT composites as the clay content was increased from 3 phr to 6 phr can be attributed to the reduced surface area due to clay-clay interaction (Ashraf et al., 2018). However, further increasing the clay content to 9 phr resulted in G_c increase simply due to the reinforcing effect of the clay particles.

It should be noted that the addition of both untreated or treated MMT resulted in lower impact properties compared to neat PHB. From the testing results, it can be suggested that MMT is not a suitable filler to improve the impact properties of PHB. It resulted in deterioration of the impact properties at higher clay content. However, the addition of MMT does offer improvement in other aspects, such as the barrier properties, which is beneficial in specific applications.

4.4 Conditioning

Typical mechanical testing of polymer composites is primarily performed in ambient laboratory conditions. However, testing is often performed in additional environmental conditions to determine properties of interest. The selection of these environmental conditions for testing is based on established limits of the composite material's usage and the environmental conditions expected in service.

The study was done between June 2016 and September 2016 in Petaling Jaya, Selangor. The monthly relative mean humidity, rainfall, and maximum and minimum temperature for those months were provided by the Department of Meteorology, Malaysia, in Table 4.15.

Table 4.15: Meteorological data for Petaling Jaya.

	Month			
	JUN	JUL	AUG	SEP
Mean Relative Humidity (%)	72.2	74.4	69.4	71.4
Daily Maximum Temperature (°C)	33.4	33.3	33.4	33.1
Daily Minimum Temperature (°C)	25.7	25.4	26.2	25.3
Daily Rainfall (ml)	288.4	251.8	124.4	269.0
No. of Raindays	11	15	11	12

4.4.1 Indoor exposure

4.4.1.1 Tensile properties

Exposure to indoor conditions simulates actual life conditions if PHB and its composites are used indoors. Indoor is the least harsh of the three conditions since the samples are protected from the sun and rain and do not directly contact soil

microorganisms. Both factors can lead to significant degradation of PHB composites. The Young's modulus, tensile strength and elongation at break are tabulated in Table 4.16.

Table 4.16: Tensile properties of PHB and its composites subjected to indoor condition.

Sample	Young's modulus (GPa)			Tensile strength (MPa)			Elongation at break (%)		
	0 months	2 months	4 months	0 months	2 months	4 months	0 months	2 months	4 months
PHB	1.95	1.94	2.06	35.55	31.29	34.55	4.14	2.48	2.57
UT5	2.12	2.07	2.23	32.07	29.11	31.76	2.91	2.08	2.16
UT10	2.21	2.11	2.31	31.36	28.29	30.24	2.66	2.07	1.90
UT20	2.68	2.37	2.49	31.28	27.28	29.04	2.25	1.83	1.77
CT5	1.97	2.34	2.25	29.97	32.34	31.62	2.78	2.24	2.37
CT10	2.12	2.44	2.44	27.44	30.41	29.74	2.19	1.91	1.92
CT20	2.36	2.75	2.60	26.28	28.03	27.53	1.93	1.67	1.75
PGV3	1.96	2.43	2.33	29.08	32.66	30.52	1.91	1.63	1.63
PGV6	2.00	2.51	2.33	29.16	31.71	30.76	1.97	1.60	1.73
PGV9	1.98	2.32	2.39	30.62	32.51	32.29	2.33	1.99	2.12
TCN3	2.22	2.71	2.58	31.22	33.13	32.92	1.83	1.55	1.68
TCN6	2.33	2.70	2.67	28.82	30.56	28.62	1.45	1.35	1.25
TCN9	2.49	2.98	2.97	26.40	26.95	27.53	1.23	1.01	1.08

The Young's modulus of the specimens in indoor condition exhibited a slightly increasing trend with increasing duration. Young's modulus for pure PHB slightly increased from 1.95 to 2.06 GPa after four months. A similar trend was observed in kenaf reinforced PHB and MMT modified PHB, as illustrated in Figure 4.37. The Young's modulus of composite CT20 and TCN3 increased from 2.36 to 2.60 GPa and 2.22 to 2.58 GPa, respectively. de Koning et al. (1993) have reported that embrittlement is a gradual process, and the microstructure of the polymer reaches equilibrium at about 150 days. The finding is in line with the observation made in this experiment. During the processing cycle in the moulding process, PHB did not have sufficient time to crystalise completely. Therefore, progressive crystallisation will continue to occur during storage. This observation was further supported by the increase in PHB density measured over the same period observed by de Koning et al. The materials would also absorb moisture from the environment over time, especially the untreated kenaf and untreated clay. The increase in moisture absorption can introduce defects in the structure, reducing its properties. Moisture can also penetrate the fibre-matrix interface, weakening the interfacial adhesion, leading to lower mechanical properties (Sanjeevi et al., 2021).

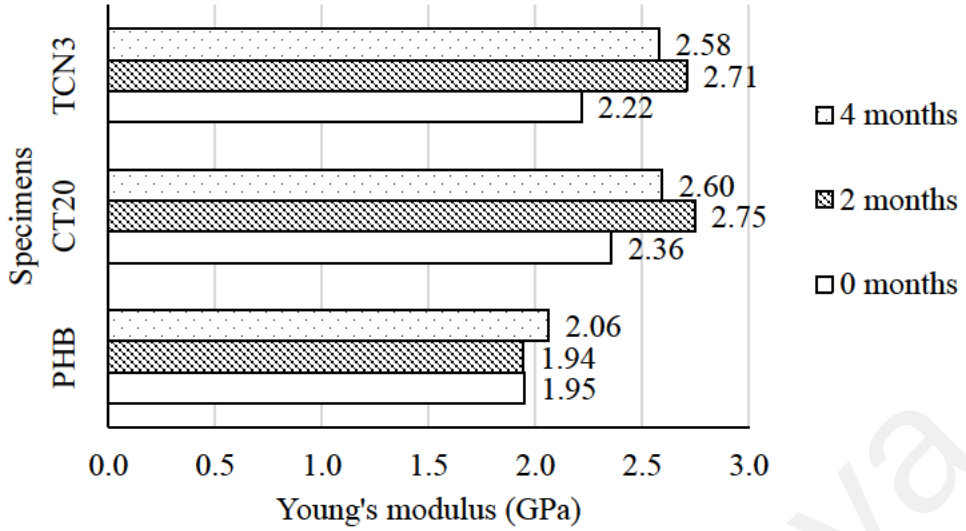

Figure 4.37: Young's modulus for PHB and its composites subjected to indoor condition.

The tensile strength of PHB is slightly reduced from 35.55 MPa to 31.29 MPa after the first two months. Then, it was increased slightly to 34.55 MPa. For CT20, after two months in indoor conditions, tensile strength increased slightly from 26.28 MPa to 28.03 MPa. Then, it decreased slightly to 27.53 MPa. MMT modified PHB also exhibited a similar trend to the kenaf reinforced composites. The initial decrease can be attributed to moisture absorption. Moisture absorption can lead to swelling and delamination of the reinforcing element, leading to lower tensile strength (Mortazavian et al., 2015). Overall, a downward trend is observed for the tensile strength of pure PHB and its composite subjected to indoor conditions, as illustrated in Figure 4.38. Generally, the changes observed for all the specimens are relatively negligible. No meaningful reduction in the energy required to break the specimen was observed in the timeline evaluated.

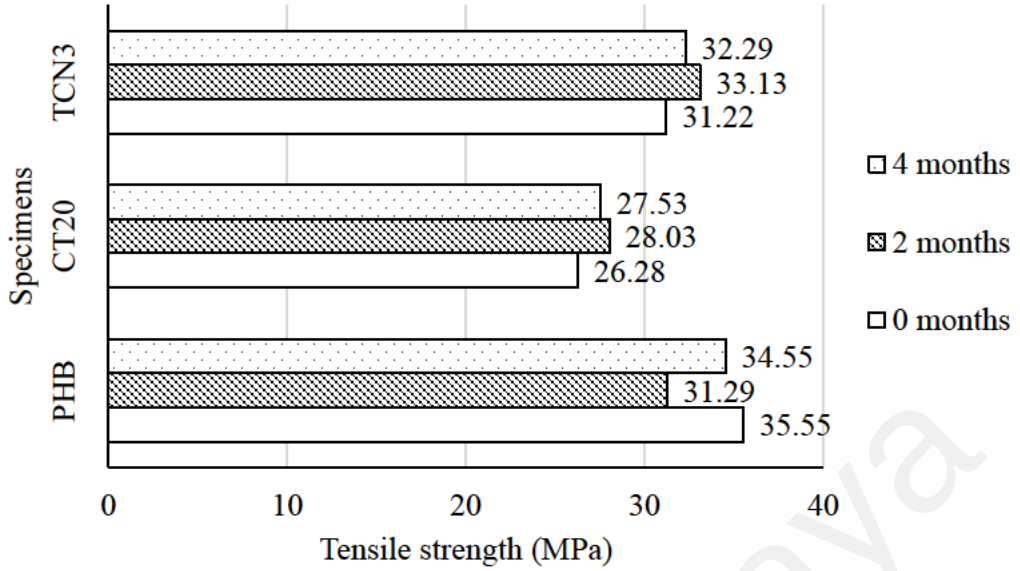

Figure 4.38: Tensile strength for PHB and its composites subjected to indoor condition.

Alata et al. (2007), in their study on the ageing of poly(3-hydroxybutyrate-co-3-hydroxyhexanoate), also reported similar tensile strength trends. The embrittlement of PHB did not result in any reduced strength. However, the change in failure mode, from ductile to brittle, can be very problematic. More ductile failure would allow engineers time to detect and take appropriate actions. In contrast, brittle fracture is usually a fast fracture. Stress needed to initiate a crack in a brittle material is lower than stress needed to grow a crack. It is fast, catastrophic with no prior warning signs (Hayes et al., 2015).

The change in fracture behaviour can be observed when studying the trend exhibited by elongation at break. The elongation at break of PHB was reduced by almost 38% after four months of exposure to indoor conditions. However, all PHB composites did not show any significant reduction in their elongation at break. Refer to Figure 4.39. Tensile strain for CT20 at zero and four months exposure is 1.93% and 1.75%, respectively. The change is relatively more minor than the change observed in pure PHB,

reducing it from 4.14% to 2.58%. This trend indicates that over the four months exposure period, PHB becomes increasingly brittle.

The tendency of material embrittlement in PHB has been reported by several researchers and is a well-known issue plaguing PHB (Crétois et al., 2016; de Koning et al., 1994; de Koning & Lemstra, 1993). During secondary crystallisation, the PHB molecule segment in the amorphous region, especially those covalently connected to the crystalline phase, exhibited reduced mobility. On the other hand, the kenaf reinforced composites, and MMT modified composites show that their tensile properties are relatively stable and consistent compared to pure PHB. A stable and consistent material is easier to evaluate by designers and engineers for application.

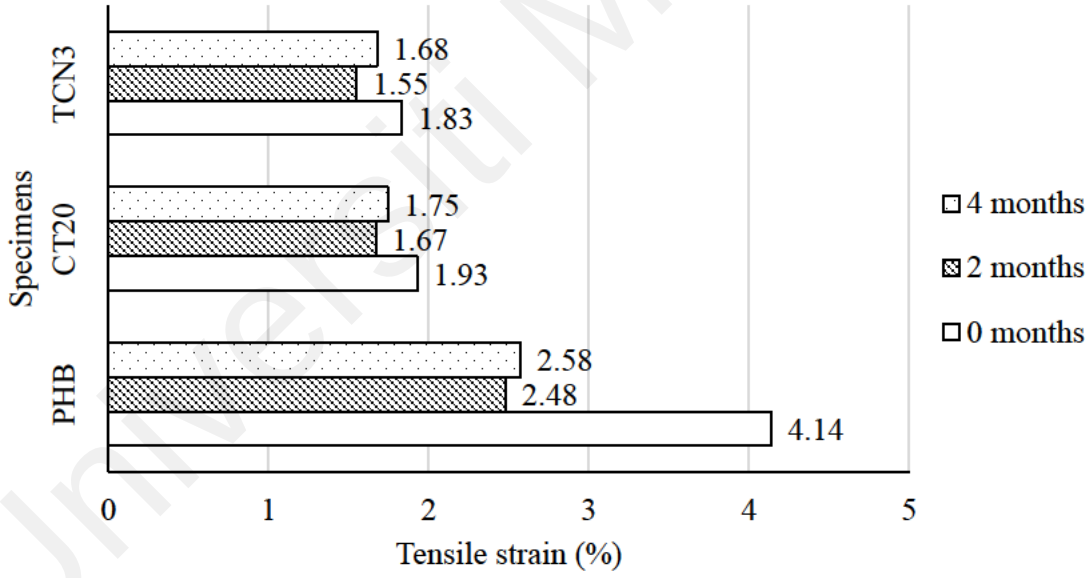

Figure 4.39: Elongation at break for PHB and its composites subjected to indoor condition.

4.4.1.2 Flexural properties

The flexural modulus and flexural strength of PHB and its composites subjected to the indoor condition are tabulated in Table 4.17. The flexural modulus and flexural strength of PHB, CT20 and TCN are illustrated in Figure 4.40 and Figure 4.41. The flexural modulus of PHB increases from 2.65 to 3.49 GPa after four months. The apparent increase in PHB can be attributed to its increasing crystallinity. Generally, the more crystalline material is stiffer compared to more amorphous material. Cretois et al. (2016) has extensively studied the secondary recrystallisation and physical aging of PHB. The researchers reported that physical ageing would cause the crystallisation peak temperature to shift to a lower temperature. Biddlestone et al. (1996) also reported that the glass transition temperature of PHB was shifted from -6°C to 3°C after a 60 minutes ageing period at -13°C. On the other hand, CT20 remains almost unchanged, and TCN3 increased slightly from 3.87 to 4.10 GPa.

Table 4.17: Flexural properties of PHB and its composites subjected to indoor conditions.

Sample	Flexural modulus (GPa)			Flexural strength (MPa)			Flexural displacement (mm/mm)		
	0 months	2 months	4 months	0 months	2 months	4 months	0 months	2 months	4 months
PHB	2.65	3.04	3.49	54.70	47.14	53.08	0.03	0.02	0.02
UT5	2.93	2.88	3.68	54.60	45.20	53.32	0.03	0.02	0.02
UT10	3.75	2.69	3.81	56.90	41.27	53.56	0.02	0.02	0.02
UT20	4.04	2.07	3.89	58.30	36.67	54.69	0.02	0.03	0.02
CT5	3.58	3.78	3.88	53.58	54.88	56.20	0.02	0.02	0.02
CT10	3.82	3.93	3.94	52.62	54.74	56.19	0.02	0.02	0.02
CT20	4.29	4.37	4.36	52.73	53.40	55.36	0.02	0.02	0.02
PGV3	3.84	4.19	3.59	49.86	49.40	48.01	0.02	0.01	0.01
PGV6	3.64	4.05	3.94	49.67	51.51	49.94	0.02	0.01	0.01
PGV9	3.72	4.01	3.84	50.73	53.86	52.75	0.02	0.02	0.02
TCN3	3.87	4.28	4.10	48.58	53.85	50.08	0.02	0.02	0.01
TCN6	4.49	4.53	4.33	46.69	47.23	45.74	0.01	0.01	0.01
TCN9	4.62	4.81	4.07	40.56	41.67	39.16	0.01	0.01	0.01

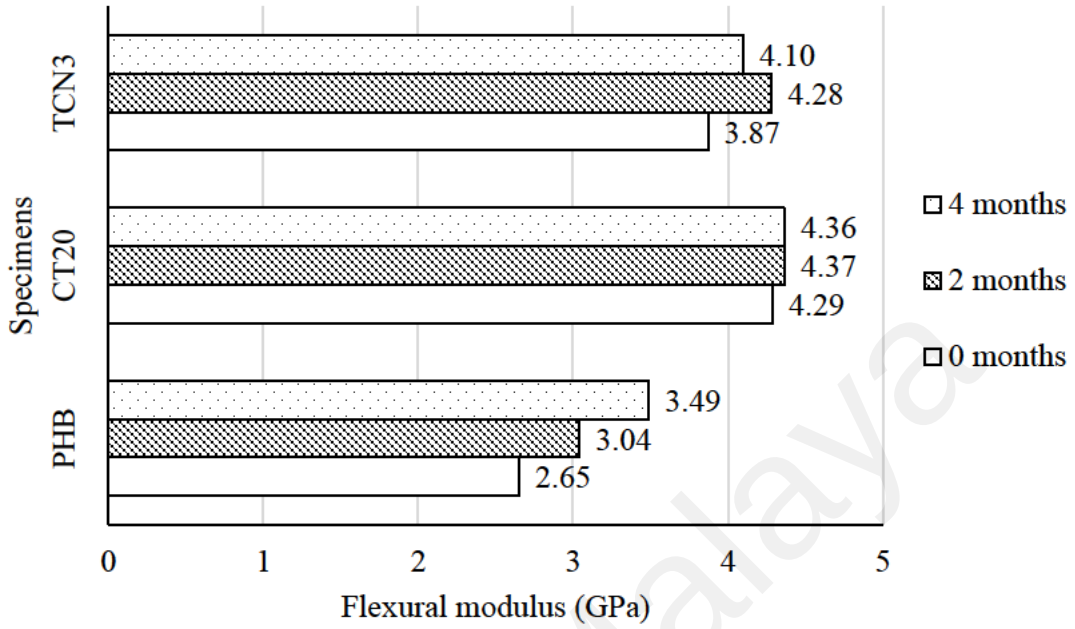

Figure 4.40: Flexural modulus for PHB and its composites subjected to indoor condition.

de Koning et al. (1994) also studied the effect of crystal morphology on the toughness of PHB. The researchers suggested that moulded PHB specimens possess a large crystalline-amorphous interface per unit volume. Any process involving this interface, such as crystal rearrangement, will give a more profound effect than other semicrystalline polymers. It can be postulated that the presence of fillers in the form of kenaf fibres or MMT particles might have interfered in the normal crystallisation behaviour of PHB, resulting in less crystalline-amorphous interphase. This interference would result in a lesser impact of secondary recrystallisation on the material properties.

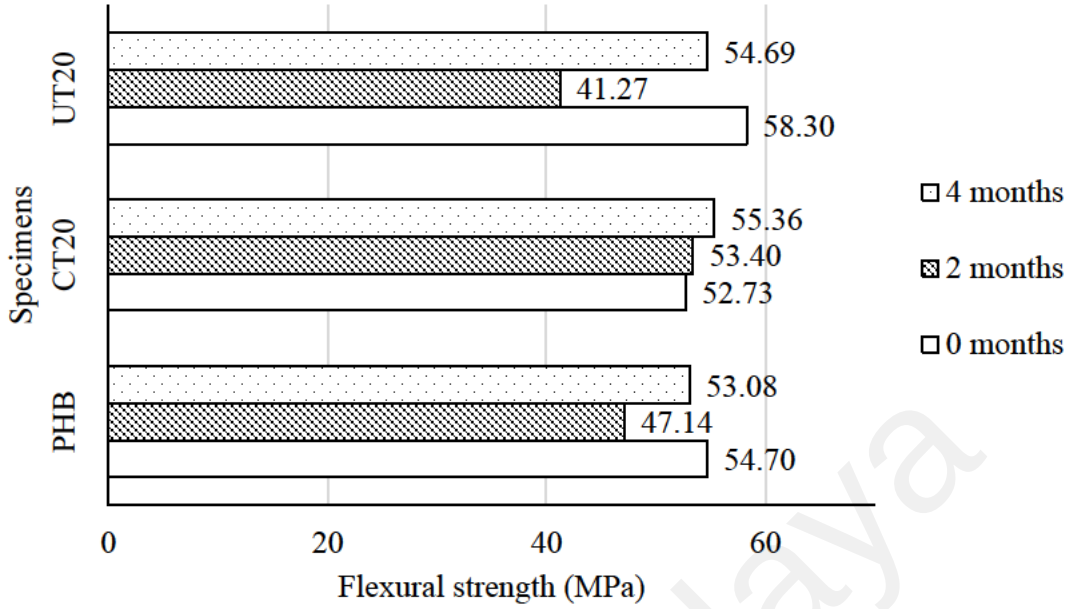

Figure 4.41: Flexural strength for PHB and its composites subjected to indoor condition.

The stability shown by surface-treated kenaf reinforce PHB composite over its untreated counterpart can be attributed to the former's reduced sensitivity to moisture (Satyanarayana et al., 2009). For example, the flexural strength of UT20 was reduced from 58.30 MPa to 41.27 MPa after two months in the indoor environment. The reduction was observed in all untreated kenaf reinforced composites, and the magnitude of reduction is higher with increasing fibre content. Moisture uptake can lead to fibre swelling, which causes dimensional instability in the material.

In general, the flexural displacement exhibited trends correlated to the flexural modulus. For example, the flexural modulus for PGV6 increased when subjected to indoor conditions for two months, from 3.64 GPa to 3.94 GPa. Correspondingly, the flexural displacement was reduced from 0.02 mm/mm to 0.01 mm/mm. However, there were instances where the reported flexural displacement remained constant. Refer to

Table 4.17. For example, the flexural displacement for CT5 at zero month and four months exposure are both 0.02 mm/mm, even though the flexural modulus changed from 3.58 GPa to 3.88 GPa. Possibly, there was a reduction in the displacement, but it was minuscule.

4.4.2 Outdoor exposure

4.4.2.1 Tensile properties

The Young's modulus, tensile strength and elongation at break for specimens subjected to the outdoor condition are tabulated in Table 4.18. Based on the meteorological data in Table 4.15, the relative humidity during the exposure months ranges between 69.4% to 74.4% relative humidity. Temperature ranges from 25.4°C to 33.4°C with average daily rainfall of around 233.4 ml. The outdoor condition is generally more humid than the indoor one, with cyclical exposure to UV and relatively elevated temperatures. This difference is due to the indoor specimens being shielded from direct sunlight and rainfall.

The Young's modulus for PHB exhibited no significant trend after exposure to outdoor conditions for four months. Untreated kenaf reinforced PHB composites exhibited a reduction in its Young's modulus, from 2.68 GPa at zero month to 2.26 GPa at four months. Treated kenaf PHB composites and treated MMT modified PHB exhibited similar behaviour. Both show Young's modulus increase after the first two months. However, between two to four months, a negligible difference was observed. The trend was shown by all treated kenaf reinforced PHB composites, and MMT modified composites regardless of filler loading and are illustrated in Figure 4.42.

Untreated kenaf composites exhibited decreasing tensile strength can be attributed to the fibre composition. As discussed in section 4.1.1, untreated kenaf fibres contain more lignin and hemicellulose than alkali-treated kenaf fibres. Several researchers have reported that removal of lignin and hemicellulose resulted in lower moisture uptake (Pejic et al., 2008; Salim et al., 2020). Hemicellulose has been attributed as the main water-absorbing component, although lignin and cellulose play a minor role. Water uptake in fibre reinforced composites can lead to fibre swelling, resulting in the formation of micro-cracks at the fibre-matrix interface, reducing its strength (Dhakal et al., 2007; Halip et al., 2019; Muñoz & García-Manrique, 2015). It is also well known that higher fibre content would result in more moisture uptake.

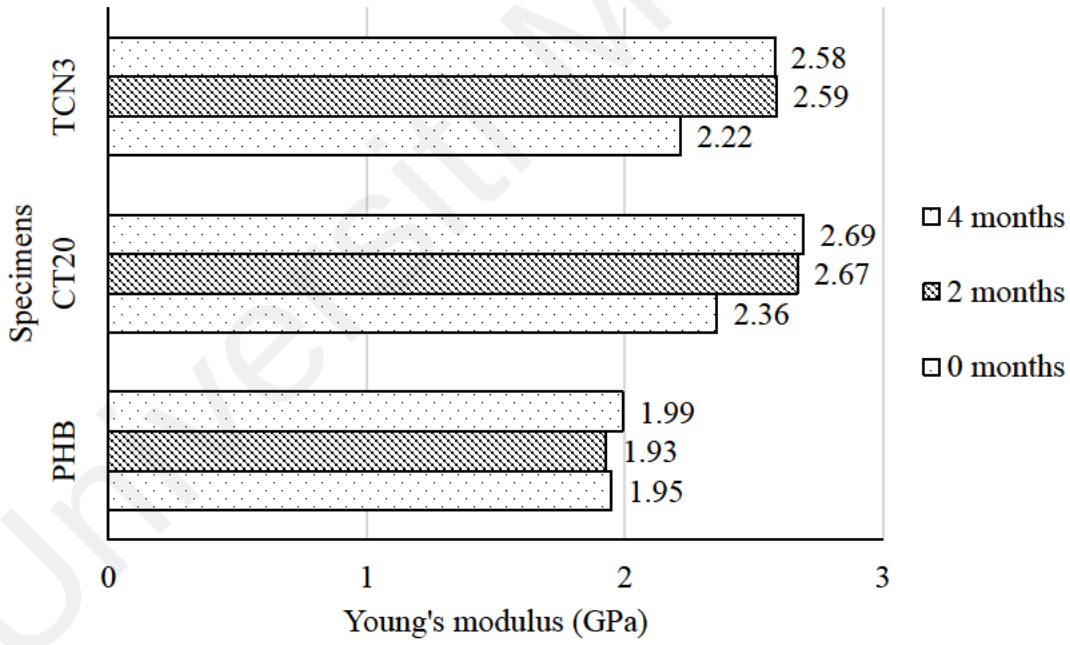

Figure 4.42: Young's modulus for PHB and its composites subjected to outdoor condition.

Lim & Kim (2016) studied the mechanism of UV degradation for poly(3-hydroxybutyrate-co-3-hydroxyhexanoate). The researchers reported that the average

molecular weight of the molecules decreased while the polydispersity index was increased as the polymer was subjected to UV. It was also reported that the crystallinity of the polymer was increased after exposure to UV. Tertyshnaya and Shibryaeva (2013) observed that a combination of exposure to UV and water causes degradation to occur via chain scission.

Table 4.18: Tensile properties of PHB and its composites subjected to outdoor condition.

Sample	Young's modulus (GPa)			Tensile strength (MPa)			Elongation at break (%)		
	0 months	2 months	4 months	0 months	2 months	4 months	0 months	2 months	4 months
PHB	1.95	1.93	1.99	35.55	31.00	32.60	4.14	2.40	2.51
UT5	2.12	2.03	2.23	32.07	29.46	29.65	2.91	2.30	2.15
UT10	2.21	2.09	2.15	31.36	28.02	28.71	2.66	2.17	2.08
UT20	2.68	2.18	2.26	31.28	26.29	26.84	2.25	2.14	2.00
CT5	1.97	2.42	2.47	29.97	32.67	31.85	2.78	2.18	2.17
CT10	2.12	2.60	2.47	27.44	30.79	28.87	2.19	1.86	1.80
CT20	2.36	2.67	2.69	26.28	27.29	27.09	1.93	1.54	1.61
PGV3	1.96	2.37	2.37	29.08	31.45	30.34	1.91	1.66	1.53
PGV6	2.00	2.30	2.34	29.16	31.46	30.23	1.97	1.75	1.65
PGV9	1.98	2.30	2.33	30.62	32.91	31.30	2.33	2.10	1.82
TCN3	2.22	2.59	2.58	31.22	33.19	30.78	1.83	1.53	1.43
TCN6	2.33	2.69	2.78	28.82	30.78	29.36	1.45	1.34	1.27
TCN9	2.49	2.86	2.94	26.40	27.69	26.21	1.23	1.09	1.01

The tensile strength for PHB was reduced slightly after four months of outdoor exposure and is illustrated in Figure 4.43. The tensile strength was reduced from 35.55 MPa to 32.60 MPa. A similar trend was observed for UT composites, and MMT modified PHB. Tensile strength for UT20 was reduced from 31.28 MPa at zero month to 26.84 MPa at four months. On the other hand, tensile strength for CT remained relatively the same over the four months, between 26.28 MPa to 27.09 MPa. Humidity ageing is recognised as the leading cause for the long-term failure of organic composites (Akil et al., 2011; Merdas et al., 2002). Plasticisisation of the matrix, differential swelling related to concentration gradients, embrittlement linked to the degradation of the macromolecular skeleton by hydrolysis, osmotic cracking, hygrothermic shock with the change of water state and localised damage to the fibre-matrix interface can all contribute to a lower tensile strength. Fading colour from dark brown to whitish and reduced tensile strength has been widely reported as a common effect of kenaf fibre reinforced composites to UV (Abdullah et al., 2019; Akil et al., 2011; Chee et al., 2019; Merdas et al., 2002).

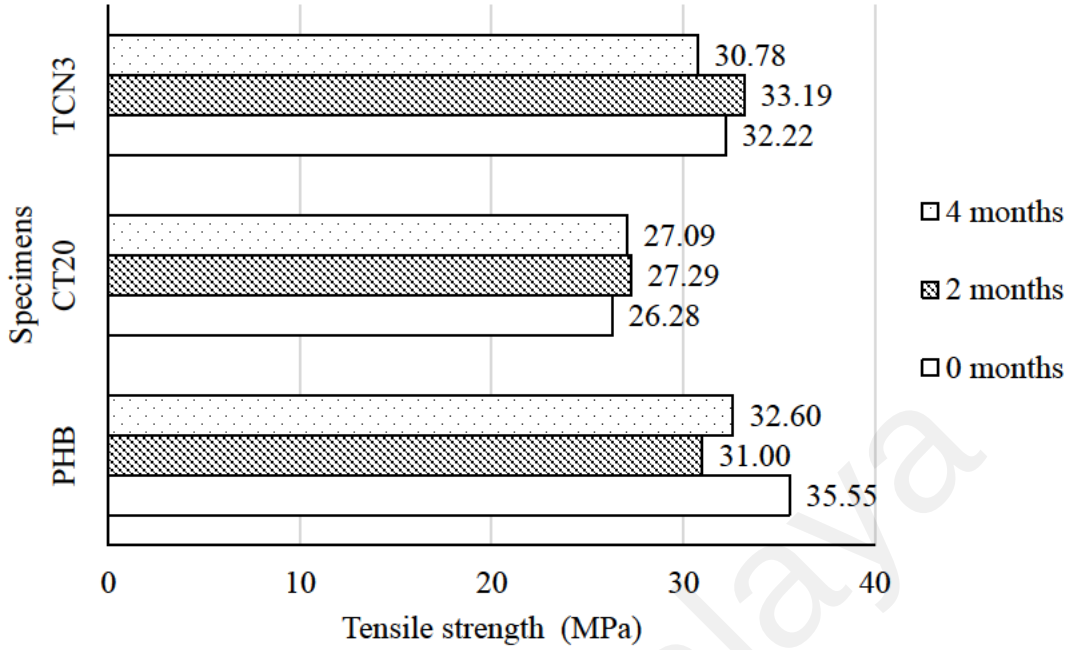

Figure 4.43: Tensile strength for PHB and its composites subjected to outdoor condition.

The elongation at break for PHB and all composites exhibited a downward trend. Refer to Figure 4.44. However, the reduction in elongation at break for pure PHB was most drastically reduced from 4.14% to 2.51% after the four months. It was reported that PHB is susceptible to UV attack, which results in the development of micro-cracks (de Koning et al., 1997). These cracks can contribute to the lowered tensile strength and elongation at break observed in the PHB samples. These micro-cracks would act as stress concentrators which accelerates the failure process. In addition, the energy need for crack initiation was also reduced.

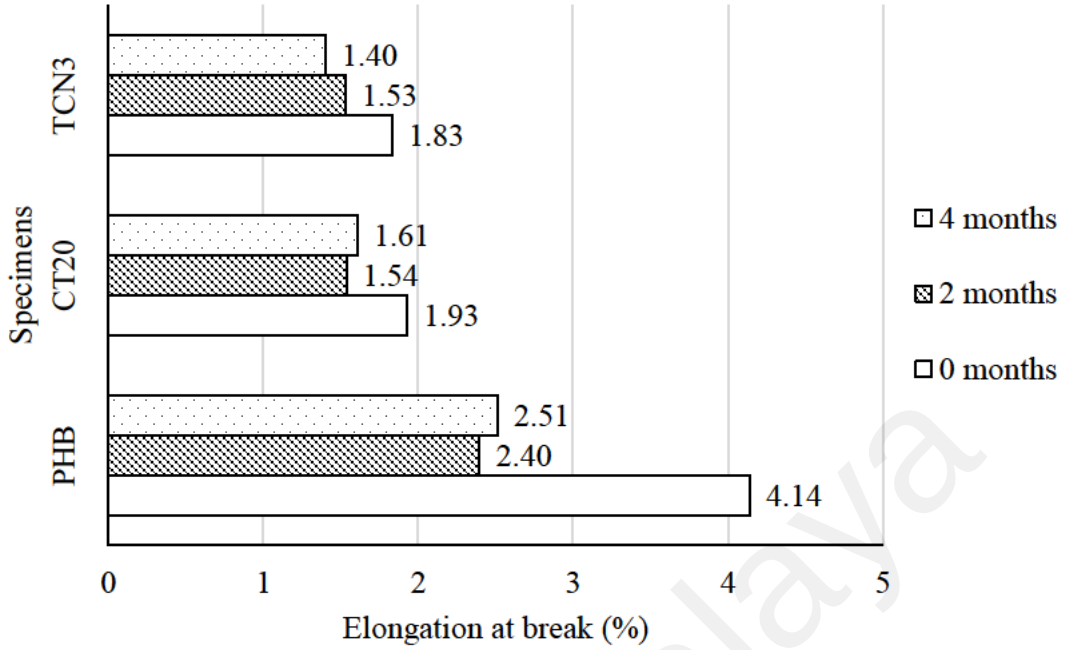

Figure 4.44: Elongation at break for PHB and its composites subjected to outdoor condition.

4.4.2.2 Flexural properties

Flexural modulus and flexural strength of PHB and its composites subjected to outdoor conditions for up to four months are tabulated in Table 4.19.

The flexural modulus for PHB and MMT modified PHB increase with increasing duration in outdoor conditions. Refer to Figure 4.45. The flexural modulus increased from 2.65 GPa at zero months to 3.47 GPa at four months. TCN3 increased from 3.87 GPa at zero month to 4.38 GPa at four months. The upward or downward trend of kenaf reinforced PHB composites can be attributed to their fibre loading. At 5% fibre loading, both treated and untreated composites exhibited increasing flexural modulus. However, the flexural modulus exhibited a downward trend at 20% fibre loading. UT20 exhibited a more pronounced reduction, from 4.04 GPa at the beginning to 3.67 GPa after two months.

Flexural modulus for CT20 composite was slightly reduced from 4.29 GPa to 4.10 GPa within the same period. This observation further reinforced the idea that the chemical treatment of kenaf improved its long-term durability, especially towards moisture and UV attack (Pejic et al., 2008; Salim et al., 2020).

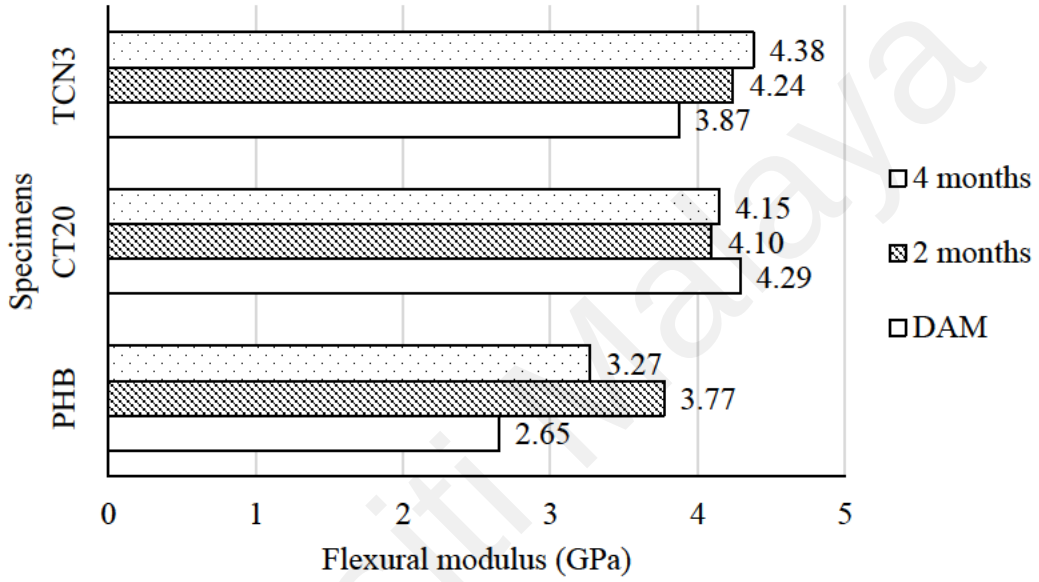

Figure 4.45: Flexural modulus for PHB and its composites subjected to outdoor condition.

Table 4.19: Flexural properties of PHB and its composites subjected to outdoor condition.

Sample	Flexural modulus (GPa)			Flexural strength (MPa)			Flexural displacement (mm/mm)		
	0 months	2 months	4 months	0 months	2 months	4 months	0 months	2 months	4 months
PHB	2.65	3.77	3.47	54.70	55.19	50.68	0.03	0.02	0.02
UT5	2.93	3.84	3.60	54.60	54.50	49.31	0.03	0.02	0.02
UT10	3.75	3.74	3.73	56.90	51.00	47.95	0.02	0.02	0.02
UT20	4.04	3.67	3.62	58.30	50.34	47.80	0.02	0.02	0.02
CT5	3.58	3.91	3.94	53.58	56.58	56.89	0.02	0.02	0.02
CT10	3.82	4.09	4.07	52.62	55.37	56.38	0.02	0.02	0.02
CT20	4.29	4.10	4.15	52.73	51.75	48.82	0.02	0.02	0.02
PGV3	3.84	4.16	4.34	49.86	49.36	48.29	0.02	0.01	0.01
PGV6	3.64	4.06	4.22	49.67	49.35	50.97	0.02	0.01	0.01
PGV9	3.72	3.97	4.07	50.73	52.86	53.10	0.02	0.02	0.02
TCN3	3.87	4.24	4.38	48.58	51.42	51.39	0.02	0.01	0.01
TCN6	4.49	4.56	4.74	46.69	46.29	44.36	0.01	0.01	0.01
TCN9	4.62	4.52	4.96	40.56	39.81	38.32	0.01	0.01	0.01

The flexural strength for MMT modified PHB did not significantly change after the four-month exposure period. Refer to Figure 4.45. For example, the flexural strength for TCN3 at zero, two months and four months exposure are 48.58 MPa, 51.42 MPa and 51.39 MPa, respectively. A similar observation was recorded for PGV modified PHB composites. UT composites exhibited decreasing flexural strength. For example, the flexural strength for UT10 was reduced from 56.90 MPa to 47.95 MPa after four months. For treated kenaf reinforced composites, specimens with the highest fibre loading of 20% exhibited decreasing flexural strength, while specimens with 5% and 10% fibre loading exhibited an increasing trend. The ageing of a composite involves multiple processes and is very complex. For kenaf reinforced PHB composites, known phenomena include moisture uptake, secondary crystallisation and physical ageing of the PHB matrix and UV attack on both fibre and matrix. This complex interaction results in the mixed behaviour observed in the flexural strength of PHB and its composites. At a glance, it can be be

postulated that outdoor exposure is more detrimental to specimens reinforced with untreated kenaf or with treated kenaf at higher fibre loading.

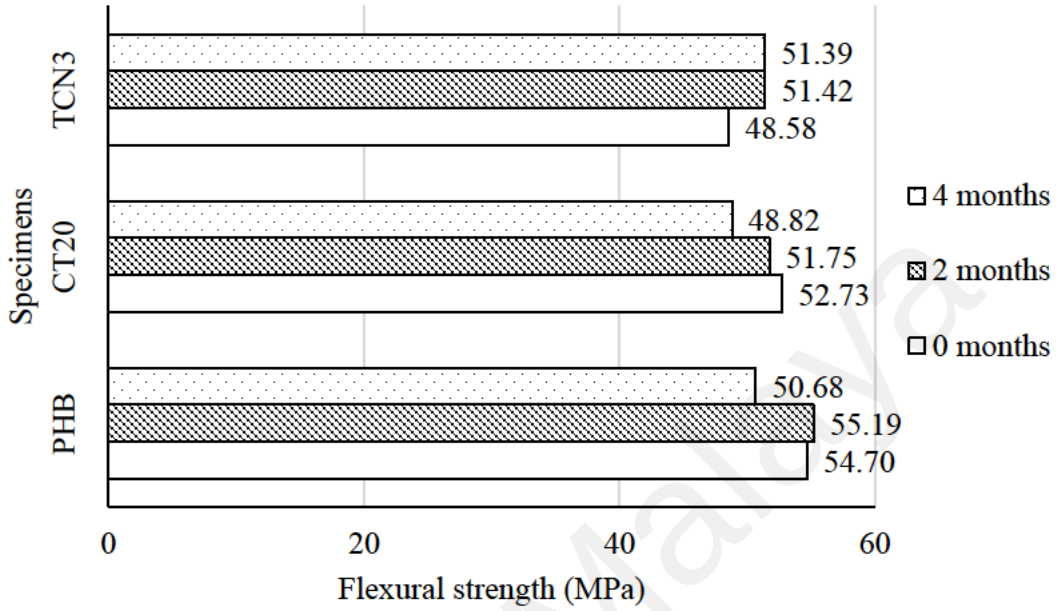

Figure 4.45: Flexural strength for PHB and its composites subjected to outdoor condition.

Similar to specimens subjected to indoor conditioning, the flexural displacement response correlates with the trend observed in flexural modulus. Specimens with higher flexural modulus exhibited lower flexural displacement than specimens with lower flexural modulus, and the increase in flexural modulus over time, due to the material increasing brittleness, is also reflected by the decrease in displacement.

4.4.3 Soil burial

4.4.3.1 Tensile properties

The Young's modulus, tensile strength and elongation at break of PHB and its composites subjected to soil burial are tabulated in Table 4.20. It was observed that for pure PHB and kenaf reinforced composites, Young's modulus (Figure 4.46), tensile

strength (Figure 4.47) and elongation at break (Figure 4.48) exhibited a decreasing trend with more prolonged exposure duration.

It can also be observed that kenaf reinforced PHB has a more significant decrease over time than neat PHB. This observation is in line with what has been reported by most researchers. Popa et al. (2018) studied the bacterial colonisation and biodegradation behaviour of PHB/cellulose fibre composites. The researchers reported that introducing cellulose fibres would increase the biodegradability of the composites. It was found that PHB/cellulose composites would have a higher amount of Aspergillus brasiliensis and Paecilomyces variotii fungi colonies over neat PHB, which suggests that the composite is a better substrate for fungi growth. The degradation rate of the composite was higher as the specimens were left in the soil for a more extended period.

A similar observation was reported by Rapa et al. in their study of PHB/wood composites degradation by Trichoderma spp. and Penicillium sp. (Râpă et al., 2011, 2014). The introduction of wood fibres at loading as low as 2% was found to increase the biodegradability rate of the specimens.

Table 4.20: Tensile properties of PHB and its composites subjected to soil burial condition.

Sample	*Young's modulus (GPa)*			*Tensile strength (MPa)*			*Elongation at break (%)*		
	0 months	2 months	4 months	0 months	2 months	4 months	0 months	2 months	4 months
PHB	1.95	1.82	1.79	35.55	26.20	28.32	4.14	1.79	2.50
5UT	2.12	1.82	1.73	32.07	29.11	26.42	2.91	1.66	2.42
10UT	2.21	2.11	1.77	31.36	28.29	24.39	2.66	1.75	2.30
20UT	2.68	2.37	1.78	31.28	27.28	21.70	2.25	1.95	2.68
5CT	1.97	2.08	2.14	29.97	29.78	27.30	2.78	2.41	2.06
10CT	2.12	2.24	2.07	27.44	27.71	25.76	2.19	2.12	2.15
20CT	2.36	2.17	1.96	26.28	21.79	18.89	1.93	1.75	1.69
3PGV	1.96	2.54	2.08	29.08	28.09	25.41	1.91	1.53	1.45
6PGV	2.00	2.02	2.05	29.16	29.21	25.75	1.97	2.00	1.69
9PGV	1.98	2.22	2.14	30.62	29.38	28.10	2.33	2.01	2.02
3TCN	2.22	2.54	2.52	31.22	31.69	30.78	1.83	1.77	1.77
6TCN	2.33	2.52	2.44	28.82	29.80	26.56	1.45	1.53	1.33
9TCN	2.49	2.64	2.56	26.40	24.30	23.72	1.23	1.08	1.09

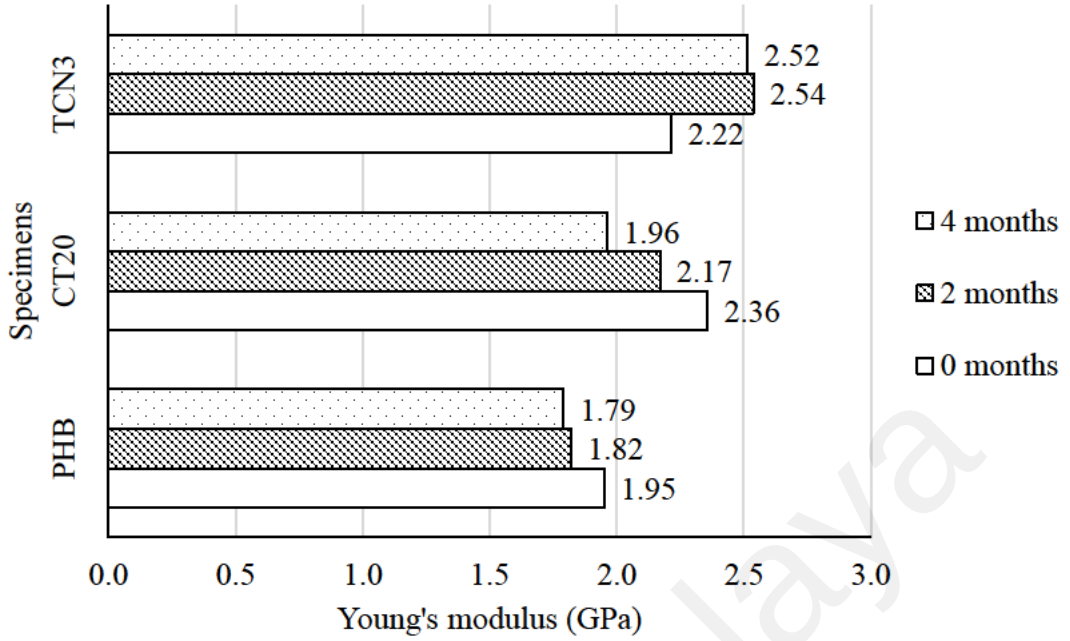

Figure 4.46: Young's modulus for PHB and its composites subjected to soil burial.

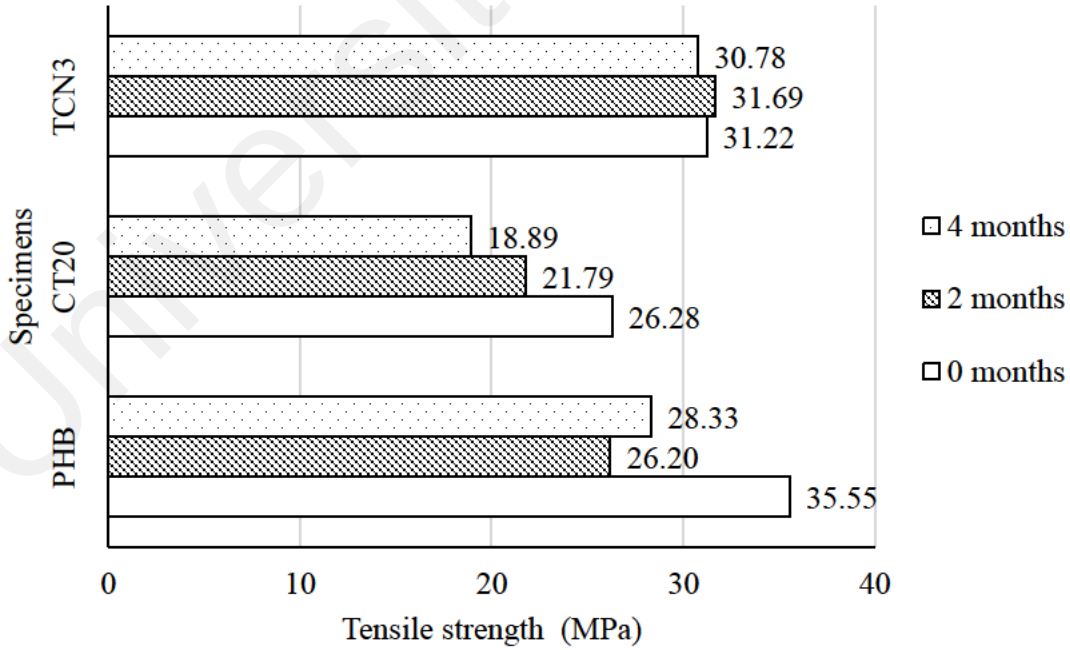

Figure 4.47: Tensile strength for PHB and its composites subjected to soil burial.

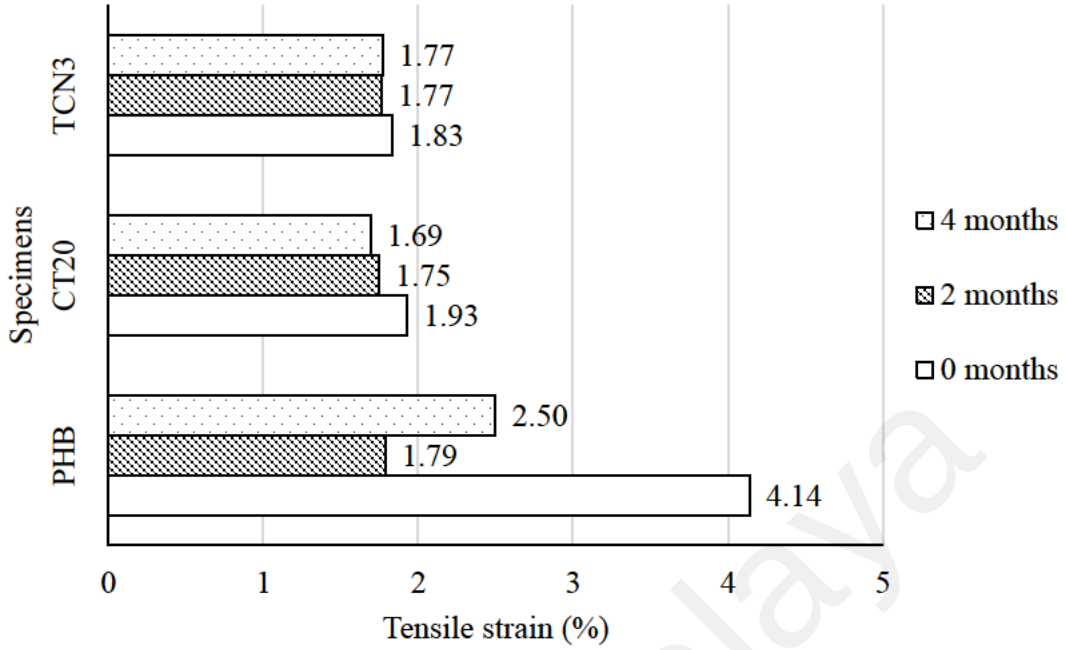

Figure 4.48: Tensile strain for PHB and its composites subjected to soil burial.

The researchers also reported an increasing degree of crystallinity in the PHB specimens after 90 days of soil burial and can be attributed to the microorganism preference of attacking the amorphous region in the polymer (Boyandin et al., 2012; Prudnikova et al., 2017; Salim et al., 2012). The amorphous region would be consumed first, leaving the crystalline region later. This behaviour resulted in the increased crystallinity observed in the samples.

The surface image of KT20 observed under an optical microscope at 40 magnification is illustrated in Figure 4.49. It was observed that the surface of kenaf reinforced PHB has extensive deterioration, which resulted from the consumption of the exposed fibres by microorganisms. The fibres exposed on the composite surface serves as an excellent landing pad for the microorganisms to initially grow. Fibres consumed by the microorganisms would leave hollowed-out "ridges" and "canyons" on the composite

surface. It would lead to a larger surface area, further accelerating the degradation process as the microorganisms now have access to the specimens' interior and outer layer. This increased network of hollow tunnels would also deteriorate its physical properties as multiple flaws were introduced into the composite structure.

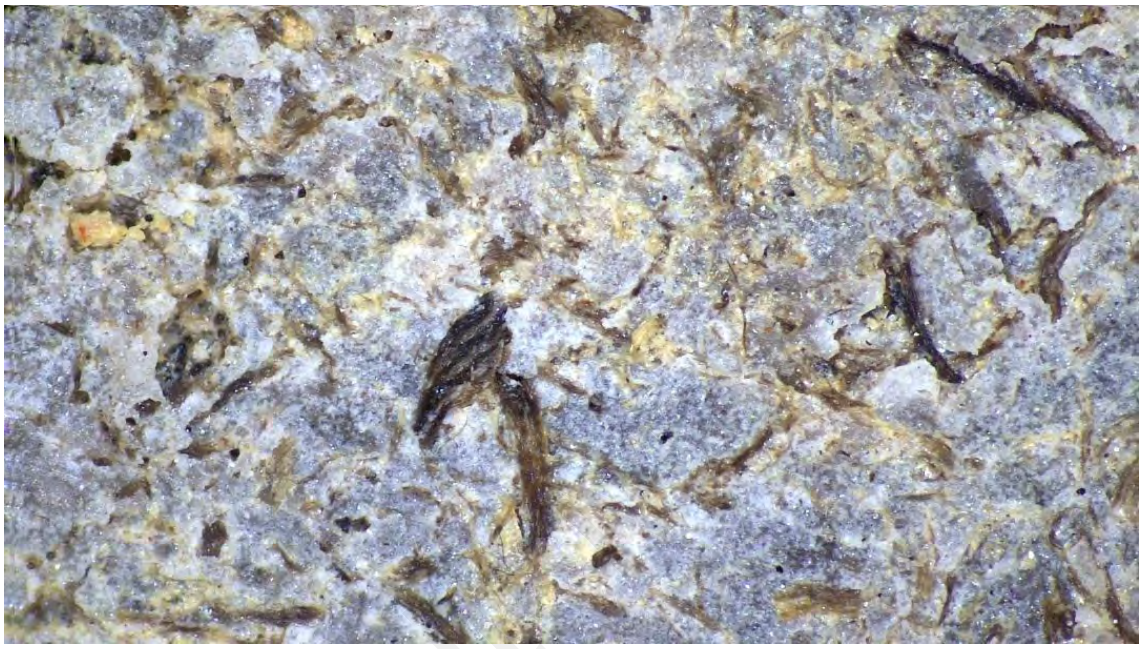

Figure 4.49: Surface of KT20 at 40 times magnification.

On the other hand, biodegradation occurring on neat PHB is limited on its surface. However, it has been extensively reported that the microorganisms attached to the surface would produce micro-sized holes on the surface of PHB (refer to Figure 4.50). Since Young's modulus is measured at lower strain levels, these imperfections have yet to significantly impact the structure, resulting in relatively unchanged Young's modulus. However, as the specimen is subjected to increasing strains, the imperfections on the specimen surfaces would act as stress concentrators, accelerating its failure resulting in lower tensile strength. As the specimens are exposed to the soil burial condition for a longer time, more and deeper holes are expected to be produced. Eventually, PHB and its

composite would lose their load-bearing capabilities as the microorganisms are further degraded.

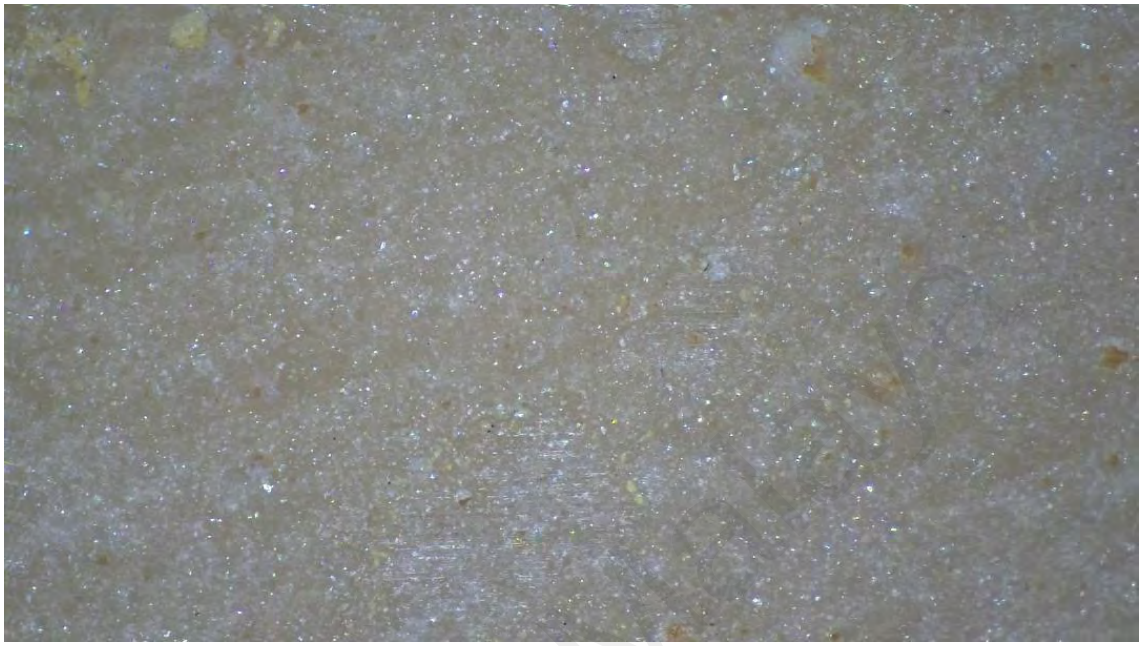

Figure 4.50: Surface of PHB at 40 times magnification.

It is interesting to note that for MMT modified PHB, it is relatively unimpacted by the conditioning. No noticeable reduction in the tensile properties was observed. Maiti et al. (2011) have suggested that MMT modified PHB has better barrier properties, preventing oxygen and moisture from reaching the sample. Biodegradation of PHB involves enzymatic hydrolysis of ester linkages by PHB depolymerase in the presence of moisture (Panayotidou et al., 2014). Therefore, the lack of moisture can cause the biodegradation process to occur slower. This capability is helpful in cases where PHB composites might be employed in conditions known to cause biodegradation, allowing the designer to tailor the biodegradability according to the requirements of applications. In addition, it is also interesting to explore the impact of these barrier properties if the MMT is employed together with cellulosic fibre reinforcement. As discussed earlier, the

mechanical properties of kenaf fibre composites deteriorate significantly due to moisture uptake. Reduction in moisture uptake in kenaf reinforced PHB composites can significantly improve its durability in the long run.

4.4.3.2 Flexural properties

Flexural modulus and flexural strength of PHB and its composites subjected to soil burial for up to four months are tabulated in Table 4.21. The flexural modulus and flexural strength for PHB, CT20 and TCN3 are illustrated in Figure 4.51 and Figure 4.52. From Figure 4.51, it can be observed that the flexural modulus for neat PHB initially increased from 2.65 GPa to 3.00 GPa after two months. However, it remained relatively unchanged at 3.04 GPa after four months. On the other hand, flexural modulus for CT20 steadily decreased from 4.29 GPa to 2.41 GPa after soil burial for four months. There was no clear trend observed for TCN3.

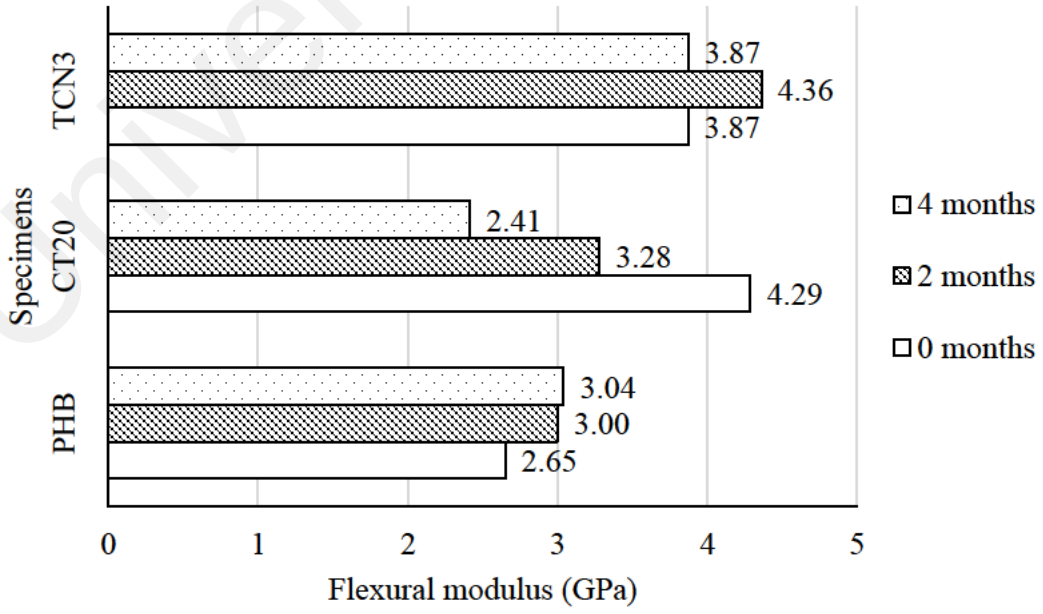

Figure 4.51: Flexural modulus for PHB and its composites subjected to soil burial.

For the flexural strength of buried specimens, the flexural strength of neat PHB decreased from 54.70 MPa to 47.14 MPa after four months. CT20 displayed a significant decrease in flexural properties, from 52.73 MPa to 32.97 MPa, after four months. TCN3, on the other hand, maintained its flexural strength at around 50 MPa. In general, the tensile strength of MMT/PHB composites is relatively unaffected by soil burial. This behaviour

Table 4.21: Flexural properties of PHB and its composites subjected to soil burial.

Sample	Flexural modulus (GPa)			Flexural strength (MPa)			Flexural displacement (mm/mm)		
	0 months	2 months	4 months	0 months	2 months	4 months	0 months	2 months	4 months
PHB	2.65	3.00	3.04	54.70	45.45	47.14	0.03	0.02	0.02
UT5	2.93	3.02	2.88	54.60	45.35	45.20	0.03	0.02	0.02
UT10	3.75	2.93	2.69	56.90	42.19	41.27	0.02	0.02	0.02
UT20	4.04	2.63	2.07	58.30	38.36	36.67	0.02	0.03	0.03
CT5	3.58	3.61	3.37	53.58	51.99	47.73	0.02	0.02	0.02
CT10	3.82	3.41	3.29	52.62	49.15	45.41	0.02	0.02	0.02
CT20	4.29	3.28	2.41	52.73	43.74	32.97	0.02	0.02	0.02
PGV3	3.84	3.87	3.84	49.86	44.79	43.33	0.02	0.01	0.01
PGV6	3.64	3.71	3.67	49.67	46.55	42.89	0.02	0.01	0.01
PGV9	3.72	3.50	3.51	50.73	49.88	46.73	0.02	0.02	0.02
TCN3	3.87	4.36	3.87	48.58	49.58	50.34	0.02	0.02	0.02
TCN6	4.49	4.15	4.22	46.69	42.48	46.13	0.01	0.01	0.01
TCN9	4.62	4.19	4.32	40.56	38.57	38.34	0.01	0.01	0.01

could be due to lesser defects present on the specimens compared to the extensive degradation observed on kenaf/PHB composite specimens. There is the possibility that the introduction of MMT has increased the time required for degradation to occur, as suggested by Maiti et al. (2011).

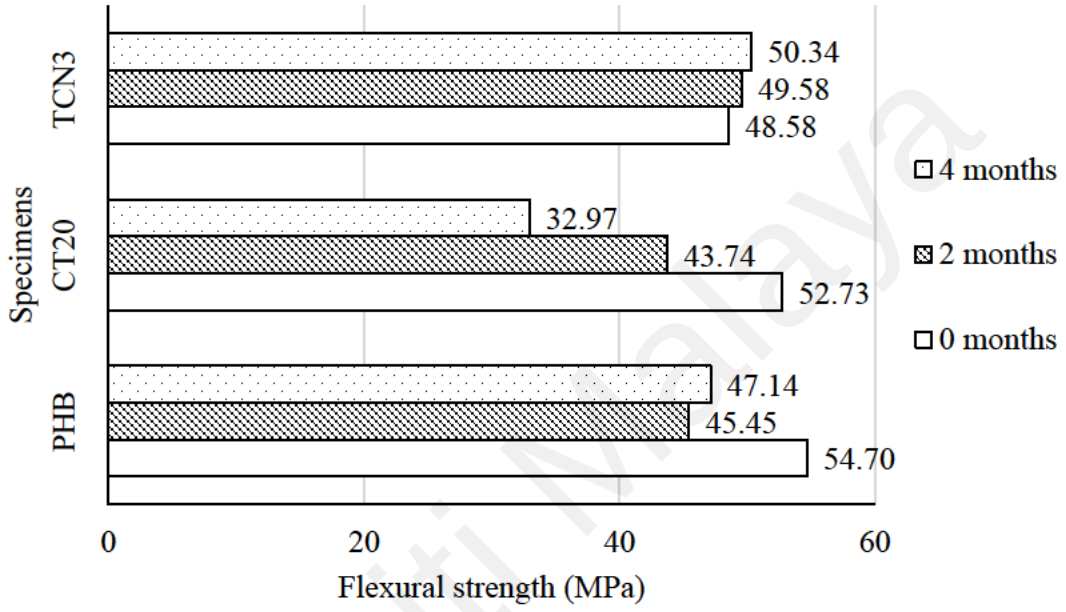

Figure 4.52: Flexural strength for PHB and its composites subjected to soil burial.

Further investigation is required to prove this hypothesis. It is possible that improved barrier properties achieved by adding MMT nanoparticles also reduce the biodegradation rate. It will allow researchers to engineer the material for applications that require the material to be buried in soil for an extended time. On the other hand, adding kenaf or potentially any other natural fibres can lead to accelerated biodegradation, especially at higher fibre loading. Flexural displacement exhibited a similar trend as observed for indoor and outdoor conditions.

CHAPTER 5:CONCLUSION

5.1 Conclusion

Kenaf/PHB and MMT/PHB composites were successfully prepared and characterised. Twin-screw extruder and injection moulding are suitable for producing complex shapes and at higher output volume. Kenaf/PHB composites exhibited up to 21% higher Young's modulus than neat PHB. A similar improvement was observed for MMT/PHB composites. However, the composites generally have lower tensile strength when compared to neat PHB, indicating the dispersion, filler wetting, and interfacial adhesion is still poor. The fibre-matrix interface is weak for kenaf/PHB composites, as gaps between the matrix and fibre are observed in the FESEM image. For MMT/composites, agglomeration was still present likely due to low shear during the compounding process, which was limited by the melt behaviour.

Untreated kenaf/PHB composites exhibited better thermal stability, a higher degree of crystallinity, slightly better thermal properties, higher flexural strength, higher critical stress intensity factor, and peak load than treated kenaf composites. The presence of lignin on the fibre surface acted as a nucleating agent for PHB, resulting in higher crystallinity of the matrix, translating into its physical properties. The presence of lignin and hemicellulose was also proposed to have shielded the cellulose portion of the natural fibres from degradation by-products of PHB, resulting in better thermal properties. On the other hand, treated kenaf fibres exhibited higher storage and loss modulus from rheology indicating better fibre-matrix interaction. It also displayed a higher critical strain energy release rate and fracture energy due to the increased roughness of the treated fibres. Even though the matrix still fails in a brittle manner, fibre pullout occurring during failure increased the fracture energy and prevented the specimens from shattering.

However, gaps between the fibres and matrix were present in both systems from the fracture images, indicating that the interfacial adhesion is still suboptimal. Alkali-treated kenaf composites have proven to be more resistant to weathering as it is less susceptible to water absorption when compared to their untreated counterpart. In this study, the introduction of the kenaf fibres has accelerated its bio-degradation regardless of surface treatment.

For MMT/PHB composites, surface treated MMT exhibited overall better performance. It has better dispersion resulting in improved mechanical properties such as Young's modulus and flexural modulus. TCN/PHB composites exhibited pseudo-solid-like rheological behaviour at lower frequencies, indicating stronger melt-particle interaction. However, treated and untreated MMT composites have lower melting temperatures and X_c than neat PHB. Agglomeration was still present even with surface treatment, resulting in reduced tensile and flexural strength. The introduction of MMT into PHB significantly decreased the impact properties. The poor properties of PHB/mmt composites reported in this work are mainly due to the poor dispersion of the nanoclay, resulting in extensive agglomerations. Since exfoliation or intercalation of the nanoclay was not achieved, improvement expected from its addition was not realised. However, it is interesting to note that the introduction of MMT into PHB delayed the degradation rate compared to neat PHB. Further investigation is required in order to understand the phenomenon better.

5.2 Suggestions for future works

Several analyses can be done to enhance the understanding of Kenaf/PHB and mmt/PHB composites. The surface morphology of the alkali-treated and untreated fibres

can be characterized by AFM. The influence of kenaf fibre and MMT on wetting and viscoelastic properties of PHB composites can be determined. Dynamic Mechanical Analyser would improve the understanding of the viscoelastic properties and determine the composites' glass transition temperature. Damping in the material can be studied to understand the ability and efficiency of the composites to dissipate energy.

The fibres can be treated chemically to improve fibre and matrix adhesion further. Treatment with organic silane or introducing a compatibilising agent into the matrix could improve the fibre matrix adhesion. For MMT modified PHB, preparing a masterbatch with higher clay content during the initial extrusion could yield a better exfoliation effect due to higher melt viscosity resulting in stronger shear forces. The preparation of a hybrid PHB composite using both treated kenaf and MMT as reinforcement is an exciting prospect, considering the potential synergistic effect of both systems. Improved barrier property of PHB after modification with PHB could further increase the lifetime of kenaf reinforced PHB composite by improving its durability to ageing.

Another interesting study would be to create “deconstructed” kenaf composites. Lignin has been shown to improve the crystallisation behaviour of PHB by acting as a nucleating agent. Taking chemical treatment further, we can generate nano-cellulose whiskers, which are purer than the alkali-treated produced in this study. The lignin then could be recovered from the cleaning reagent and processed into nanoparticles, adding value to a process by-product.

REFERENCES

Abdullah, A. H., Bakar, A. A., Ismail, H., Kahar, A. W. M., & Debnath, S. (2019). The effects of accelerated weathering on the tensile properties of kenaf reinforced biocomposites. *IOP Conference Series: Materials Science and Engineering, 495*, Article #12110.

Abral, H., Kadriadi, Mahardika, M., Handayani, D., Sugiarti, E., & Muslimin, A. N. (2019). Characterization of disintegrated bacterial cellulose nanofibers/PVA bionanocomposites prepared via ultrasonication. *International Journal of Biological Macromolecules, 135*, 591–599.

Achilias, D. S., Panayotidou, E., & Zuburtikudis, I. (2011). Thermal degradation kinetics and isoconversional analysis of biodegradable poly(3-hydroxybutyrate)/organomodified montmorillonite nanocomposites. *Thermochimica Acta, 514*(1–2), 58–66.

Akil, H. M., Omar, M. F., Mazuki, A. A. M., Safiee, S., Ishak, Z. A. M., & Abu Bakar, A. (2011). Kenaf fibre reinforced composites: A review. *Materials & Design, 32*(8), 4107–4121.

Akin, O., & Tihminlioglu, F. (2018). Effects of organo-modified clay addition and temperature on the water vapor barrier properties of polyhydroxy butyrate homo and copolymer nanocomposite films for packaging applications. *Journal of Polymers and the Environment, 26*(3), 1121–1132.

Alata, H., Aoyama, T., & Inoue, Y. (2007). Effect of aging on the mechanical properties of poly(3-hydroxybutyrate-co- 3-hydroxyhexanoate). *Macromolecules, 40*(13), 4546-4551.

Anderson, A. J., & Dawes, E. A. (1990). Occurrence, metabolism, metabolic role, and industrial uses of bacterial polyhydroxyalkanoates. *Microbiological Reviews, 54*(4), 450–472.

Ariffin, H., Nishida, H., Shirai, Y., & Hassan, M. A. (2008). Determination of multiple thermal degradation mechanisms of poly(3-hydroxybutyrate). *Polymer Degradation and Stability, 93*(8), 1433–1439.

Arjmandi, R., Hassan, A., Eichhorn, S. J., Mohamad Haafiz, M. K., Zakaria, Z., & Tanjung, F. A. (2015). Enhanced ductility and tensile properties of hybrid montmorillonite/cellulose nanowhiskers reinforced polylactic acid nanocomposites. *Journal of Materials Science, 50*(8), 3118–3130.

Arrigo, R., Morici, E., & Dintcheva, N. T. (2017). High-performance thermoplastic elastomers/carbon nanotubes nanocomposites: Mechanical behaviour, rheology, and durability. *Polymer Composites, 38*(S1), E381–E391.

Arseneau, D. F. (1971). Competitive reactions in the thermal decomposition of cellulose. *Canadian Journal of Chemistry, 49*(4), 632–638.

Arthur, J. C. (1989). 2 - Chemical modification of cellulose and its derivatives. In Allen G. Bevington & J. C. (Eds.), *Comprehensive polymer science and supplements* (pp. 49–80). Pergamon.

Ashraf, M. A., Peng, W., Zare, Y., & Rhee, K. Y. (2018). Effects of size and aggregation/agglomeration of nanoparticles on the interfacial/interphase properties and tensile strength of polymer nanocomposites. *Nanoscale Research Letters, 13*(1), 214.

Asim, M., Jawaid, M., Abdan, K., & Ishak, M. R. (2016). Effect of alkali and silane treatments on mechanical and fibre-matrix bond strength of kenaf and pineapple leaf fibres. *Journal of Bionic Engineering, 13*(3), 426–435.

Asrar, J., & Gruys, K. J. (2005). Biodegradable Polymer (Biopol®). In Steinbüchel, A., (2005) *Biopolymers Online*. https://onlinelibrary.wiley.com/doi/10.1002/3527600035.bpol4003

Asrar, J., Shah, D. T., & Tran, M. (2000). *Hydroxy-terminated polyhydroxyalkanoates*. (European Patent No. EP1088093B1), European Patent Office.

Avella, M., Martuscelli, E., & Raimo, M. (2000). Review Properties of blends and composites based on poly(3-hydroxy)butyrate (PHB) and poly(3-hydroxybutyrate-hydroxyvalerate) (PHBV) copolymers. *Journal of Materials Science, 35*(3), 523–545.

Avossa, J., Pota, G., Vitiello, G., Macagnano, A., Zanfardino, A., Di Napoli, M., Pezzella, A., D'Errico, G., Varcamonti, M., & Luciani, G. (2021). Multifunctional mats by antimicrobial nanoparticles decoration for bioinspired smart wound dressing solutions. *Materials Science and Engineering: C*, 123, 111954.

Barham, P. J., & Keller, A. (1986). The relationship between microstructure and mode of fracture in polyhydroxybutyrate. *Journal of Polymer Science Part B: Polymer Physics, 24*(1), 69–77.

Barham, P. J., Keller, A., Otun, E. L., & Holmes, P. A. (1984). Crystallisation and morphology of a bacterial thermoplastic: poly-3-hydroxybutyrate. *Journal of Materials Science, 19*(9), 2781–2794.

Barkoula, N. M., Garkhail, S. K., & Peijs, T. (2010). Biodegradable composites based on flax/polyhydroxybutyrate and its copolymer with hydroxyvalerate. *Industrial Crops and Products, 31*(1), 34–42.

Bauer, H., & Owen, A. J. (1988). Some structural and mechanical properties of bacterially produced poly-β-hydroxybutyrate-co-β-hydroxyvalerate. *Colloid and Polymer Science, 266*(3), 241–247.

Bhat, A. H., Dasan, Y. K., Khan, I., Soleimani, H., & Usmani, A. (2017). Application of nanocrystalline cellulose: Processing and biomedical applications. In Cellulose-Reinforced Nanofibre Composites: Production, Properties and Applications (pp. 215-240). Elsevier Inc.

Biddlestone, F., Harris, A., Hay, J. N., & Hammond, T. (1996). The physical ageing of amorphous poly(hydroxybutyrate). Polymer International, 39(3), 221–229.

Bodros, E., Pillin, I., Montrelay, N., & Baley, C. (2007). Could biopolymers reinforced by randomly scattered flax fibre be used in structural applications? *Composites Science and Technology, 67*(3), 462–470.

Bordes, P., Hablot, E., Pollet, E., & Avérous, L. (2009). Effect of clay organomodifiers on degradation of polyhydroxyalkanoates. *Polymer Degradation and Stability, 94*(5), 789–796.

Bordes, P., Pollet, E., Bourbigot, S., & Avérous, L. (2008). Structure and properties of PHA/clay nano-biocomposites prepared by melt intercalation. *Macromolecular Chemistry and Physics, 209*(14), 1473–1484.

Boyandin, A. N., Prudnikova, S. V, Filipenko, M. L., Khrapov, E. A., Vasil'ev, A. D., & Volova, T. G. (2012). Biodegradation of polyhydroxyalkanoates by soil microbial communities of different structures and detection of PHA degrading microorganisms. *Applied Biochemistry and Microbiology, 48*(1), 28–36.

Briassoulis, D., Tserotas, P., & Athanasoulia, I.-G. (2021). Alternative optimization routes for improving the performance of poly(3-hydroxybutyrate) (PHB) based plastics. *Journal of Cleaner Production, 318*, Article #128555.

Brooks, A. L., Wang, S., & Jambeck, J. R. (2018). The Chinese import ban and its impact on global plastic waste trade. *Science Advances, 4*(6).

Bruno, M., Tavares, M. I., Motta, L., Miguez, E., Preto, M., & Fernandez, A. (2008). Evaluation of PHB/Clay nanocomposite by spin-lattice relaxation time. *Materials Research-Ibero-American Journal of Materials, 11*(4).

Bucci, D., Alberti, L., Souza, O., & Barcellos, I. (2014). Study on physical and mechanical properties of PHB biocomposites with rice hull ash. *Materials Science Forum*, 775–776, 557–561.

Cai, M., Takagi, H., Nakagaito, A. N., Katoh, M., Ueki, T., Waterhouse, G. I. N., & Li, Y. (2015). Influence of alkali treatment on internal microstructure and tensile properties of abaca fibres. *Industrial Crops and Products, 65*, 27–35.

Campo, E. A. (2008). *Selection of polymeric materials: How to select design properties from different standards*. William Andrew.

Chandrasekar, M., Ishak, M. R., Sapuan, S. M., Leman, Z., & Jawaid, M. (2017). A review on the characterisation of natural fibres and their composites after alkali treatment and water absorption. *Plastics, Rubber and Composites, 46*(3), 119–136.

Chee, S. S., Jawaid, M., Sultan, M. T. H., Alothman, O. Y., & Abdullah, L. C. (2019). Accelerated weathering and soil burial effects on colour, biodegradability and thermal properties of bamboo/kenaf/epoxy hybrid composites. *Polymer Testing, 79*, Article #106054.

Choi, G. G., Kim, H. W., & Rhee, Y. H. (2004). Enzymatic and non-enzymatic degradation of poly (3-hydroxybutyrate-co-3-hydroxyvalerate) copolyesters produced by Alcaligenes sp. MT-16. *Journal of Microbiology (Seoul, Korea), 42*(4), 346–352.

Choi, J. & Lee, S. Y. (1997). Process analysis and economic evaluation for Poly(3-hydroxybutyrate) production by fermentation. *Bioprocess Engineering 17*, 335–342.

Chow, W. S., Ishak, Z. A. M., Karger-Kocsis, J., Apostolov, A. A., & Ishiaku, U. S. (2003). Compatibilizing effect of maleated polypropylene on the mechanical properties and morphology of injection molded polyamide 6/polypropylene/organoclay nanocomposites. *Polymer, 44*(24), 7427–7440.

Chun, K. S., Husseinsyah, S., & Yeng, C. M. (2015). Torque rheological properties of polypropylene/cocoa pod husk composites. *Journal of Thermoplastic Composite Materials, 30*(9), 1217–1227.

Council, N. R. (1996). Shipboard Pollution Control: U.S. Navy Compliance with MARPOL Annex V. The National Academies Press.

Crétois, R., Chenal, J. M., Sheibat-Othman, N., Monnier, A., Martin, C., Astruz, O., Kurusu, R., & Demarquette, N. R. (2016). Physical explanations about the improvement of polyhydroxybutyrate ductility: Hidden effect of plasticiser on physical ageing. *Polymer, 102*, 176-182.

Cyras, V. P., Manfredi, L. B., Ton-That, M. T., & Vázquez, A. (2008). Physical and mechanical properties of thermoplastic starch/montmorillonite nanocomposite films. *Carbohydrate Polymers, 73*(1), 55–63.

Darlington, M. W., & Mcginley, P. (1975). Fibre orientation distribution in short fibre reinforced plastics. *Journal of Materials Science, 10*, 906–910.

de Carvalho Arjona, J., das Graças Silva-Valenzuela, M., Wang, S.-H., & Valenzuela-Diaz, F. R. (2021). Biodegradable nanocomposite microcapsules for controlled release of urea. *Polymers, 13*(5), 722.

de Koning, G. J. M., Kellerhals, M., van Meurs, C., & Witholt, B. (1997). A process for the recovery of poly(hydroxyalkanoates) from Pseudomonads Part 2: Process development and economic evaluation. *Bioprocess Engineering, 17(*1), 15–21.

de Koning, G. J. M., & Lemstra, P. J. (1993). Crystallisation phenomena in bacterial poly[(R)-3-hydroxybutyrate]: 2. Embrittlement and rejuvenation. *Polymer, 34*(19), 4089-4094.

de Koning, G. J. M., Scheeren, A. H. C., Lemstra, P. J., Peeters, M., & Reynaers, H. (1994). Crystallisation phenomena in bacterial poly[(R)-3-hydroxybutyrate]: 3. Toughening via texture changes. *Polymer, 35*(21), 4598-4605.

de Moraes, J. O., Müller, C. M. O., & Laurindo, J. B. (2011). Influence of the simultaneous addition of bentonite and cellulose fibres on the mechanical and barrier properties of starch composite-films. *Food Science and Technology International, 18*(1), 35–45.

Dhakal, H. N., Zhang, Z. Y., & Richardson, M. O. W. (2007). Effect of water absorption on the mechanical properties of hemp fibre reinforced unsaturated polyester composites. *Composites Science and Technology, 67*(7), 1674–1683.

Dhar, P., Bhardwaj, U., Kumar, A., & Katiyar, V. (2015). Poly (3-hydroxybutyrate)/cellulose nanocrystal films for food packaging applications: Barrier and migration studies. Polymer *Engineering & Science, 55*(10), 2388–2395.

Djafari Petroudy, S. R. (2017). 3 - Physical and mechanical properties of natural fibres. In M. Fan M. & Fu F. (Eds.), *Advanced high strength natural fibre composites in construction*. (pp. 59–83). Woodhead Publishing.

Doi, Y., Kanesawa, Y., Kunioka, M., & Saito, T. (1990). Biodegradation of microbial copolyesters: poly(3-hydroxybutyrate-co-3-hydroxyvalerate) and poly(3-hydroxybutyrate-co-4-hydroxybutyrate). *Macromolecules, 23*(1), 26–31.

Dufresne, A. (2013). Nanocellulose: a new ageless bionanomaterial. *Materials Today, 16*(6), 220–227.

El-Shekeil, Y. A., Sapuan, S. M., Khalina, A., Zainudin, E. S., & Al-Shuja'a, O. M. (2012). Effect of alkali treatment on mechanical and thermal properties of Kenaf fibre-reinforced thermoplastic polyurethane composite. *Journal of Thermal Analysis and Calorimetry, 109*(3), 1435–1443.

Fatou, J. G. (1984). Crystallisation, morphology and properties of polymers. Die *Makromolekulare Chemie, 7*(S19841), 131–146.

Ferreira, D. P., Cruz, J., & Fangueiro, R. (2019). Chapter 1 - Surface modification of natural fibres in polymer composites. In Koronis G. & Silva A. (Eds.), *Green composites for automotive applications*. (pp. 3–41). Woodhead Publishing.

Fiore, V., Di Bella, G., & Valenza, A. (2015). The effect of alkaline treatment on mechanical properties of kenaf fibres and their epoxy composites. *Composites Part B: Engineering, 68*, 14–21.

Fitaroni, L., De Lima, J., Cruz, S., & Waldman, W. (2015). Thermal stability of polypropylene–montmorillonite clay nanocomposites: Limitation of the thermogravimetric analysis. *Polymer Degradation and Stability, 111*, 102–108.

Folkes, M. (1979). [Review of the book *Polymer engineering composites*, edited by Richardson M.O.W.] *British Polymer Journal, 11*(4), 219.

Frone, A. N., Batalu, D., Chiulan, I., Oprea, M., Gabor, A. R., Nicolae, C.-A., Raditoiu, V., et al. (2019). Morpho-Structural, Thermal and Mechanical Properties of PLA/PHB/Cellulose Biodegradable Nanocomposites Obtained by Compression Molding, Extrusion, and 3D Printing. *Nanomaterials, 10*(1), 51.

Garvey, C. J., Parker, I. H., & Simon, G. P. (2005). On the interpretation of X-ray diffraction powder patterns in terms of the nanostructure of cellulose I fibres. *Macromolecular Chemistry and Physics, 206*(15), 1568–1575.

Geyer, R., Jambeck, J. R., & Law, K. L. (2017). Production, use, and fate of all plastics ever made. *Science Advances, 3*(7), e1700782.

Gogolewski, S., Jovanovic, M., Perren, S. M., Dillon, J. G., & Hughes, M. K. (1993). The effect of melt-processing on the degradation of selected polyhydroxyacids: polylactides, polyhydroxybutyrate, and polyhydroxybutyrate-co-valerates. *Polymer Degradation and Stability, 40*(3), 313–322.

Grassie, N., Murray, E. J., & Holmes, P. A. (1984). The thermal degradation of poly(-(d)-β-hydroxybutyric acid): Part 2—Changes in molecular weight. *Polymer Degradation and Stability, 6*(2), 95–103.

Gross, R. A., & Kalra, B. (2002). *Biodegradable polymers for the environment*. *Science (New York, N.Y.), 297*(5582), 803–807.

Gunning, M. A., Geever, L. M., Killion, J. A., Lyons, J. G., & Higginbotham, C. L. (2013). Mechanical and biodegradation performance of short natural fibre polyhydroxybutyrate composites. *Polymer Testing, 32*(8), 1603–1611.

Halip, J. A., Hua, L. S., Ashaari, Z., Tahir, P. M., Chen, L. W., & Anwar Uyup, M. K. (2019). 8 - Effect of treatment on water absorption behaviour of natural fibre–reinforced polymer composites. In Jawaid, M., Thariq, M., & Saba, N. (Eds.), *Fibre-reinforced composites and hybrid composites* (pp. 141–156). Woodhead Publishing.

Hankermeyer, C. R., & Tjeerdema, R. S. (1999). Polyhydroxybutyrate: Plastic made and degraded by microorganisms. In Ware G.W. (Eds.), Reviews of Environmental Contamination and Toxicology. Reviews of Environmental Contamination and Toxicology, vol 159. Springer, New York, NY.

Hassan, A., Yahya, R., Yahaya, A. H., Tahir, A. R. M., & Hornsby, P. R. (2004). Tensile, impact and fibre length properties of injection-molded short and long glass fibre-reinforced polyamide 6,6 composites. *Journal of Reinforced Plastics and Composites, 23*(9), 969–986.

Hassan, A., Hassan, A. A., & Mohd Rafiq, M. I. (2011). Impact properties of injection molded glass fibre/polyamide-6 composites: effect of testing parameters. *Journal of Reinforced Plastics and Composites, 30*(10), 889–898.

Hassan, Aziz, Isa, M. R. M., Ishak, Z. A. M., Ishak, N. A., Rahman, N. A., & Salleh, F. M. (2018). Characterisation of sodium hydroxide-treated kenaf fibres for biodegradable composite application. *High Performance Polymers, 30*(8), 890–899.

Hassan, A., Muhammad Rafiq, M. I., & Zainal Ariffin, M. I. (2019). Improving thermal and mechanical properties of injection moulded kenaf fibre-reinforced polyhydroxy-butyrate composites through fibre surface treatment. *Bioresources; 14*(2)

Hayes, M. D., Edwards, D. B., & Shah, A. R. (2015). 4 - Fractography Basics. In Hayes, M. D., Edwards, D. B., & Shah A.R., (Eds.), *Fractography in failure analysis of polymers*. (pp. 48–92). William Andrew Publishing.

Herrera-Franco, P. J., & Valadez-González, A. (2005). A study of the mechanical properties of short natural-fibre reinforced composites. *Composites Part B: Engineering, 36*(8), 597–608.

Hodgkinson, J. M. (2000). 7 - Flexure. In Hodgkinson, J.M., (Ed*.), Mechanical testing of advanced fibre composites* (pp. 124–142). Woodhead Publishing.

Holmes, P. A. (1985). Applications of PHB - a microbially produced biodegradable thermoplastic. *Physics in Technology, 16*(1), 32–36.

Holmes, P. A. (1988). Biologically produced (R)-3-hydroxy-alkanoate polymers and copolymers. In Bassett, D.C., (Ed.), *Developments in crystalline polymers* (pp. 1–65). Springer Netherlands.

Hong, S.-G., & Huang, S.-C. (2015). Crystallisation properties of polyhydroxybutyrate with modified silicas. *Journal of Polymer Research, 22*(4), 61.

Hosokawa, M. N., Darros, A. B., Moris, V. A. da S., & de Paiva, J. M. F. (2017). Polyhydroxybutyrate composites with random mats of sisal and coconut fibres. *Materials Research, 20*, 279–290.

Hossain, S. I., Hasan, M., Hasan, M. N., & Hassan, A. (2013). Effect of chemical treatment on physical, mechanical and thermal properties of ladies finger natural fibre. *Advances in Materials Science and Engineering, 2013*, Article #824274.

Ibrahim, N. A., Hadithon, K. A., & Abdan, K. (2009). Effect of fibre treatment on mechanical properties of kenaf fibre-ecoflex composites. *Journal of Reinforced Plastics and Composites, 29*(14), 2192–2198.

Issaadi, K., Habi, A., Grohens, Y., & Pillin, I. (2015). Effect of the montmorillonite intercalant and anhydride maleic grafting on polylactic acid structure and properties. *Applied Clay Science, 107*, 62–69.

Jalalvandi, E., Majid, R. A., Ghanbari, T., & Ilbeygi, H. (2013). Effects of montmorillonite (MMT) on morphological, tensile, physical barrier properties and biodegradability of polylactic acid/starch/MMT nanocomposites. *Journal of Thermoplastic Composite Materials, 28*(4), 496–509.

Jayakumar, A., Prabhu, K., Shah, L., & Radha, P. (2020). Biologically and environmentally benign approach for PHB-silver nanocomposite synthesis and its characterisation. *Polymer Testing, 81*, Article #106197.

Jendrossek, D., & Handrick, R. (2002). Microbial degradation of polyhydroxyalkanoates. Annual *Review of Microbiology, 56*, 403–432.

Jiang, Z., Zhang, H., Han, J., Liu, Z., Liu, Y., & Tang, L. (2016). Percolation model of reinforcement efficiency for carbon nanotubes dispersed in thermoplastics. *Composites Part A: Applied Science and Manufacturing, 86*, 49–56.

Jimenez, G., Ogata, N., Kawai, H., & Ogihara, T. (1997). Structure and thermal/mechanical properties of poly (ϵ-caprolactone)-clay blend. *Journal of Applied Polymer Science, 64*(11), 2211–2220.

Kabir, M. M., Wang, H., Lau, K. T., & Cardona, F. (2012). Chemical treatments on plant-based natural fibre reinforced polymer composites: An overview. *Composites Part B: Engineering, 43*(7), 2883–2892.

Kaci, M., Hamma, A., Pillin, I., & Grohens, Y. (2009). Effect of reprocessing cycles on the morphology and properties of poly(propylene)/wood flour composites compatibilised with EBAGMA terpolymer. *Macromolecular Materials and Engineering, 294*, 532–540.

Kargarzadeh, H., Ahmad, I., Abdullah, I., Dufresne, A., Zainudin, S. Y., & Sheltami, R. M. (2012). Effects of hydrolysis conditions on the morphology, crystallinity, and thermal stability of cellulose nanocrystals extracted from kenaf bast fibres. *Cellulose, 19*(3), 855–866.

Kaynak, C., Nakas, G. I., & Isitman, N. A. (2009). Mechanical properties, flammability and char morphology of epoxy resin/montmorillonite nanocomposites. *Applied Clay Science, 46*(3), 319–324.

Kazerani, T., Zhao, G., & Zhao, J. (2010). Dynamic fracturing simulation of brittle material using the distinct lattice spring method with a full rate-dependent cohesive law. *Rock Mechanics and Rock Engineering, 43*.

Kim, H.-Y., Park, S. S., & Lim, S.-T. (2015). Preparation, characterization and utilization of starch nanoparticles. *Colloids and Surfaces B: Biointerfaces, 126*, 607–620.

Kiran, G. S., Jackson, S. A., Priyadharsini, S., Dobson, A. D. W., & Selvin, J. (2017). Synthesis of Nm-PHB (nanomelanin-polyhydroxy butyrate) nanocomposite film and its protective effect against biofilm-forming multi drug resistant Staphylococcus aureus. *Scientific Reports, 7*(1), 9167.

Khoshnava, S. M., Rostami, R., Ismail, M., Rahmat, A. R., & Ogunbode, B. E. (2017). Woven hybrid biocomposite: Mechanical properties of woven kenaf bast fibre/oil palm empty fruit bunches hybrid reinforced poly hydroxybutyrate biocomposite as non-structural building materials. *Construction and Building Materials, 154*, 155–166.

Krishnaiah, P., Ratnam, C. T., & Manickam, S. (2017). Enhancements in crystallinity, thermal stability, tensile modulus and strength of sisal fibres and their PP composites induced by the synergistic effects of alkali and high intensity ultrasound (HIU) treatments. *Ultrasonics Sonochemistry, 34*, 729–742.

Kusmono, & Arifin Mohd Ishak, Z. (2013). effect of clay addition on mechanical properties of unsaturated polyester/glass fibre composites. *International Journal of Polymer Science, 2013*, Article #797109.

Lan, C.-H., & Sun, Y.-M. (2017). Influence of the surface properties of nano-silica on the dispersion and isothermal crystallisation kinetics of PHB/silica nanocomposites. *Materials Chemistry and Physics, 199*, 88–97.

Laura, P., & Kennedy, E. (2018). Plastic Recycling Is Broken. Here's How to Fix It. [Internet]. National Geographic. 2018 [cited 20 January 2021]. National Geographic.

Lenz, R. W., JTEC monograph on biodegradable polymers and plastics in Japan: Research, development, and applications (1995). Baltimore, MD; International Technology Research Institute, JTEC/STEC Program, Loyola College in Maryland.

Lertwimolnun, W., & Vergnes, B. (2005). Influence of compatibiliser and processing conditions on the dispersion of nanoclay in a polypropylene matrix. *Polymer, 46*(10), 3462–3471.

Li, Z., Yang, J., & Loh, X. J. (2016). Polyhydroxyalkanoates: opening doors for a sustainable future. *NPG Asia Materials, 8*(4), e265–e265.

Liang, Z.-M., Yin, J., & Xu, H.-J. (2003). Polyimide/montmorillonite nanocomposites based on thermally stable, rigid-rod aromatic amine modifiers. *Polymer, 44*(5), 1391–1399.

Lim, J., & Kim, J. (2016). UV-photodegradation of poly(3-hydroxybutyrate-co-3-hydroxyhexanoate) (PHB-HHx). *Macromolecular Research, 24*(1), 9–13.

Lim, K. H., Majid, M. S. A., Ridzuan, M. J. M., Basaruddin, K. S., & Afendi, M. (2017). Effect of nano-clay fillers on mechanical and morphological properties of Napier/epoxy composites. *Journal of Physics: Conference Series, 908*, Article #12010.

Liu, X., & Wu, Q. (2001). PP/clay nanocomposites prepared by grafting-melt intercalation. *Polymer, 42*(25), 10013–10019.

Madison, L. L., & Huisman, G. W. (1999). Metabolic engineering of poly(3-hydroxyalkanoates): from DNA to plastic. *Microbiology and Molecular Biology Reviews, 63*(1), 21–53.

Maiti, P., Batt, C. A., & Giannelis, E. P. (2003). Biodegradable polyester / layered silicate nanocomposites. *MRS Online Proceedings Library, 740*(1), 53.

Maiti, P., Batt, C. A., & Giannelis, E. P. (2007). New biodegradable polyhydroxybutyrate/layered silicate nanocomposites. *Biomacromolecules, 8*(11), 3393–3400.

Maiti, P., Batt, C., & Giannelis, E. (2011). Biodegradable polyester/layered silicate nanocomposites. *MRS Proceedings, 740*, 5.

Manavitehrani, I., Fathi, A., Badr, H., Daly, S., Negahi Shirazi, A., & Dehghani, F. (2016). Biomedical applications of biodegradable polyesters. *Polymers, 8*(1).

Manikandan, N. A., Pakshirajan, K., & Pugazhenthi, G. (2020). Preparation and characterisation of environmentally safe and highly biodegradable microbial polyhydroxybutyrate (PHB) based graphene nanocomposites for potential food packaging applications. International *Journal of Biological Macromolecules, 154*, 866–877.

Manshor, M. R., Anuar, H., Nur Aimi, M. N., Ahmad Fitrie, M. I., Wan Nazri, W. B., Sapuan, S. M., El-Shekeil, Y. A., & Wahit, M. U. (2014). Mechanical, thermal and morphological properties of durian skin fibre reinforced PLA biocomposites. *Materials and Design, 59*, 279–286.

Marchessault, R. H., & Yu, G. (2005). Crystallisation and material properties of polyhydroxyalkanoates PHAs). In Steinbüchel A. (Ed.), *Biopolymers Online*.

Meischel, M., Eichler, J., Martinelli, E., Karr, U., Weigel, J., Schmöller, G., Tschegg, E. K., Fischerauer, S., Weinberg, A. M., & Stanzl-Tschegg, S. E. (2016). Adhesive strength of bone-implant interfaces and in-vivo degradation of PHB composites for load-bearing applications. *Journal of the Mechanical Behavior of Biomedical Materials, 53*, 104–118.

Melo, J. D. D., Carvalho, L. F. M., Medeiros, A. M., Souto, C. R. O., & Paskocimas, C. A. (2012). A biodegradable composite material based on polyhydroxybutyrate (PHB) and carnauba fibres. *Composites Part B: Engineering, 43*(7), 2827–2835.

Merdas, I., Thominette, F., Tcharkhtchi, A., & Verdu, J. (2002). Factors governing water absorption by composite matrices. *Composites Science and Technology, 62*(4), 487–492.

Mitomo, H., & Ota, E. (1991). Thermal decomposition of polyhydroxybutyrate and its copolymer. *Journal of Textile Society, 47*(2), 89–94.

Modesti, M., Lorenzetti, A., Bon, D., & Besco, S. (2005). Effect of processing conditions on morphology and mechanical properties of compatibilised polypropylene nanocomposites. *Polymer, 46*, 10237–10245.

Mohamed El-Hadi, A. (2014). Investigation of the effect of nano-clay type on the non-isothermal crystallisation kinetics and morphology of poly(3(R)-hydroxybutyrate) PHB/clay nanocomposites. *Polymer Bulletin, 71*(6), 1449–1470.

Mortazavian, V., Fatemi, A., & Khosrovaneh, A. (2015). Effect of water absorption on tensile and fatigue behaviours of two short glass fibre reinforced thermoplastics. *SAE International Journal of Materials and Manufacturing, 8*.

Mousavioun, P., Halley, P. J., & Doherty, W. O. S. (2013). Thermophysical properties and rheology of PHB/lignin blends. *Industrial Crops and Products, 50*, 270–275.

Muhammadi, Shabina, Afzal, M., & Hameed, S. (2015). Bacterial polyhydroxyalkanoates-eco-friendly next generation plastic: Production, biocompatibility, biodegradation, physical properties and applications. *Green Chemistry Letters and Reviews, 8*(3–4), 56–77.

Muneer, F., Rasul, I., Azeem, F., Siddique, M. H., Zubair, M., & Nadeem, H. (2020). Microbial polyhydroxyalkanoates (PHAs): Efficient replacement of synthetic polymers. *Journal of Polymers and the Environment, 28*(9), 2301–2323.

Muñoz, E., & García-Manrique, J. A. (2015). Water absorption behaviour and its effect on the mechanical properties of flax fibre reinforced bioepoxy composites. *International Journal of Polymer Science, 2015*, Article #390275.

Nor Mas Mira Abdul Rahman. (2013). Preparation and characterisation of glass fibre/nanoclay/polypropylene nanocomposites (Publication No 5986) [Doctoral Dissertation Universiti Malaya], UM Students Repository.

Ogata, N., Kawakage, S., & Ogihara, T. (1997). Structure and thermal/mechanical properties of poly(ethylene oxide) - clay mineral blends. *Polymer, 38*(20), 5115–5118.

Ollier, R. P., D'Amico, D. A., Schroeder, W. F., Cyras, V. P., & Alvarez, V. A. (2018). Effect of clay treatment on the thermal degradation of PHB based nanocomposites. *Applied Clay Science, 163*, 146–152.

Ouajai, S., & Shanks, R. A. (2005). Composition, structure and thermal degradation of hemp cellulose after chemical treatments. *Polymer Degradation and Stability, 89*(2), 327–335.

Owen, A. J. (1985). Some dynamic mechanical properties of microbially produced poly-B-hydroxybutyrate/B-hydroxyvalerate copolymers. *Colloid and Polymer Science, 263*(10), 799–803.

Padermshoke, A., Katsumoto, Y., Sato, H., Ekgasit, S., Noda, I., & Ozaki, Y. (2005). Melting behaviour of poly(3-hydroxybutyrate) investigated by two-dimensional infrared

correlation spectroscopy. *Spectrochimica Acta Part A: Molecular and Biomolecular Spectroscopy, 61*(4), 541–550.

Panayotidou, E., Baklavaridis, A., Zuburtikudis, I., & Achilias, D. S. (2014). Nanocomposites of poly(3-hydroxybutyrate)/organomodified montmorillonite: Effect of the nanofiller on the polymer's biodegradation. *Journal of Applied Polymer Science, 132*(11).

Pang, C., Shanks, R. A., & Daver, F. (2015). Characterisation of kenaf fibre composites prepared with tributyl citrate plasticized cellulose acetate. *Composites Part A: Applied Science and Manufacturing, 70*, 52–58.

Park, S., Baker, J. O., Himmel, M. E., Parilla, P. A., & Johnson, D. K. (2010). Cellulose crystallinity index: measurement techniques and their impact on interpreting cellulase performance. *Biotechnology for Biofuels, 3*(1), 10

Pavlidou, S., & Papaspyrides, C. D. (2008). A review on polymer–layered silicate nanocomposites. *Progress in Polymer Science, 33*(12), 1119–1198.

Pejic, B., Kostic, M., Skundric, P., & Praskalo, J. (2008). The effects of hemicelluloses and lignin removal on water uptake behaviour of hemp fibres. *Bioresource Technology, 99*, 7152–7159.

Pickering, K. L., Efendy, M. G. A., & Le, T. M. (2016). A review of recent developments in natural fibre composites and their mechanical performance. *Composites Part A: Applied Science and Manufacturing, 83*, 98–112.

Poirier, Y., Nawrath, C., & Somerville, C. (1995). Production of polyhydroxyalkanoates, a family of biodegradable plastics and elastomers, in bacteria and plants. *Bio/Technology, 13*(2), 142–150.

Popa, E., Râpă, M., Cornea, C. P., Popa, V., Mitelut, A., Popa, O., Cristea, M., & Popa, M. (2018). PHB/cellulose fibres composites colonisation and biodegradation behaviour. *Materiale Plastice, 55*, 48–53.

Prudnikova, S. V, Vinogradova, O. N., & Trusova, M. Y. (2017). Specific character of bacterial biodegradation of polyhydroxyalkanoates with different chemical structure in soil. *Doklady Biochemistry and Biophysics, 473*(1), 94–97.

Râpă, M., Popa, M., Cornea, C. P., Popa, V., Grosu, E., Geicu, M., Stoica, P., Elisabeta, E., & Popa, E. (2014). Degradation study by trichoderma spp. of poly (3-hydroxybuthyrate) and wood fibres composites. *Romanian Biotechnological Letters, 19*, 9390–9399.

Râpă, M., Popa, M., Grosu, E., Geicu, M., & Stoica, P. (2011). Evaluation of the biodegrading action of the Penicillium Sp. on some composites based on PHB. *Romanian Journal of Physics, 16*, 9–18.

Reis, K. C., Pereira, L., Melo, I. C. N. A., Marconcini, J. M., Trugilho, P. F., & Tonoli, G. H. D. (2015) Particles of Coffee Wastes as Reinforcement in Polyhydroxybutyrate (PHB) Based Composites. *Materials Research, 18*(3), 546-552.

Righetti, M. C., Aliotta, L., Mallegni, N., Gazzano, M., Passaglia, E., Cinelli, P., & Lazzeri, A. (2019). Constrained amorphous interphase and mechanical properties of poly(3-hydroxybutyrate-co-3-hydroxyvalerate). *Frontiers in Chemistry, 7*, p. 790.

Roy, A., Chakraborty, S., Kundu, S. P., Basak, R. K., Basu Majumder, S., & Adhikari, B. (2012). Improvement in mechanical properties of jute fibres through mild alkali treatment as demonstrated by utilisation of the Weibull distribution model. *Bioresource Technology, 107*, 222–228.

Roy, S., & Rhim, J.-W. (2021). New insight into melanin for food packaging and biotechnology applications. *Critical Reviews in Food Science and Nutrition*, 1–27.

Saba, N., Jawaid, M., Alothman, O. Y., & Paridah, M. T. (2016). A review on dynamic mechanical properties of natural fibre reinforced polymer composites. *Construction and Building Materials, 106*, 149–159.

Salehabadi, A., Bakar, M. A., & Bakar, N. H. H. A. (2014). Effect of organo-modified nanoclay on the thermal and bulk structural properties of poly(3-hydroxybutyrate)-epoxidized natural rubber blends: Formation of multi-components biobased nanohybrids. *Materials, 7*(6), 4508–4523.

Salim, M. S., Ariawan, D., Ahmad Rasyid, M. F., Mat Taib, R., Ahmad Thirmizir, M. Z., & Mohd Ishak, Z. A. (2020). Accelerated weathering and water absorption behaviour of kenaf fibre reinforced acrylic based polyester composites. *Frontiers in Materials, 7*, 26.

Salim, Y. S., Sharon, A., Vigneswari, S., Mohamad Ibrahim, M. N., & Amirul, A. A. (2012). Environmental degradation of microbial polyhydroxyalkanoates and oil palm-based composites. *Applied Biochemistry and Biotechnology, 167*(2), 314–326.

Salleh, F. M., Hassan, A., Yahya, R., & Azzahari, A. D. (2014). Effects of extrusion temperature on the rheological, dynamic mechanical and tensile properties of kenaf fibre/HDPE composites. *Composites Part B: Engineering, 58*, 259–266.

Sánchez-Safont, E. L., Aldureid, A., Lagarón, J. M., Cabedo, L., & Gámez-Pérez, J. (2020). Study of the compatibilisation effect of different reactive agents in PHB/natural fibre-based composites. *Polymers, 12*(9).

Sanjeevi, S., Shanmugam, V., Kumar, S., Ganesan, V., Sas, G., Johnson, D. J., Shanmugam, M., Ayyanar, A., Naresh, K., Neisiany, R. E., & Das, O. (2021). Effects of water absorption on the mechanical properties of hybrid natural fibre/phenol formaldehyde composites. *Scientific Reports, 11*(1), 13385.

Satyanarayana, K. G., Arizaga, G. G. C., & Wypych, F. (2009). Biodegradable composites based on lignocellulosic fibres-An overview. *Progress in Polymer Science, 34*(9), 982–1021.

Segal, L., Creely, J. J., Martin, A. E., & Conrad, C. M. (1959). An empirical method for estimating the degree of crystallinity of native cellulose using the X-Ray diffractometer. *Textile Research Journal, 29*(10), 786–794.

Seoane, I. T., Manfredi, L. B., Cyras, V. P., Torre, L., Fortunati, E., & Puglia, D. (2017). Effect of cellulose nanocrystals and bacterial cellulose on disintegrability in composting conditions of plasticized phb nanocomposites. *Polymers, 9*(11).

Sgriccia, N., Hawley, M. C., & Misra, M. (2008). Characterisation of natural fibre surfaces and natural fibre composites. *Composites Part A: Applied Science and Manufacturing, 39*(10), 1632–1637.

Shahinur, S., Hasan, M., Ahsan, Q., & Haider, J. (2020). Effect of chemical treatment on thermal properties of jute fibre used in polymer composites. *Journal of Composites Science, 4*, 1–13.

Shangguan, Y.-Y., Wang, Y.-W., Wu, Q., & Chen, G.-Q. (2006). The mechanical properties and in vitro biodegradation and biocompatibility of UV-treated poly(3-hydroxybutyrate-co-3-hydroxyhexanoate). *Biomaterials, 27*(11), 2349–2357.

Shen, D. K., & Gu, S. (2009). The mechanism for thermal decomposition of cellulose and its main products. *Bioresource Technology, 100*(24), 6496–6504.

Singh, I., & Chaitanya, S. (2015). Injection molding of natural fibre reinforced composites. In Thakur, V. K., & Kessler, M. R. (Eds.),*Green Biorenewable Biocomposites* (pp. 77–130). New York, Apple Academic Press

Smith, E. (1968). Crack bifurcation in brittle solids. *Journal of the Mechanics and Physics of Solids, 16*(5), 329–336.

Smith, M. K. M., Paleri, D. M., Abdelwahab, M., Mielewski, D. F., Misra, M., & Mohanty, A. K. (2020). Sustainable composites from poly(3-hydroxybutyrate) (PHB) bioplastic and agave natural fibre. *Green Chemistry, 22*(12), 3906–3916.

Sri Aprilia, N. A., Davoudpour, Y., Zulqarnain, W., Abdul Khalil, H. P. S., Mohamad Hazwan, C. I. C., Hossain, M. S., Dungani, R., Fizree, H. M., Zaidon, A., & Mohamad Haafiz, M. K. (2016). Physicochemical characterisation of microcrystalline cellulose extracted from kenaf bast. *BioResources, 11*(2).

Sudesh, K., Abe, H., & Doi, Y. (2000). Synthesis, structure and properties of polyhydroxyalkanoates: biological polyesters. *Progress in Polymer Science, 25*(10), 1503–1555.

Suryanto, H., Marsyahyo, E., Irawan, Y., & Soenoko, R. (2014). Effect of alkali treatment on crystalline structure of cellulose fibre from mendong (Fimbristylis globulosa) straw. *Key Engineering Materials, 594–595*, 720–724.

Takahashi, K., & Choi, N.-S. (1991). Influence of fibre weight fraction on failure mechanisms of poly(ethylene terephthalate) reinforced by short-glass-fibres. *Journal of Materials Science, 26*(17), 4648–4656.

Tertyshnaya, Y. V, & Shibryaeva, L. S. (2013). Degradation of poly(3-hydroxybutyrate) and its blends during treatment with UV light and water. *Polymer Science Series B, 55*(3), 164–168.

Thankappan, S., Abraham, J., George, S. C., & Thomas, S. (2018). Rheological characterisation of nanocomposites. in characterisation of nanomaterials. *Advances and Key Technologies* (pp. 167–189). Elsevier.

Theocaris, P. S., & Papadopoulos, G. A. (1986). Crack propagation and bifurcation in fibre-composite models-ii: Hard-soft-hard sequence of phases. *Journal of Reinforced Plastics and Composites, 5*(2), 120–140.

Thomason, J. L., Vlug, M. A., Schipper, G., & Krikor, H. G. L. T. (1996). Influence of fibre length and concentration on the properties of glass fibre-reinforced polypropylene: Part 3. Strength and strain at failure. *Composites Part A: Applied Science and Manufacturing, 27*(11), 1075–1084.

Ublekov, F., Budurova, D., Staneva, M., Natova, M., & Penchev, H. (2018). Self-supporting electrospun PHB and PHBV/organoclay nanocomposite fibrous scaffolds. *Materials Letters, 218*, 353–356.

Vahabi, H., Michely, L., Moradkhani, G., Akbari, V., Cochez, M., Vagner, C., Renard, E., Saeb, M. R., & Langlois, V. (2019). Thermal stability and flammability behaviour of poly(3-hydroxybutyrate) (PHB) based composites. *Materials, 12*(14), 2239.

Van Soest, P. J., & Wine, R. H. (1968). Determination of lignin and cellulose in acid-detergent fibre with permanganate. *Journal of Association of Official Analytical Chemists, 51*(4), 780–785.

Ventura, H., Claramunt, J., Rodríguez-Pérez, M. A., & Ardanuy, M. (2017). Effects of hydrothermal aging on the water uptake and tensile properties of PHB/flax fabric biocomposites. *Polymer Degradation and Stability, 142*, 129–138.

Vinayagamoorthy, R. (2020). Influence of fibre pretreatments on characteristics of green fabric materials. *Polymers and Polymer Composites, September 2021*, 1039-1054

Vishtal, A., & Retulainen, E. (2014). Boosting the extensibility potential of fibre networks: A Review. *Bioresources, 9*,

Volova, T., Shishatskaya, E., Sevastianov, V., Efremov, S., & Mogilnaya, O. (2003). Results of biomedical investigations of PHB and PHB/PHV fibres. *Biochemical Engineering Journal, 16*(2), 125–133.

Wang, C., Bai, S., Yue, X., Long, B., & Choo-Smith, L.-P. (2016). Relationship between chemical composition, crystallinity, orientation and tensile strength of kenaf fibre. *Fibers and Polymers, 17*(11), 1757–1764.

Wang, P. H., Ghoshal, S., Gulgunje, P., Verghese, N., & Kumar, S. (2016). Polypropylene nanocomposites with polymer coated multiwall carbon nanotubes. *Polymer, 100*, 244–258.

Wang, S., Chen, W., Xiang, H., Yang, J., Zhou, Z., & Zhu, M. (2016). Modification and potential application of short-chain-length polyhydroxyalkanoate (SCL-PHA). *Polymers, 8*(8).

Wang, X., & Petrů, M. (2019). Effect of Hygrothermal aging and surface treatment on the dynamic mechanical behaviour of flax fibre reinforced composites. *Materials, 12*(15).

Weihua, K., He, Y., Asakawa, N., & Inoue, Y. (2004). Effect of lignin particles as a nucleating agent on crystallisation of poly(3-hydroxybutyrate). *Journal of Applied Polymer Science, 94*(6), 2466–2474.

Wong, S., Shanks, R., & Hodzic, A. (2004). Interfacial improvements in poly(3-hydroxybutyrate)-flax fibre composites with hydrogen bonding additives. *Composites Science and Technology, 64*(9), 1321–1330.

Wu, Y.-L., Wang, H., Qiu, Y.-K., Liow, S. S., Li, Z., & Loh, X. J. (2016). PHB-based gels as delivery agents of chemotherapeutics for the effective shrinkage of tumors. *Advanced Healthcare Materials, 5*(20), 2679–2685.

Xiang, H., Wen, X., Miu, X., Li, Y., Zhou, Z., & Zhu, M. (2016). Thermal depolymerisation mechanisms of poly(3-hydroxybutyrate-co-3-hydroxyvalerate). *Progress in Natural Science: Materials International, 26*(1), 58–64.

Xie, W., Gao, Z., Liu, K., Pan, W. P., Vaia, R., Hunter, D., & Singh, A. (2001). Thermal characterisation of organically modified montmorillonite. *Thermochimica Acta, 367*(368), 339–350.

Yang, B., Nar, M., Visi, D. K., Allen, M., Ayre, B., Webber, C. L., Lu, H., & D'Souza, N. A. (2014). Effects of chemical versus enzymatic processing of kenaf fibres on poly(hydroxybutyrate-co-valerate)/poly(butylene adipate-co-terephthalate) composite properties. *Composites Part B: Engineering, 56*, 926–933.

Yang, H., Yan, R., Chen, H., Lee, D. H., & Zheng, C. (2007). Characteristics of hemicellulose, cellulose and lignin pyrolysis. *Fuel, 86*(12–13), 1781–1788.